UNIVERSIDAD DE CHILE
FACULTAD DE CIENCIAS FÍSICAS Y MATEMÁTICAS
DEPARTAMENTO DE GEOLOGÍA

NEOTECTONICS AND CRUSTAL FAULT CHARACTERIZATON IN THE AYSÉN REGION (~44º-47ºS), NORTHERN PATAGONIAN ANDES, CHILE

TESIS PARA OPTAR AL GRADO DE MAGÍSTER EN CIENCIAS, MENCIÓN GEOLOGÌA

MARIO ADRIANO PERSICO BLANCO

PROFESOR GUÍA:
GREGORY PAUL DE PASCALE

PROFESOR CO-GUÍA:
DANIEL MONCADA DE LA ROSA

MIEMBROS DE LA COMISIÓN:
MARCELO FARÍAS THIERS
GABRIEL EASTON VARGAS

SANTIAGO DE CHILE
2021

RESUMEN DE LA TESIS PARA OPTAR AL TITULO DE: Magíster en Ciencias, mención Geología

POR: Mario Adriano Persico Blanco

FECHA: 14/04/2021

PROFESOR GUÍA: Gregory Paul De Pascale

Abstract

The Northern Patagonian Andes constitutes part of one of the most geologically active orogens in the world, with the longest active volcanic chain and the greatest recorded earthquake in history (Mw 9.5 Valdivia 1960 Earthquake). In 2007, a seismic swarm with magnitudes up to Mw 6.2 occurred in the Aysén fiord associated to submarine crustal faults related to the Liquiñe-Ofqui Fault Zone (LOFZ), triggering earthquakes and landslides that induced a tsunami, causing 12 deaths. However, very little is known about the active tectonic framework and the potential seismogenic crustal faults in the Aysén Region, mainly due to dense vegetation and widespread Quaternary volcanic and glacial cover.

Six (6) previously unmapped faults are documented in this work. Based on the presence of uncemented (unhealed) fault rocks, geomorphological and stratigraphic observations, in addition to recent microseismicity studies in the Puyuhuapi area, I propose that these faults are potentially active, and thus correspond to sources of potential coseismic hazard for the Aysén Region. Based on scaling relationships, these faults are capable of generating earthquakes of magnitudes up to at least Mw 6.5.

Additionally, eight (8) new thermochronological cooling ages along the Exploradores Valley reflect progressive younger cooling ages towards the main trace of the LOFZ. Notably, samples from the same elevation present younger AHe ages at the eastern side of the LOFZ (1.5 ± 0.15 Ma) than samples located at the western side of the fault (2.0 ± 0.07 to 2.37 ± 0.32), which are at least 0.5 Ma older.

Results from this work present evidence of previously unmapped faults and neotectonic activity along the LOFZ that are compatible with the current stress regime in the Aysén Region, and thus correspond to potential sources of coseismic hazard for the region that should be considered and included in local and regional seismic hazard models, in addition to providing a better understanding of the neotectonic framework of the area about the subducted Chile Ridge.

Resumen

Los Andes Patagónicos del Norte constituyen parte de uno de los orógenos más activos del mundo, con la cadena volcánica active más larga y el mayor terremoto registrado de la historia (Terremoto de Valdivia de 1960 de Mw 9.5). En 2007, un enjambre sísmico con magnitudes máximas de Mw 6.2 ocurrió en el fiordo de Aysén asociado a fallas corticales submarinas relacionadas a la Zona de Falla Liquiñe-Ofqui (ZFLO), gatillando terremotos y remociones en masa que provocaron un tsunami, causando 12 muertes. Sin embargo, poco es lo que se conoce acerca del régimen tectónico active y del potencial sismogénico de fallas corticales en la región de Aysén, principalmente debido a la densa vegetación y extensa cubierta volcánica y glacial cuaternaria.

Seis (6) fallas previamente no mapeadas son documentadas en este trabajo. Basado en la presencia de rocas de falla no cementadas (o selladas), observaciones geomorfológicas y estratigráficas, junto con estudios recientes de microsismicidad en el área de Puyuhuapi, se propone que estas fallas son potencialmente activas y, por lo tanto, corresponden a potenciales fuentes de peligro cosísmico para la región de Aysén. Basado en relaciones de escala, estas fallas son capaces de generar terremotos de magnitudes hasta al menos Mw 6.5.

Adicionalmente, nuevas edades termocronológicas a lo largo del Valle Exploradores reflejan edades de enfriamiento progresivamente más jóvenes hacia la traza principal de la ZFLO. En particular, muestras a la misma elevación presentan edades AHe más jóvenes en el lado este de la ZFLO (1.5 ± 0.15 Ma) que las ubicadas en el lado oeste de la falla (2.0 ± 0.07 a 2.37 ± 0.32), siendo al menos 0.5 Ma más antiguas.

Los resultados de este trabajo presentan evidencia de fallas previamente no mapeadas y actividad neotectónica a lo largo de la LOFZ que son compatibles con el régimen de estrés actual en la Región de Aysén y, por lo tanto, corresponden a fuentes potenciales de amenaza cosísmica para la región que deben ser consideradas e incluidas en la escala local y modelos regionales de riesgo sísmico, además de proporcionar una mejor comprensión del marco neotectónico del área sobre la subducción del Ridge de Chile.

ACKNOWLEDGMENTS

First of all thanks to the Chilean national research agency (CONICYT), to the project Fondecyt Nº11160038: “Quantifying Seismic Hazard Along Chile's fastest slipping crustal Fault, the Liquiñe-Ofqui Fault Zone (LOFZ), Patagonia”, and to the Andean Geothermal Center of Excellence (CEGA) FONDAP/CONICYT Project Nº15090013 for supporting this MSc thesis.

Thanks to my supervisor, Dr. Gregory De Pascale, for his support throughout my MSc. I really appreciate the opportunities that he gave me and the fieldwork experiences we had together. Thanks to Dr. Daniel Moncada for his help and fruitful discussions during fieldwork in Patagonia. Thanks to Dr. Marcelo Farías, Dr. Daniel Moncada and Dr. Gabriel Easton for previous reviews and comments to this thesis.

Thanks to my office postgraduate colleagues for the numberless discussions and opinions during these years: Jose Araya, Francisca Sandoval, Gonzalo Silva, Sebastian Herrera, Huber Rivera. All your opinions have made this thesis a much improved document and I really appreciate it.

Thanks to Roberto from the Mineral separation Lab of the Universidad de Chile. Without his help the mineral separation would not have been possible. Thanks for your time, patience and dedication in teaching me. Thanks to Julie Fosdick for thermochronology analysis in the Basin Analysis & Helium Thermochronology Lab at the University of Connecticut.

Finally, but not less important, thanks to all my family. Your support has been essential during these years. Without it this thesis would not have been possible.

TABLE OF CONTENTS

LIST OF FIGURES

LIST OF TABLES

1 INTRODUCTION

1.1 Abstract

This chapter is an introduction to this thesis focused on the crustal faults as potential seismogenic sources in the Aysén Region, Patagonia. It presents a brief motivation of this study, the working hypothesis, the main scientific questions to be achieved and a general background of the Northern Patagonian Andes geology.

1.2 Motivation

Conventional seismic hazard analysis is based primarily on earthquake frequency obtained from historical catalogues of seismicity (e.g. Allen et al., 1965; Wesnousky et al., 1984, 1986; Dimaté et al., 1999), but the uncertainty in such analyses is large when the historical and instrumental records of earthquake recurrence time is too short to define seismic rates (Allen et al., 1965; Allen, 1975; Anderson, 1979; Wesnousky et al., 1984, 1986). In contrast to seismic catalogues, the geological identification of Quaternary active faults are used to reduce these uncertainties, as moderate to large earthquakes occur when crustal faults rupture, and faults that deform Quaternary deposits are now commonly accepted as sources of seismic hazard (Allen et al., 1965, 1975; Matsuda, 1977; Anderson, 1979; Wesnousky, 1986 and references therein) Therefore, detailed mapping and field characterization of active faults constitutes a first order input for accurate geohazard assessment, including strong ground motions, fault ruptures and potential earthquake effects (landslides, lateral spreading, and liquefaction), especially in regions where seismological record is short and poorly constrained. In addition, the geometry and architecture of upper

crustal faults and their damage zones enhances rock permeability and controls the pathways for heat and hydrothermal fluid flow of geothermal systems in the upper crust (e.g. Sibson, 1994, 1996; Cox, 1999; Zhang et al., 2008; Sanchez et al., 2013; Perez-Flores et al., 2016). The Northern Patagonian Andes has abundant thermal springs that show potential for geothermal energy, so understanding fault networks and where potential seismic sources are located in this region is critical prior to exploration or development of these geothermal fields, in addition to better characterization of the seismic hazard.

The Northern Patagonian Andes are part of the longest active mountain chain on Earth, characterized by a continuous orogenic belt that extends for more than 7,000 km in length and up to 500 km in width (e.g. Dewey and Bird, 1970). The most prominent feature of the Northern Patagonian Andes is the Liquiñe-Ofqui Fault Zone (LOFZ), a 1,200 km long intra-arc fault system that corresponds to one of the most important seismogenic sources in the Aysén Region, where earthquakes up to Mw 6.2 have occurred (Lange et al., 2008; Legrand et al., 2011; Russo et al., 2011; Vargas et al., 2013; Cisternas et al., 2017), including big landslides (Sepulveda et al., 2010) and the greatest instrumentally recorded earthquake in the Earth (1960 Valdivia earthquake; e.g. Cifuentes, 1989; Dzierma et al., 2012; Cisternas et al., 2017) (Figure 1.1).

However, little is known about the active tectonic framework and the potential seismogenic crustal structures in this region of the Andes, mainly due to poor weather conditions, dense vegetation and wide quaternary volcanic and glacial cover. Moreover, the geology and fault characterization in this region are currently mapped at scales that are of limited use for neotectonic investigations (e.g. 1:1,000,000 scale map of "Servicio Nacional de Geología y Minería" (Sernageomin, 2002), although with localized mapping at scales of

1:50,000 (e.g. Puyuhuapi), which provides limited insight to the regional active structures and to the local, regional and fault rupture models.

In this context, some questions arise from the crustal tectonics in the Patagonian Andes:

- Are there any other active tectonic structures in the Aysén Region?
- Are any of these structures an important seismic hazard source to the region?
- How do these crustal faults relate to the geothermal systems of the region?

1.3 Working Hypothesis

A) If the Patagonian Andes are an active orogen characterized by the oblique subduction of the Nazca Plate, then there should be evidence of Quaternary active structures accommodating crustal deformation.

B) If faults are found in the field that have fault rocks such as gouge, breccia, and cataclasite and have geomorphic expression, then perhaps these faults are active structure currently accommodating the oblique subduction in the crust.

C) If these crustal faults are active, they may be sources of seismic and coseismic hazard (earthquakes, liquefaction, and landslides).

1.4 Research Goals

1.4.1 Main Goal

The main research goal of this thesis is to recognize and characterize crustal faults in the Aysén Region related to tectonic deformation both within and adjacent to the LOFZ. As faults are both potential source of sesimic hazard and conduits for geothermal fluid flow, better mapping and field characterization will provide new insights into the geothermal regime and will help for future assessment of associated coseismic geohazards (earthquakes, landslides, lateral spreading and liquefaction) in the region.

1.4.2 Specific goals

The specific research goals of this thesis are:

- Improve mapping of the geology, geomorphology, and structures in the Aysén Region.
- Document and characterize new crustal faults in the region to better understand the relation between structures, fluids and geothermal heat flow.
- Assess new crustal faults as potential seismogenic sources in the region.

1.5 Northern Patagonian Andes Geological Background

1.5.1 Tectonic Setting

The Northern Patagonian Andes is located in the Southeastern Circum-Pacific basin, between latitudes 39º and 47ºS. It is characterized by the oblique subduction of the oceanic Nazca plate under the continental South-American plate since 26 Ma, with at a rate of 6-8 cm/yr (e.g., Pardo-Casas and Molnar, 1987; Angermann et al., 1999) (Figure 1.1). At 47°S, an active oceanic ridge (Chile Ridge) collides with the continental margin at the Chile Triple Junction (e.g. Miller et al., 2005), where the Nazca, South American and Antarctic Plate meets the Peru-Chile trench, marking the transition between the Northern and Southern Patagonian Andes (e.g., Ramos and Gighlione, 2008). North of the Chile Triple Junction, the subduction is characterized by the Nazca Plate beneath the South American plate in a northeast direction since the early Miocene at a rate of 7 cm/yr (e.g. Pardo-Casas and Molnar, 1987; Angermann et al., 1999; Wang et al., 2007; DeMets et al., 2010). South of it, the Antarctic Plate subducts beneath the South American plate since 16 Ma at a rate of 2 cm/yr (Pardo-Casas and Molnar, 1987; Angermann et al., 1999) (Figure 1.1). The Chile Ridge collision was proposed to be in part responsible for topographic changes and landscape evolution of the upper crust (e.g., Guillaume et al., 2010; Georgieva et al., 2016). In contrast, Christeleit et al. (2017), based on numerical modeling, concludes that subduction and migration of the Chile Ridge has little influence on the thermal evolution of the shallow crust, attributing topographic and geomorphic changes mainly to post-glacial isostatic effects during the late Quaternary. In addition, collision and northward migration of the Chile Triple Junction has been proposed to generate the translation of the Chiloé microplate, a fore-arc sliver decoupled from the South American by the intra-arc LOFZ

(Beck, 1983; Forsythe and Nelson, 1985; Wang et al., 2007; Lange et al., 2008; Melnick et al., 2009; Georgieva et al., 2016). The subduction of the Chile Ridge has also been associated with an astenospheric slab window, which therefore produces the proposed Patagonian arc volcanic gap between 46-49ºS (Ramos and Kay, 1992; Gorring et al., 1997; Stern, 2004) and back-arc volcanism with primitive magmatic signature and mantle xenoliths (e.g. Gorring et al., 1997; Guivel et al., 1999, 2006; Parada et al., 2001; Jalowitzki et al., 2017).

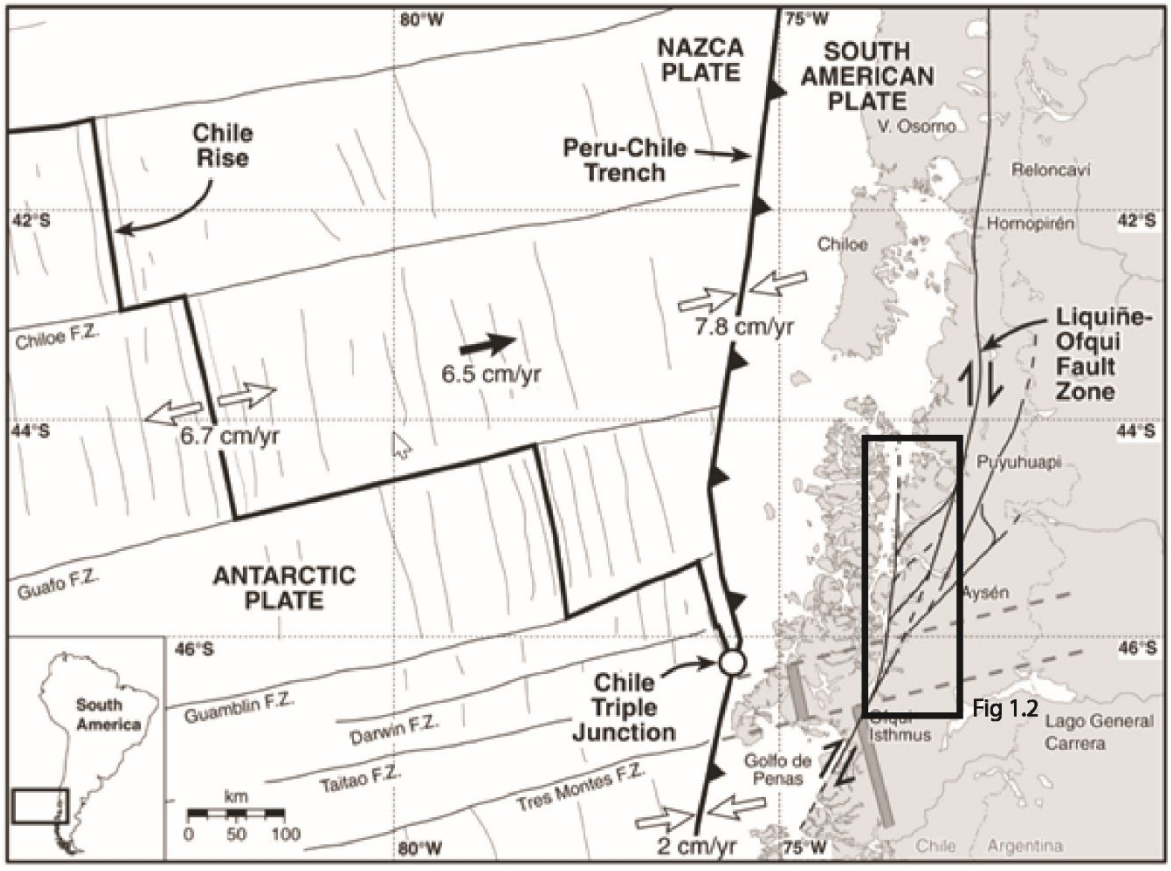

Figure 1.1. Tectonic map of the Southeast Pacific showing the plate configuration of the Southern Andes continental margin. The Peru-Chile Trench is the subduction boundary between the Nazca and the South American plates (modified from Thomson, 2002). Black rectangle shows the study area of this work.

1.5.2 Regional Geology

The geology of the Aysén Region comprises Paleozoic to Cenozoic volcanic, sedimentary and intrusive rocks that are variably folded and deformed (e.g. Hervé, 1994; Charrier et al., 2007) (Figure 1.2). The oldest exposed units in the region correspond to metamorphic complexes of Late Paleozoic age that were accreted to the western Gondwana margin (e.g. Hervé, 1994; Hervé et al., 1998; Hervé et al., 2007, 2008). They consist of polydeformed turbidite successions with minor bodies of cherts, limestones, schists and metabasites, all regionally metamorphosed to green-schist facies (Hervé et al., 2008). Mesozoic units in the area correspond to thick volcanic deposits of the Chon-Aike magmatic province (e.g. Pankhurst et al., 1992, 1998, 1999; Hervé et al., 1999, 2007; De la Cruz et al., 1994) and sedimentary marine and continental successions of Jurassic – Early Cretaceous age that were accumulated in a back-arc basin environment (e.g. Charrier et al., 2007; Scalabrino et al,. 2010). These units (Paleozoic and Mesozoic) are intruded by the North Patagonian Batholith, a huge meso-Cenozoic (191 to 10 Ma) plutonic belt hundreds of kilometers long and tens of kilometers wide, spanning between 39°S and 47°S and interpreted as the exposed roots of the Andean magmatic arc (e.g. Pankhurst et al., 1992, 1998) (Figure 1.2).

Cenozoic units found in the region correspond to tertiary volcanosedimentary successions, also intruded by the North Patagonian Batholith, and Quaternary deposits composed of Holocene volcanics (e.g. Hervé et al., 1994) (Figure 1.2). During the late Cenozoic, the Patagonian Andes relief was also subjected to repeated glaciation periods, with the Last Glacial Maximum occurring during around 18-12 Ka, where almost the whole Patagonian orogen was covered under thick ice sheets (Mercer, 1983; Ton-That et al., 1999;

Hulton et al., 2002; Lagabrielle et al., 2010). One of the most outstanding features in Aysén is the Southern Volcanic Zone, a Quaternary volcanic arc that includes over 200 large stratovolcanoes and several small monogenetic cones along the main axis of the Andes (e.g. Stern, 2004; Cembrano y Lara, 2009; Vargas et al., 2013).

1.5.3 Structural Geology

The main structural feature of the Northern Patagonian Andes is the LOFZ (Figure 1.2; Figure 1.3). It is 1,200 km-long intra-arc strike-slip fault system typically defined as a series of major NNE-striking, right-lateral, strike-slip faults associated with NE-striking dextral faults interpreted as being the result of strike-slip partitioning of weak crustal lithosphere in the region of the Andean magmatic arc (e.g. Forsythe and Nelson, 1985; Herve and Ota, 1993; Herve, 1994; Forsythe and Prior, 1992; Cembrano et al., 1996; 2002; Lavenu and Cembrano, 1999; Thomson, 2002; Cembrano and Lara, 2009; Melnick et al., 2009). The LOFZ partially controls the occurrence, spatial distribution, geochemistry and geometry of major stratovolcanoes and minor eruptive centers (e.g. Hervé, 1994; Pankhurst, 1992; Stern, 2004; Lara et al., 2008; Cembrano and Lara, 2009; Vargas et al., 2013). Present-day activity of the LOFZ would absorb a minimum of 6.5 mm/yr of northward motion of the forearc, as recorded by a limited GPS campaign and widespread crustal seismicity (Wang et al., 2007; Lange et al., 2008). Forsythe and Prior (1992) estimated a minimum slip rate of 1 mm/yr for the LOFZ based on 1,200 m of relative subsidence at Laguna San Rafael as a result of a dip-slip component of a portion of the LOFZ. Hervé et al. (1994) calculated exhumation rates in excess of 1 mm/yr based on Ar/Ar thermochronology on exhumed plutonic rocks of the Patagonian Batholith. In the Holocene, Hervé and Ota (1993) inferred late Holocene uplift rates of more than 3 mm/yr within the LOFZ based on

^{14}C ages on shell materials from elevated beaches (up to 30 m.a.s.l) in continental Chiloé at 42-43ºS associated to coseismic deformation. In addition, Cembrano et al. (2002) based on thermochronological Ar/Ar analysis obtained an average exhumation rate for the LOFZ in excess of 1.7 mm/yr for Miocene Patagonian Batholith rocks at 44ºS.

A second important structural feature in the Southern Andes are the Andean Transverse Faults (ATF; Rosenau et al., 2006; Sanchez et al., 2013; Perez-Flores et al., 2016; Siegfield 2016) (Figure 1.3). The ATF corresponds to a series of discrete, NW-striking sinistral strike-slip faults inherited from pre-Andean geological processes associated with the occurrence of earthquakes, late Cenozoic deformation, quaternary volcanism and geothermal areas (e.g. Rosenau et al., 2006; Lange et al., 2008; Pérez-Flores et al., 2016; Sielfeld et al., 2016). Remote sensing, field observations and geophysical evidence such as shallow seismicity, Vp/Vs tomography and magnetic anomalies suggest that the ATF are deep-seated lithospheric-scale structures with present-day activity (Yáñez et al., 1998; Sánchez et al., 2013; Perez-Flores et al., 2016). No slip-rates have been reported for these structures.

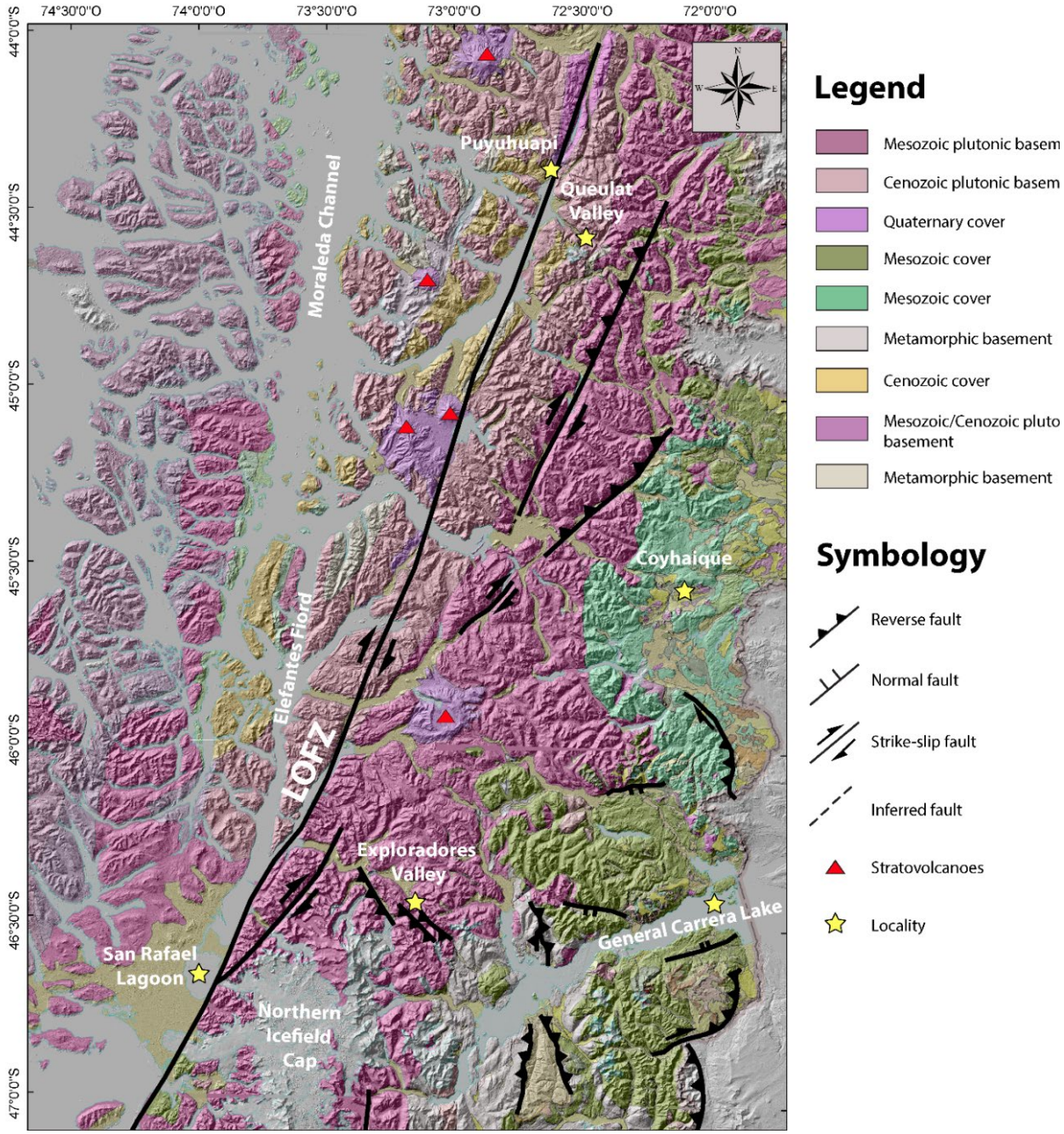

Figure 1.2. Regional Map of the Aysén Region showing the main geological units and tectonic structures. This map was developed from data compiled from Thomson (2002), Sernageomin (2002), Cembrano and Lara (2009), Scalabrino et al. (2010), Vargas et al. (2013) and Georgieva et al. (2016).

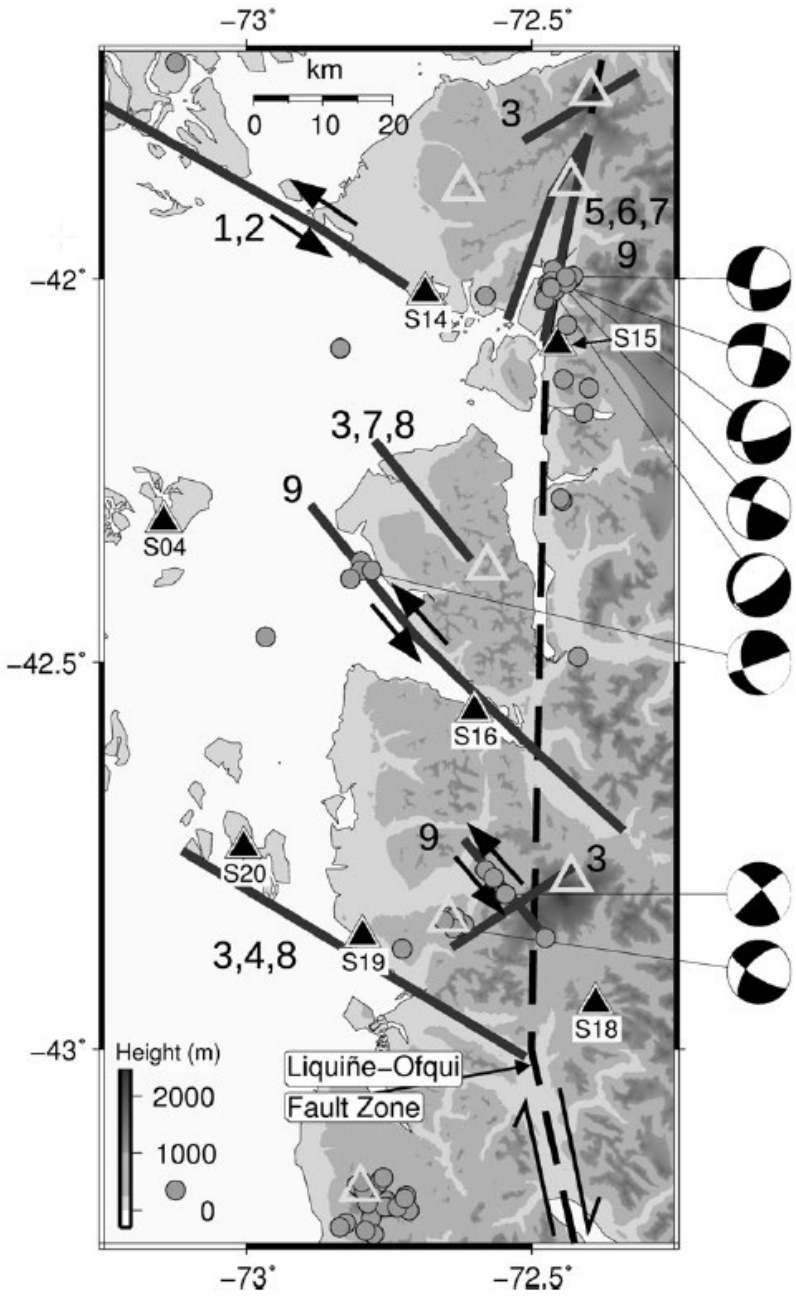

Figure 1.3. Digital elevation model of the Northern Patagonian Andes between 41.5 and 43.5ºS, showing the Liquiñe-Ofqui Fault Zone (black dashed lines) and the NW-striking Andean Transverse Faults (black solid lines). Modified from Lange et al. (2008). Black triangles show seismic stations used. White triangles show Holocene volcanic centers.

1.5.4 Seismicity

Crustal seismicity in the Northern Patagonian Andes is characterized by several shallow earthquakes with magnitudes > Mw 6 and depths less than 35 km over the last 50 years (Centro Sismológico Nacional; Chinn and Isacks; 1983; Lange et al., 2008; Legrand et al., 2011; Vargas et al., 2013; Agurto-Detzel et al., 2014) (Figure 1.4; Figure 1.5). However, plate boundary earthquakes here are common, including the greatest ever recorded earthquake (1960 Valdivia Mw 9.5 earthquake; e.g. Cifuentes, 1989; Dzierma et al., 2012; Cisternas et al., 2017). Recently, the latter found new evidence of a seismic sequence preceding the 1960 mega-earthquake, providing new insights on the time-dependent evolution of the seismogenic zone of the southern Central Andes. In addition, in 2007 a seismic swarm occurred in the Aysén Fiord at ~45.5°S, with the greatest event with a magnitude of 6.2 Mw and calculated maximum depth of 9 km, where the moment tensor solutions also indicate dextral strike-slip movements associated to a NS-striking splay of the LOFZ (Barrientos et al., 2007; Legrand et al., 2011; Vargas et al., 2013). In 2016 an Mw 7.6 earthquake struck the Chiloé island in the south of Chile, which has been interpreted as a sign of seismic reawakening of the 1960 Valdivia earthquake rupture segment (Ruiz et al., 2017). Additionally, (Lange et al. (2008) identified different seismic clusters using 7 seismic stations with magnitudes up to 3.8 Mw and depths less than 25 km along the LOFZ between 41.5 and 43.5°S (Figure 1.4). The main cluster recorded was at ~43°S near Hornopirén, with focus depths of less than 10 km and coincident with a trace of the LOFZ. Other historical earthquakes correspond to a 6.0 Mw event attributed to an eruption of the Hudson volcano in 1965 at 46ºS (Rosenau et al., 2006).

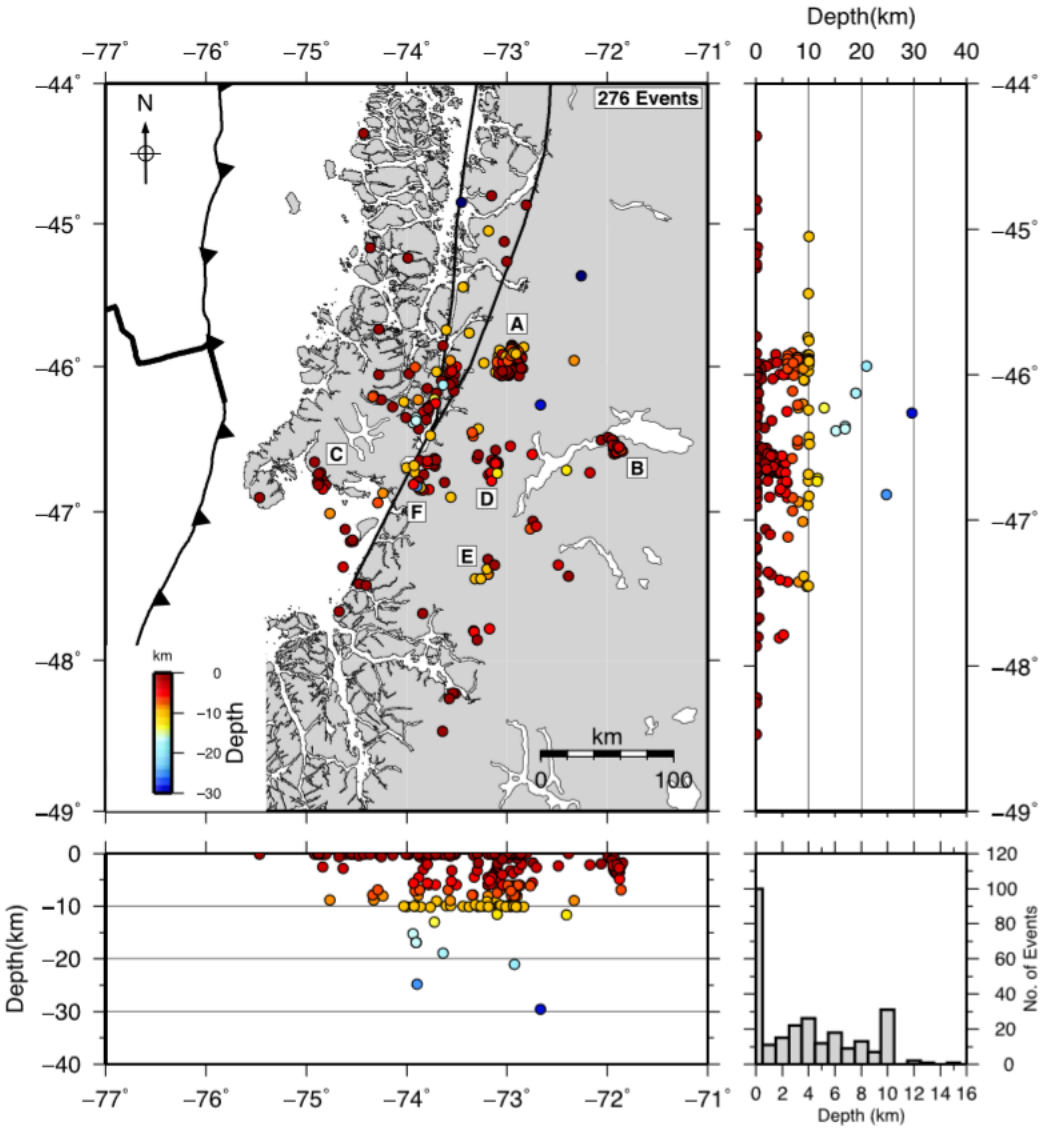

Figure 1.4. Crustal seismicity colored by depth of the Aysén Region between 44° and 48°S (modified from Agurto-Detzel et al., 2014).

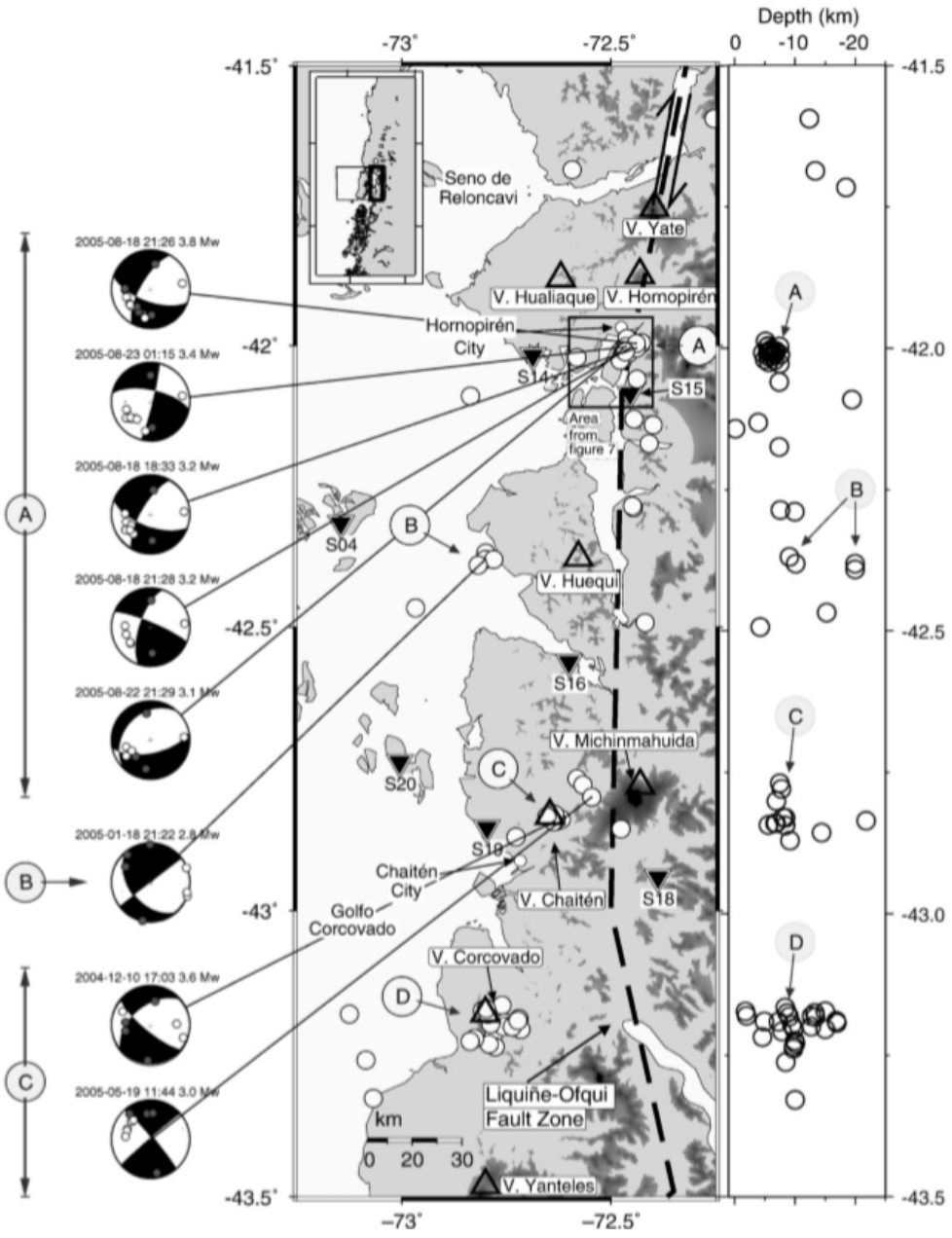

Figure 1.5. Map showing crustal seismicity with depths less than 25 km and focal mechanism solutions along the LOFZ between 41.5°S and 43.5°S obtained from Lange et al (2008). Seismic stations are indicated by inverted triangles. Volcanoes are indicated with upright triangles. Letters a-d correspond to different seismic clusters identified by Lange et al. (2008).

1.5.5 Volcanism

The Northern Patagonia is part of the southernmost segment of the Southern Volcanic Zone (SVZ), a quaternary volcanic arc composed of both major stratovolcanoes and minor eruptive centers that extends from 33° to 46°S for more than 1200 km (Figure 1.6; Stern, 2004). This volcanism is mostly controlled by the dehydration of the subducted Nazca Plate and subsequent partial melting of the mantle, usually with participation of the mantle lithosphere or the continental crust (Hildreth and Moorbath, 1998). This leads to different geochemical composition of the volcanic products, reflecting different tectono-magmatic processes (Hildreth and Moorbath, 1998; McGee et al., 2016).

Between 37° and 46°S, the Andean volcanism is mainly basaltic to andesitic, with some explosive products of more silicic composition (López et al., 1995; Cembrano and Lara, 2009). The basic volcanism is closely associated to NNE and NE-striking tension cracks with primitive minor Holocene monogenetic eruptive cones spatially correlated with the main and adjacent fault traces of the LOFZ (Lara et al., 2008; Cembrano and Lara, 2009) (Figure 1.6) like the historically active Llaima volcano which developed along a NE fissural range with almost 40 minor centres aligned along a NE-striking arc structure (Moreno and Naranjo, 2003; Naranjo and Moreno, 2005). According to Lara et al. (2006) and Cembrano and Lara (2009), dacitic to rhyolitic volcanism can result from more complex evolution in some cases associated with WNW-striking basement structures like the Puyehue-Cordón Caulle, which is a NW-striking central volcano and fissure system associated to the LOFZ that experienced large explosive eruptions on 1960 and since 2011 (Vargas et al., 2013) (Figure 1.6).

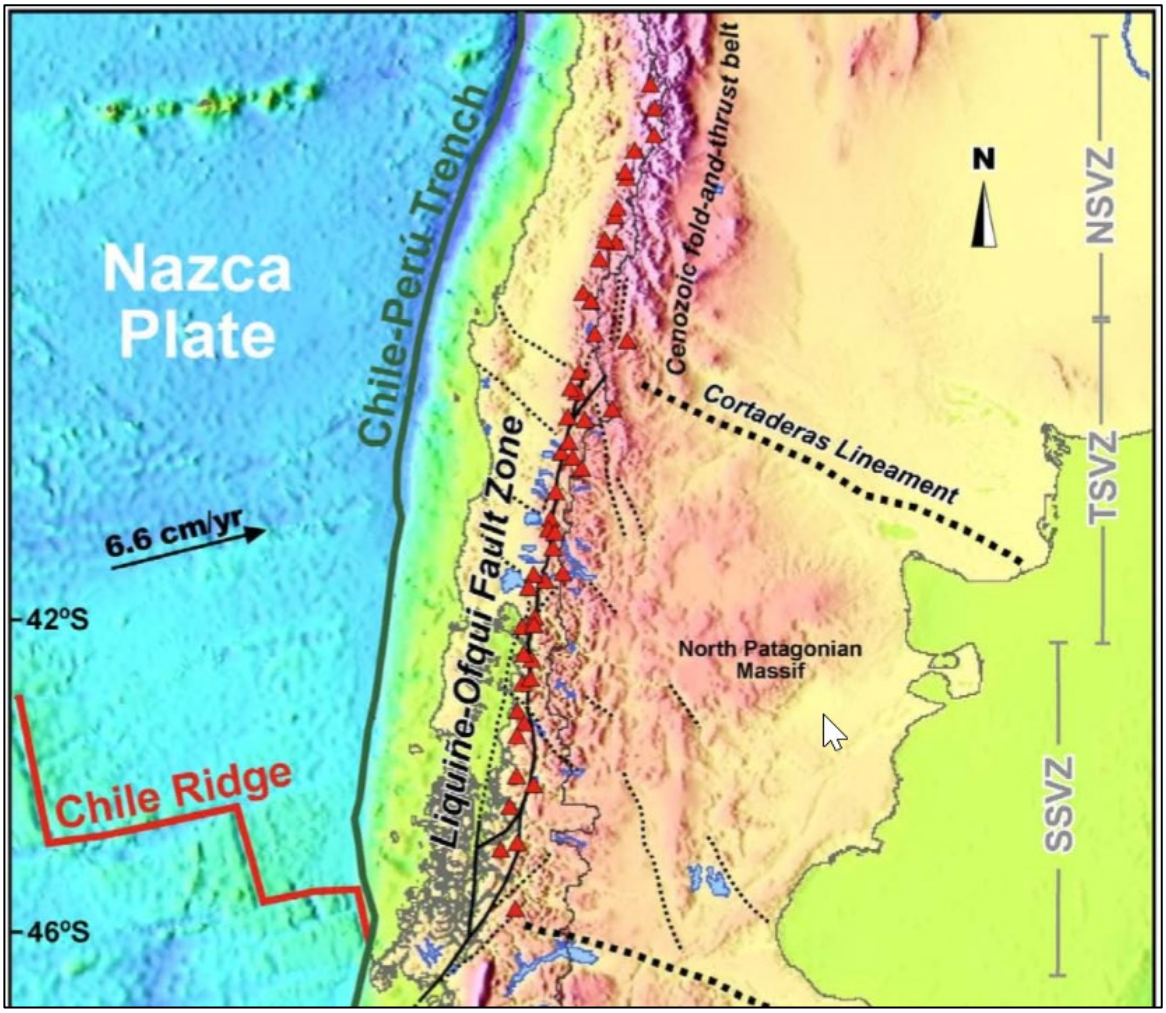

Figure 1.6. Tectonic Map of the Northern Patagonian Andes showing the spatial relation between the quaternary volcanic arc (red triangles) of the SVZ and the Liquiñe-Ofqui Fault Zone (solid black line). Modified from Cembrano and Lara (2009).

1.5.6 Geomorphology and Quaternary geology

The Patagonian Andes landscape is characterized by deep glacial valleys and fiords with reliefs of 1 to 2 km as a result of extensive glaciation during the late Cenozoic (e.g., Christeleit et al., 2017). The oldest known glacial tills are bracketed by basalt flows of 7 to 3 Ma, with the Greatest Patagonian Glaciation (GPG) around 1 Ma ago, suggesting that glaciations started during the late Miocene and continued until today in the Patagonian

Andes (Mercer and Sutter, 1982; Ton-That et al., 1999; Guivel et al., 2006). During the Last Glacial Maximum (LGM) before ~17 Ka, the entire Patagonian Andes was covered under thick ice deposits (e.g. Christeleit et al., 2017; Figure 1.7). Furthermore, Thomson (2010) proposes that glaciations can be a destructive and a constructive process of mountain building in the Patagonian Andes. The first process would be through glacial erosion, while the second would be due to passive exhumation because of isostatic response, or by inhibiting glacial erosion in regions with cool climates, thus promoting orogenic growth. Glaciations, accompanied by Holocene volcanic eruptions of the SVZ, are the main factors that control the geomorphology of the Patagonian Andes.

Other important geomorphic factors in this region of the Patagonian Andes are major landslides. On April 21, 2007, the Aysén Fjord earthquake (Mw 6.2) triggered hundreds of landslides in the epicentral area along the fjord coast and surroundings. Some of these landslides induced large tsunami waves within the fjord causing fatalities and damaging several salmon farms, the most important economic activity of the area (Sepulveda et al., 2010). The landslides included rockslides and avalanches, rock falls, shallow soil and soil–rock slides, and debris flows (Sepulveda et al., 2010).

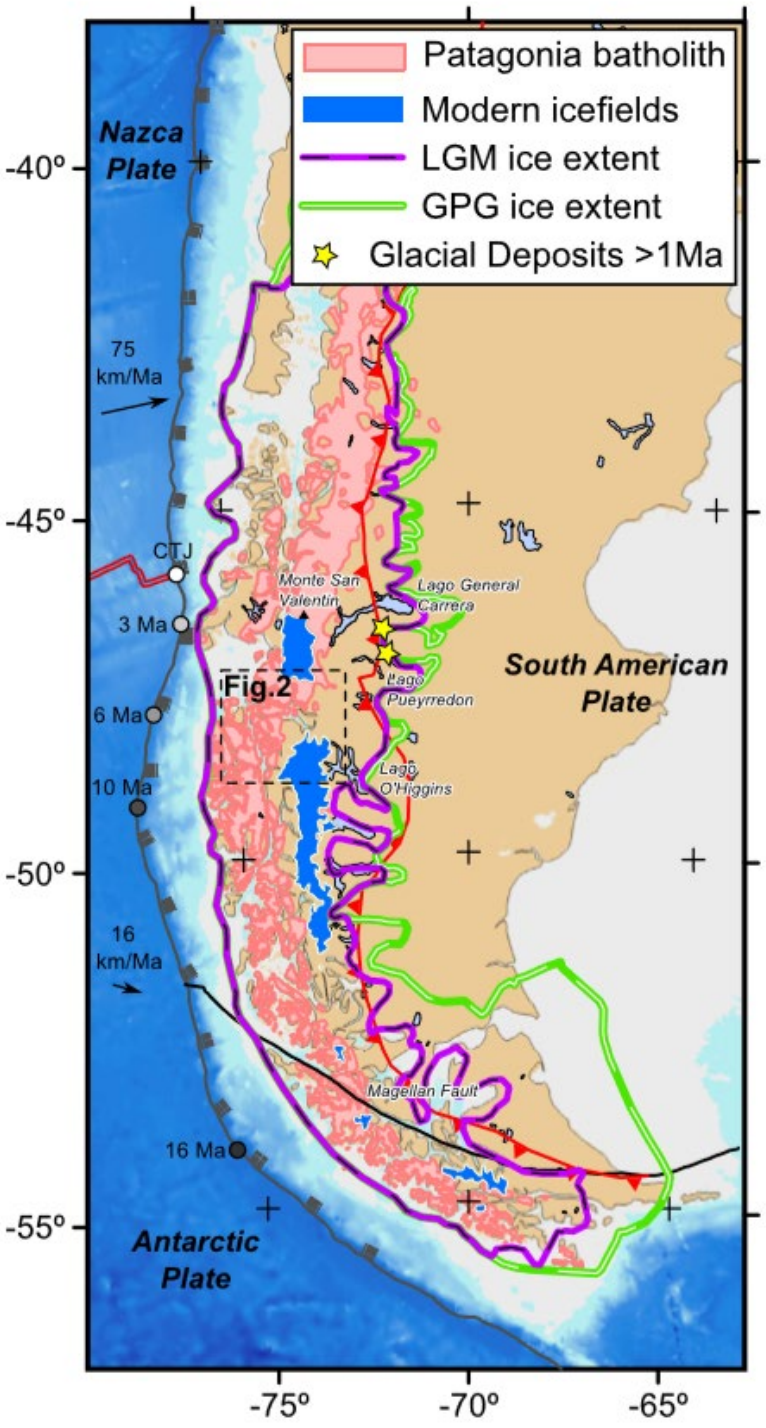

Figure 1.7. Map of the Patagonian Andes, showing the ice extent of late Cenozoic glaciations and the distribution of the Patagonian Batholith (obtained from Christeleit et al., 2017). GPG: Greatest Patagonian Glaciation; LGM: Last Glacial Maximum.

1.5.7 A review of fault zones

Faults are commonly defined as a planar fracture in a volume of rock, across which there has been significant displacement as a result of rock-mass movement. However, faults are more complex than planar features and usually correspond to heterogeneous and anisotropic zones of discontinuity in the crust, characterized by a fault core, and damage zone within relatively undeformed bedrock (e.g. Sibson, 1977; Chester and Logan, 1986; Caine et al., 1996; Figure 1.8). Most of the strain or slip in fault zones is accomodated in the fault core, indicated by fault rocks such as fault breccias, cataclasites and gouge if faults are developed in the brittle regime (upper crust), or mylonites if faults nucleate and develop in the ductile regime (deep crust) (e.g. Sibson, 1977; Caine et al., 1996; Sibson et al., 2003; Figure 1.9). The damage zone comprises a network of subsidiary minor structures bounding the fault core, including small faults, veins and subsidiary fractures (e.g. Chester and Logan, 1986; Caine et al., 1996, 2010, 2017).

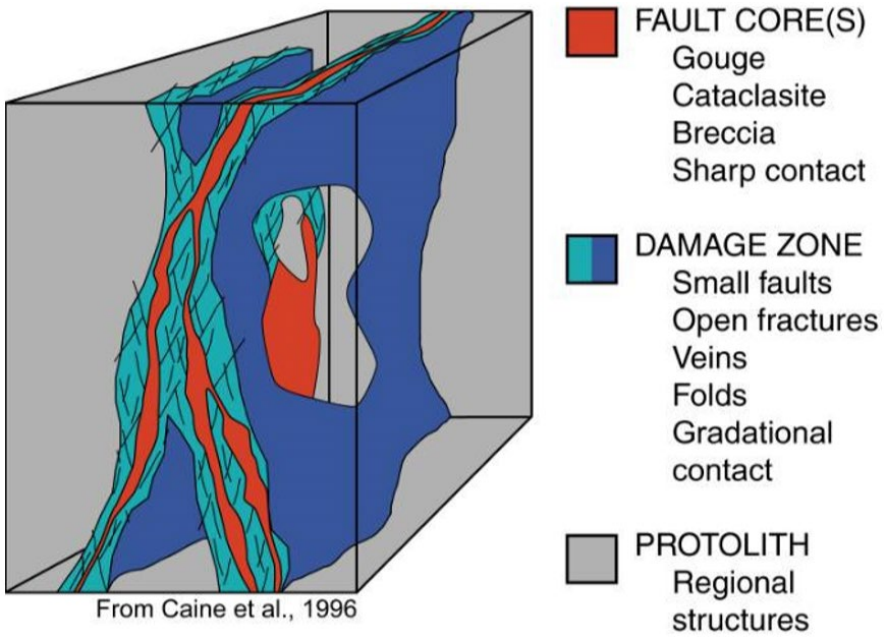

Figure 1.8. Conceptual model of fault zones. Extracted from Caine et al., 1996.

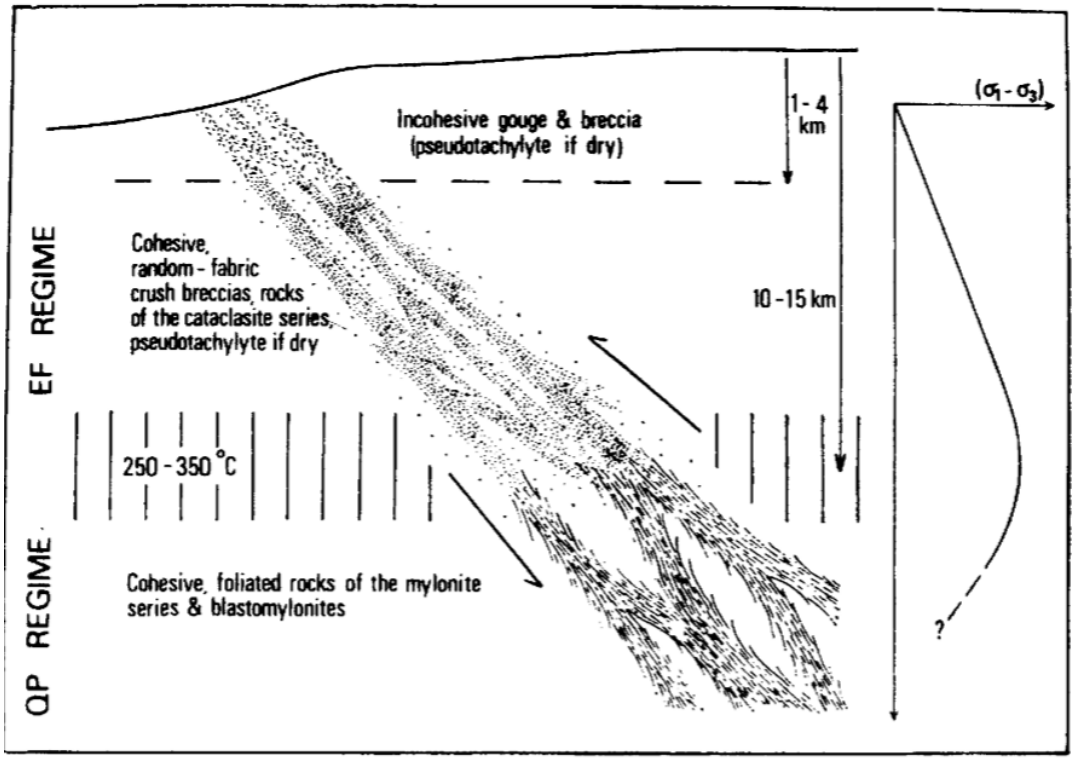

Figure 1.9. Conceptual model of fault zones and fault rocks developed in the elastic-frictional (EF) or brittle regime and quasi-plastic (QP) or ductile regime . Extracted from Sibson (1977).

1.6 Structure of the thesis

This thesis is organized into five (5) different chapters. Chapter 1 presents an introduction with the motivation for this work, the working hypothesis with the main research goals, a general background of the Northern Patagonian Andes geology and a review of fault zones.

Chapter 2 presents the methodology and activities used to achieve the proposed goals of this thesis. It outlines the literature review and desktop data compilation, fieldwork mapping techniques used for fault characterization, structure from motion models derived from Drone photogrammetry and thermocronometric analysis. For more details see methodology section of chapter 3.

Chapters 3 presents the main results of this work, related to newly identified crustal faults, their kinematic analysis and preliminar potential earthquake magnitudes, and geological mapping along the Exploradores Valley with new thermochronological ages.

Chapter 4 present a discussion of the main results presented in Chapter 3, related to style of deformation of new faults reported in this work and their seismogenic potential with the related uncertainties in earthquake magnitudes, the geothermal implications of this new faults and the interpretation of thermochronological ages along the Exploradores Valley.

Chapter 5 presents the main conclusions derived from chapters 3 and 4. It highlights the principal contributions of this thesis and suggest ideas for future work regarding neotectonics of the Northern Patagonian Andes.

2 METHODOLOGY

2.1 Abstract

This chapter presents the methodology and activities used to achieve the proposed research goals described above. This includes desktop data compilation of previous crustal faults, field mapping and outcrop characterization of crustal faults, use of digital 3D models for recent deformation events and thermochronological analysis of intrusive rocks of the Patagonian Batholith.

2.2 Desktop data compilation

The first part of this work consisted of a literature review of the geology of the region, followed by analysis and photointerpretation of satellite images, Google Earth data, Digital Elevation Models and a desktop review and compilation of previous maps of the study area using the ArcGIS 10.0 and Adobe Illustrator 6.0 software's. Digital Elevation Models used were taken from the USGS earth explorer web page and correspond to ASTER Global DEM satellite images of 30-m spatial resolution per pixel. Special emphasis was put in the compilation of tectonic structures in the whole region from existing maps and literature. Thus, a regional geological map was compiled with a detailed selection of the mapped faults, however, any lineaments and inferred faults previously mapped without any field evidence (e.g. photographs) of displacements or presence of fault rocks were excluded from this compilation. Table 2.1 presents the reported faults for the Aysén Region with their respective seismogenic parameters as derived from the literature.

2.2.1 Known crustal faults in the Aysén Region

In Table 2.1 a list of existing faults in the Aysén Region with their seismogenic parameters region is presented. Fault coordinates which have no outcrop or specific location where obtained from the maps which show those faults (see references in table).

Table 2.1. Compilation of data on known or suspected faults in the Aysén Region and related seismogenic parameters.

Fault Name	N (m)*	E (m)*	Style	Length (km)	Dip (°)	Seismogentic thickness (km)	Surface Width (Fault Zone – m)	Estimated Mw	Relevant Study
Rio Cuervo	4975422	653180	Dextral	30-40	60-90	?	313 - 852	7,1	Vargas et al. 2013; Villalobos 2017
Punta Cola	4972832	656374	Dextral-Reverse	15-20	80	?	242 - 1000	6,2	Vargas et al. 2013; Villalobos 2017
Los Palos	4979036	679416	Dextral	10-15	50-80	?	250 - 300	6,2	Vargas et al. 2013
Quitralco	4975422	653180	Dextral	15	75-85	?	?	6,2	Vargas et al. 2013; Villalobos 2017
Exploradores	4845378	655615	Reverse	~ 15	60-80	?	10 - 15	?	Georgieva et al. 2016
Cachet	4762482	632522	Dextral	~ 60	60-90	?	?	?	Georgieva et al. 2016
El Saltón	4734576	648547	Normal	~ 20	50-80	?	?	?	Georgieva et al. 2016
Rio Mañihuales (Riesco)	4943112	665636	Dextral-Reverse	~ 30	50-80	?	?	7,1	Thomson 2002; Vargas et al. 2013
Azul-Tigre (Queulat shear zone)	4999360	691310	Dextral-Reverse	15-200?	?	?	?	?	Thomson 2002; Cembrano et al. 2002
Main LOFZ	41°-47°S		Dextral-Reverse	200-1200	Vertical	?	?	?	Vargas et al., 2013

***: Coordinates in UTM (WGS84).**

?: Not reported by the author.

2.3 *Field mapping and outcrop characterization*

Fieldwork consisted of field mapping, desktop mapping validation, with emphasis on structural, bedrock, and Quaternary geology of the study area. Standard techniques of field mapping were applied, including rock type characterization, structural measurements and photographs of the studied outcrops and geomorphological observations that could suggest any recent tectonic deformation. Structural data was treated using the FaultKin7 software.

Due to the ongoing construction of the Carretera Austral (or Austral Highway), there are numerous fresh road cuts that allow observation and characterization of new outcrops and structures. By 4x4, we screened every road outcrop of the Carretera Austral from Puyuhuapi to Puerto Río Tranquilo (Figure 1.1) for faults and documented them using standard field techniques (strike and dip, fault rock characterization, etc) where they were present. Because there are not road cuts throughout the whole region, certainly there are other faults within the study area, even along the areas we worked that were not documented because of limited access and outcrops.

2.4 Structure from Motion (SfM) and geomorphic models

In order to develop 3D models of some faults, thousands of photographs were taken during both fieldtrips using a DJI Phantom 4 Quadcopter (i.e. Unmanned Aerial Vehicle (UAV) or Drone), with the purpose of building Structure from Motion models to better quantify fault parameters (e.g. Johnson et al., 2014). These photographs were loaded into photogrammetric processing software (Agisoft Standard Photoscan Pro 1.3.2). This software first aligns all the photos finding matching points between overlapping images, and then builds a sparse point cloud model, where each point represents a common pixel identified between images. Based on the estimated camera position, the software calculates depth

information for each photo to be combined into a single dense point cloud. After dense point cloud has been built it is possible to generate polygonal mesh model based on the dense cloud data, obtaining the final 3D model. This helps to better constrain fault parameters such as strike and dip of the fault plane, vertical throw of the fault, length of the fault, etc. Although these parameters can also be obtained in the field, the high resolution of the model combined with 3D structural modeling software's allows us to measure these parameters very precisely to characterize the faults and tectonic geomorphology.

2.5 Apatite (U-Th)/He Thermochronometry

The Apatite (U-Th)/He system corresponds to a low-temperature (< 70ºC) thermochronometer based on the accumulation of 4He isotope inside the apatite crystal as a product of U and Th alpha-decay. This accumulation occurs only at temperatures below 70-75ºC (e.g., Ehlers et al., 2003; Shuster et al. 2006). At higher temperatures, He is removed by diffusion as fast as it is produced by radiogenic decay. As bedrock moves upward through the upper crust, it cools below the closure temperature and thus starts accumulating He, providing time information on the cooling and exhumation history of the bedrock knowing the geothermal gradient of the crust. Therefore, thermochronology has been widely used to estimate average exhumation rates, as represented by the time-of-flight from the closure depth to the topographic surface (e.g. McPhillips et al., 2010). Another conventional method is the age-elevation-relationship method, used to estimate the rate that bedrock moves upward towards the surface. For example, consider a scenario with a closure depth of 2 km below the topographic surface and AHe age of 4 Ma. This means that the bedrock sample moved upward 2 km from 4 to 0 Ma, which gives an average exhumation rate of 0.5 km/Ma.

2.5.1 Sample Preparation

Eight new samples were collected in the field along an east-west transect in the Exploradores Valley and Bay for apatite thermochronological analysis. Apatite mineral grains were separated in the Mineral Separation Laboratory of the Department of Geology at Universidad de Chile. First, the rock samples were crushed with a "tooth-shape" iron crusher and run through a disc pulverizer until it was a very fined grained rock powder. This powder was then sieved using a 0.5 mm grid, obtaining a first sample concentrate. Second, the sample concentrate passed through the "Gemini" shacking mineral separation table, where a heavy mineral concentrate was obtained. Third, this heavy mineral concentrate passed through a Franz magnetic separator from 0 to 1.7 mA by steps of 0.2 mA, obtaining a non-magnetic concentrate. Then, this non-magnetic concentrate passed through two dense liquids with densities of 2.8 (Bromoform) and 3.3 g/cm^3 (Diiodomethane), obtaining a first apatite and heavy-mineral concentrate respectively. Finally, the apatite concentrate were seen under a binocular lense and cleaned for accessory minerals (impurities) by hand-picking with a thin paintbrush, obtaining a final mineral concentrate. Apatite concentrates were stored in plastic vials of 60 ml of capacity and then sent to Dr. Julie Fosdick for U-Th-He analysis to the Basin Analysis & Helium Thermochronology Laboratory (BAHTL) in the University of Connecticut, USA.

3 CHARACTERIZATION OF CRUSTAL FAULTS AND THERMOCHRONOMETRY IN THE AYSÉN REGION, PATAGONIAN ANDES, CHILE

This chapter, entitled "**Characterization of Crustal Faults and Thermochronometry In the Aysén Region, Patagonian Andes, Chile"** corresponds to a manuscript in progress that will be submitted to a peer journal review, and thus has its own abstract, introduction, methodology, results, discussion and conclusions.

3.1 Abstract

The Northern Patagonian Andes constitutes part of one of the most geologically active orogens in the world, with the longest active volcanic chain and the greatest recorded earthquake in history (Mw 9.5 Valdivia 1960 Earthquake). In 2007, a seismic swarm with magnitudes up to Mw 6.2 occurred in the Aysén fiord associated to submarine crustal faults related to the Liquiñe-Ofqui Fault Zone (LOFZ), triggering earthquakes and landslides that induced a tsunami, causing 12 deaths. However, very little is known about the active tectonic framework, and relation with these fault and regional geothermal systems and the potential seismogenic crustal structures in the Aysén Region, mainly due to dense vegetation and widespread Quaternary volcanic and glacial cover. Using conventional fieldwork mapping methods, combined with remote sensing using satellite data and Structure from Motion (SfM) models, we document and characterize six previously un-identified crustal faults near the LOFZ in Aysén. Based on geomorphological observations and fault rock characteristics, such as deflected rivers and uncemented cataclasite, fault breccia and gouge, it is proposed that these faults are potentially active, and thus crustal sources of coseismic hazard for the region, which based on scaling relations are capable of generating earthquakes of magnitudes up to Mw 6.0-7.0. In addition, these faults would accommodate upper crustal

deformation during late Cenozoic evolution of the Patagonian Andes. Further work here will allow a better understanding and characterization of these faults, however these should be included in local and regional seismic hazard and fault rupture models.

3.2 Introduction

Conventional seismic hazard analysis is based primarily on earthquake frequency obtained from historical catalogues of seismicity (e.g. Allen et al., 1965; Wesnousky et al., 1984, 1986; Dimaté et al., 1999; Zamudio et al., 2005), but the uncertainty in such analyses is large when the historical and instrumental records of earthquake recurrence is too short to define seismic rates (Allen et al., 1965; Allen, 1975; Anderson, 1979; Wesnousky et al, 1984, 1986). In contrast to seismic catalogues, the geological identification of Quaternary active faults are used to reduce these uncertainties, as moderate to large earthquakes occur when crustal faults rupture, and faults that deform Quaternary deposits are now commonly accepted as sources of seismic hazard (Allen et al., 1965, 1975; Matsuda, 1977; Anderson, 1979; Wesnousky, 1986 and references therein) Therefore, detailed mapping and field characterization of active faults constitutes a first order input for accurate geohazard assessment, including strong ground motions, fault ruptures and potential earthquake effects (landslides, lateral spreading, and liquefaction), especially in regions where seismological record is short and poorly constrained. In addition, the geometry and architecture of upper crustal faults and their damage zones enhances rock permeability and controls the pathways for heat and hydrothermal fluid flow of geothermal systems in the upper crust (e.g. Sibson, 1994, 1996; Cox, 1999; Zhang et al., 2008; Sanchez et al., 2013; Perez-Flores et al., 2016). The Northern Patagonian Andes has abundant thermal springs which show potential for geothermal energy, so understanding fault networks and where potential seismic sources are located in this region is critical prior to exploration or development of these geothermal fields, in addition to better characterization of the seismic hazard.

The Northern Patagonian Andes are part of the longest active mountain chain on Earth, characterized by a continuous orogenic belt that extends for more than 7.000 km in length and up to 500 km in width (e.g. Dewey and Bird, 1970). This area comprises the Chile Triple Junction, where the Nazca, Antarctica and South American plates join and an active oceanic ridge collides with the South American continent (e.g. Miller et al., 2005) (Figure 3.1). The most prominent feature of the Northern Patagonian Andes is the Liquiñe-Ofqui Fault Zone (LOFZ), a 1,200 km long intra-arc fault system that accommodates oblique subduction between Nazca and South American plates (Beck, 1993; Hervé and Ota, 1993; Hervé, 1994; Cembrano et al., 1996, 2002; Arancibia et al., 1999; Lavenu and Cembrano, 1999, 2009; Georgieva et al., 2016, Catalán et al., 2017) (Figure 3.1). The LOFZ coincides spatially the Southern Volcanic Zone, and active volcanic arc that extends for more than 1,000 km in the Southern Andes, where location and geochemistry of main stratovolcanoes and minor monogenetic cones are controlled primarily by crustal thickness and the presence of active tectonic structures (e.g. López-Escobar et al., 1995; Stern, 2004; Cembrano and Lara, 2009; Vargas et al., 2013). In addition, the LOFZ is one of the most important seismogenic sources in the Aysén Region (Perucca et al., 2007), where earthquakes up to Mw 6.2 have occurred (Lange et al., 2008; Legrand et al., 2011; Russo et al., 2011; Vargas et al., 2013; Cisternas et al., 2017), including big landslides (Sepulveda et al., 2010) and the greatest instrumentally recorded earthquake in the Earth (1960 Valdivia earthquake; e.g. Cifuentes, 1989; Dzierma et al., 2012; Cisternas et al., 2017). Also, some authors based on thermochronological studies suggested the key role that the LOFZ plays in the Cenozoic exhumation of the Patagonian Andes (e.g. Cembrano et al., 1996, 2002; Thomson, 2002; Georgieva et al., 2016).

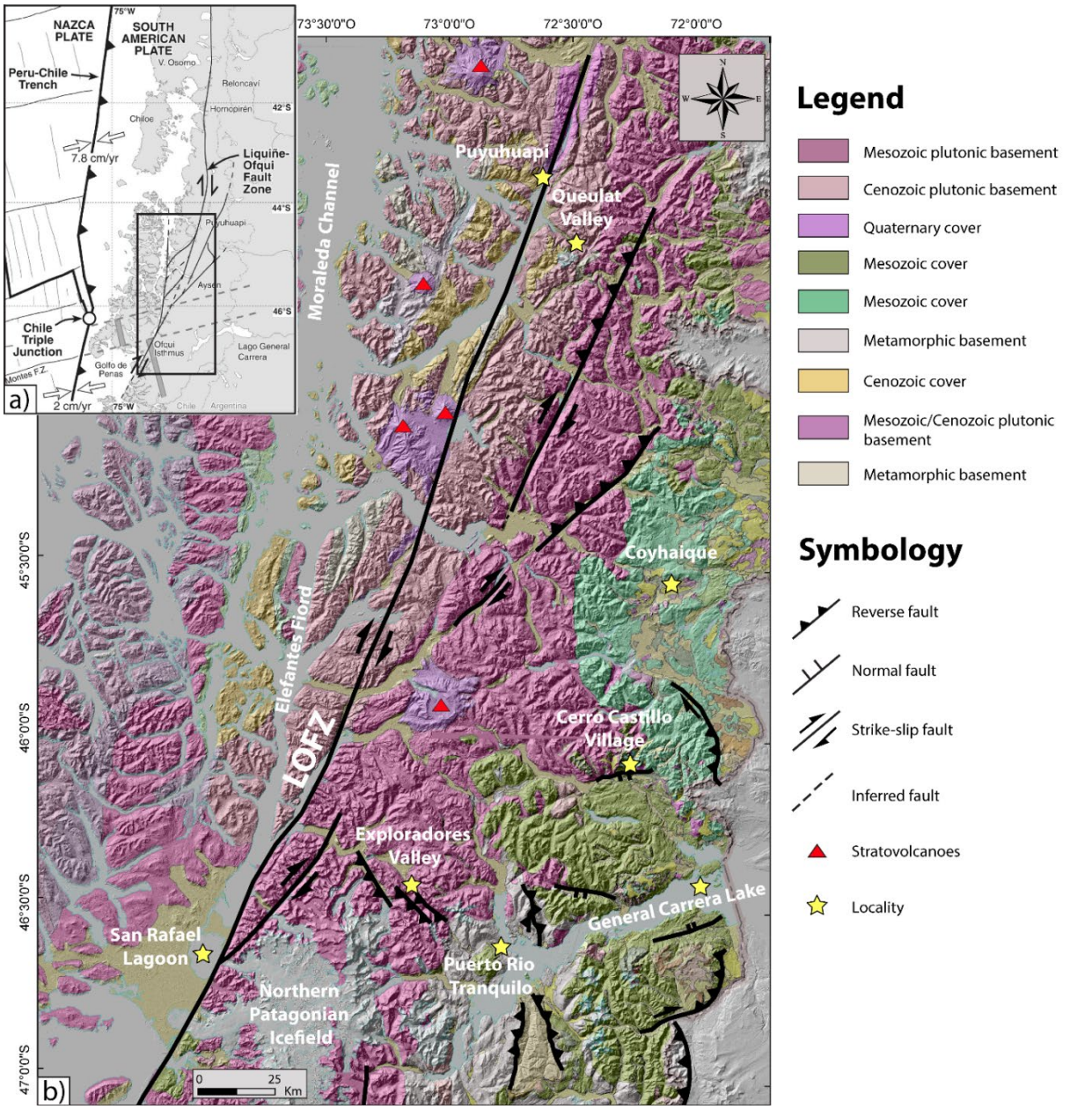

Figure 3.1. a) Tectonic map of the Southeast Pacific showing tectonic plate configuration of the Southern Andes continental margin. Black square shows area of figure b). b) Regional Map of the Aysén Region showing the main geological units and tectonic structures. Compiled from Thomson (2002), Sernageomin (2002), Cembrano and Lara (2009), Scalabrino et al. (2010), Vargas et al. (2013) and Georgieva et al. (2016).

However, little is known about the active tectonic framework and the potential seismogenic crustal structures in this region of the Andes, mainly due to poor weather conditions, dense vegetation and wide quaternary volcanic and glacial cover. Moreover, the geology and fault characterization in this region are currently mapped at scales that are of limited use for neotectonic investigations (e.g. 1:1,000,000 scale map of "Servicio Nacional de Geología y Minería" (Sernageomin, 2002), although with localized mapping at scales of 1:50,000 (e.g. Puyuhuapi), which provides limited insight to the regional active structures and to the local, regional and fault rupture models.

Here we investigate and document previously un-identified crustal faults in the Aysén Region found during field mapping and remote sensing investigations that suppose potential sources of seismic hazard and accommodate crustal deformation in this region of the Patagonian Andes. Using conventional fieldwork methods, combined with remote sensing using satellite data and Structure from Motion models, we characterize these previously undocumented structures and discuss their potential seismic hazard in order to get a better understanding of the seismotectonic framework in the region.

3.3 Methodology

This research combines a number of different methods from desktop work and remote sensing to conventional field mapping and outcrop characterization.

3.3.1 Desktop work

The first part of this work consisted of a literature review of the geology of the region, followed by analysis and photointerpretation of satellite images, Google Earth data, Digital Elevation Models and a desktop review and compilation of previous maps of the study area using the ArcGIS 10.0 and Adobe Illustrator 6.0 software's. Digital Elevation Models used

were taken from the USGS earth explorer web page and correspond to ASTER Global DEM satellite images of 30-m spatial resolution per pixel. Special emphasis was put in the compilation of tectonic structures in the whole region from existing maps and literature. Thus, a regional geological map was compiled with a detailed selection of the mapped faults (Figure 3.1); however, any lineament or inferred faults previously mapped without any field evidence (e.g. photographs) of displacements or presence of fault rocks were excluded from this compilation. Table 1.1 presents the reported faults for the Aysén Region with their respective seismogenic parameters as derived from the literature.

3.3.1.1 Known crustal faults in the Aysén Region

In Table 3.1 a list of existing faults in the Aysén Region with their seismogenic parameters is presented. Fault coordinates which have no outcrop or specific location were obtained from the maps which show those faults (see references in table).

Table 3.1. Compilation of data on known or suspected faults in the Aysén Region and related seismogenic parameters.

Fault Name	N (m)*	E (m)*	Style	Length (km)	Dip (degrees)	Seismogentic thickness (km)	Surface Width (Fault Zone – m)	Estimated Mw	Relevant Study
Rio Cuervo	4975422	653180	Dextral	30-40	60-90	?	313 - 852	7,1	Vargas et al. 2013; Villalobos 2017
Punta Cola	4972832	656374	Dextral-Reverse	15-20	80	?	242 - 1000	6,2	Vargas et al. 2013; Villalobos 2017
Los Palos	4979036	679416	Dextral	10-15	50-80	?	250 - 300 m	6,2	Vargas et al. 2013
Quitralco	4975422	653180	Dextral	15	75-85	?	?	6,2	Vargas et al. 2013; Villalobos 2017
Exploradores	4845378	655615	Reverse	~ 15	60-80	?	10 - 15		Georgieva et al. 2016
Cachet	4762482	632522	Dextral	~ 60	60-90	?	?	?	Georgieva et al. 2016
El Saltón	4734576	648547	Normal	~ 20	?	?	?	?	Georgieva et al. 2016
Rio Mañihuales (Riesco)	4943112	665636	Dextral-Reverse	~ 30	50-80	?	?	7,1	Thomson 2002; Vargas et al. 2013
Azul-Tigre (Queulat shear zone)	4999360	691310	Dextral-Reverse	15-200?	?	?	?	?	Thomson 2002; Cembrano et al. 2002

***: Coordinates in UTM (WGS84).**

?: Not reported by the author.

3.3.2 Remote sensing, field mapping and outcrop characterization

Fieldwork consisted of field mapping, desktop mapping validation, with emphasis on structural, bedrock, and Quaternary geology of the study area. Standard techniques of field mapping were applied, including rock type characterization, structural measurements, photographs of the studied outcrops and geomorphological observations that could suggest any recent tectonic deformation. Remote sensing and satellite imagery based on Google

Earth and digital elevation models of 12.5m-resolution, extracted from the Alos Palsar satellite were both used a base maps for remote mapping. Conventional field mapping was also carried along the Exploradores Valley, with emphasis in structural data, petrographic characterization and geomorphic mapping.

Due to the ongoing construction of the Carretera Austral (or Austral Highway), there are numerous fresh road cuts that allow observation and characterization of new outcrops and structures. By 4x4, we screened every road outcrop of the Carretera Austral from Puyuhuapi to Puerto Río Tranquilo (Figure 3.1; Figure 3.2) for faults and documented them using standard field techniques (strike and dip, fault rock characterization, etc.) where they were present. Because there are not road cuts throughout the whole region, certainly there are other faults within the study area, even along the areas we worked that were not documented because of limited access and outcrops.

3.3.3 Structure from Motion (SfM) and geomorphic models

In order to develop 3D models of some faults, thousands of photographs were taken during both fieldtrips using a DJI Phantom 4 Quadcopter (i.e. Unmanned Aerial Vehicle (UAV) or Drone), with the purpose of building Structure from Motion models to better quantify fault parameters (e.g. Johnson et al., 2014). These photographs were loaded into photogrammetric processing software (Agisoft Standard Photoscan Pro 1.3.2). This software first aligns all the photos finding matching points between overlapping images, and then builds a sparse point cloud model, where each point represents a common pixel identified between images. Based on the estimated camera position, the software calculates depth information for each photo to be combined into a single dense point cloud. After dense point cloud has been built it is possible to generate polygonal mesh model based on the dense cloud data, obtaining the final 3D model. This helps to better constrain fault parameters such

as strike and dip of the fault plane, vertical throw of the fault, length of the fault, etc. Although these parameters can also be obtained in the field, the high resolution of the model combined with 3D structural modeling software's (Arcgis 10.0 / Move 2015 / Leapfrog), allows us to measure these parameters very precisely to characterize the faults and tectonic geomorphology.

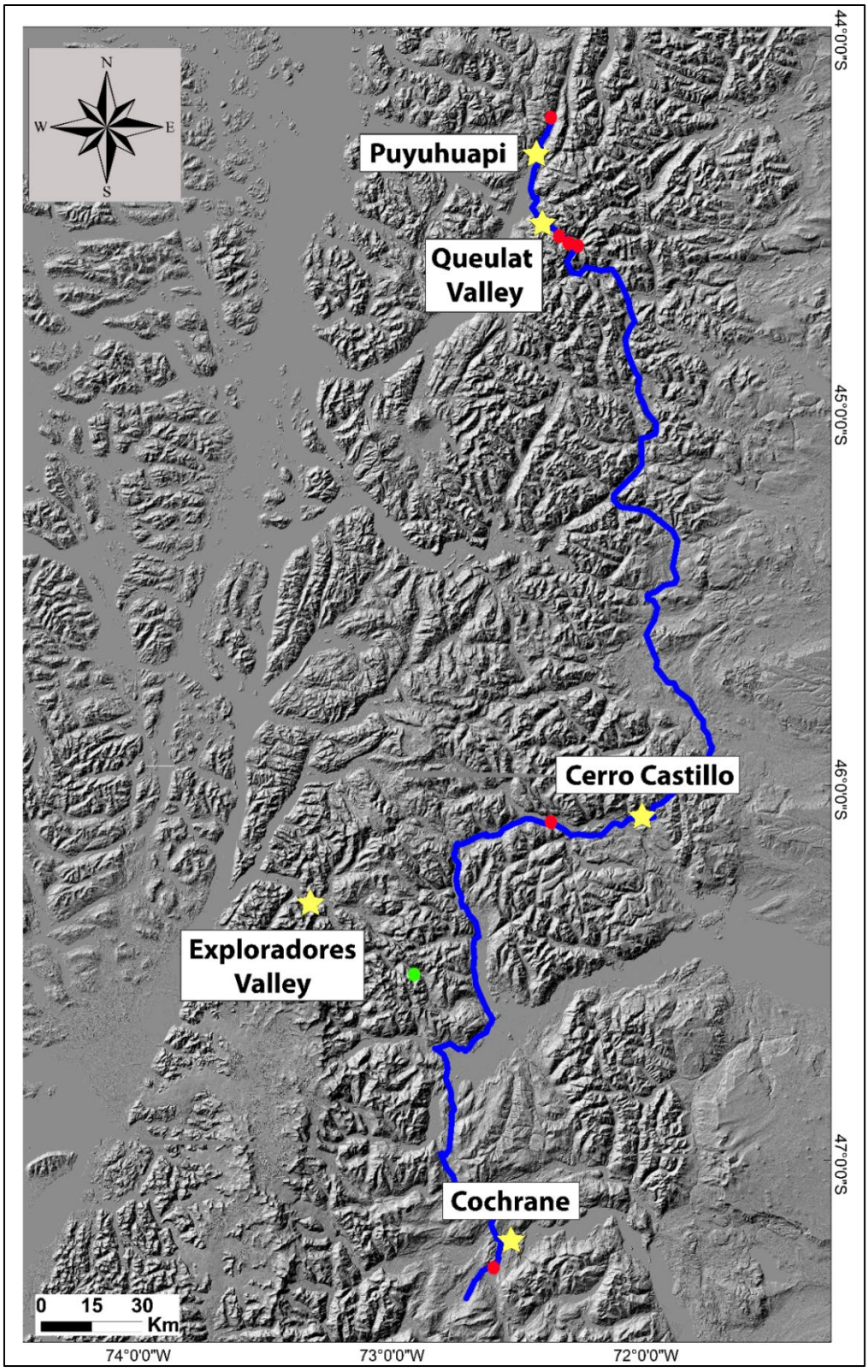

Figure 3.2. Hillshade map of the Aysén Region. The blue line corresponds to the Carretera Austral. The red dots shown correspond to the outcrops of the faults documented in this study. The green dot corresponds to the Exploradores Fault from Georgieva et al. (2016).

3.3.4 Apatite (U-Th)/He Thermochronometry

The Apatite (U-Th)/He system corresponds to a low-temperature (< 70ºC) thermochronometer based on the accumulation of 4He isotope inside the apatite crystal as a product of U and Th alpha-decay. This accumulation occurs only at temperatures below 70-75ºC (e.g., Ehlers et al., 2003; Shuster et al. 2006). At higher temperatures, He is removed by diffusion as fast as it is produced by radiogenic decay. As bedrock moves upward through the upper crust, it cools below the closure temperature and thus starts accumulating He, providing time information on the cooling and exhumation history of the bedrock knowing the geothermal gradient of the crust. Therefore, thermochronology has been widely used to estimate average exhumation rates, as represented by the time-of-flight from the closure depth to the topographic surface (e.g. McPhillips et al., 2010). Another conventional method is the age-elevation-relationship method, used to estimate the rate that bedrock moves upward towards the surface. For example, consider a scenario with a closure depth of 2 km below the topographic surface and AHe age of 4 Ma. This means that the bedrock sample moved upward 2 km from 4 to 0 Ma, which gives an average exhumation rate of 0.5 km/Ma. Samples were all collected along the Exploradores Valley outcrops, with a mean elevation of 20 m above sea level and all sample locations were photographed in the field with location noted with a GPS and on the field map. Sample locations are shown in Figure 4.3 and Table 4.1.

3.3.4.1 Sample Preparation and Analysis

Apatite mineral grains were separated from eight samples collected in the field along an east-west transect along the Exploradores Valley. Mineral Separation was done in the Mineral Separation Laboratory of the Department of Geology at Universidad de Chile. First, the rock samples were crushed with a “tooth-shape” iron crusher and run through a disc

pulverizer until it was a very fined grained rock powder. This powder was then sieved using a 0.5 mm grid, obtaining a first sample concentrate. Second, the sample concentrate passed through the "Gemini" shaking mineral separation table, where a heavy mineral concentrate was obtained. Third, this heavy mineral concentrate passed through a Franz magnetic separator from 0 to 1.7 mA by steps of 0.2 mA, obtaining a non-magnetic concentrate. Then, this non-magnetic concentrate passed through two dense liquids with densities of 2.8 (Bromoform) and 3.3 g/cm^3 (Diiodomethane), obtaining a first apatite and heavy-mineral concentrate respectively. Finally, the apatite concentrate were seen under a binocular lense and cleaned for accessory minerals (impurities) by hand-picking with a thin paintbrush, obtaining a final mineral concentrate. Apatite concentrates were stored in plastic vials of 60 ml of capacity and then sent to Dr. Julie Fosdick for U-Th-He analysis to the Basin Analysis & Helium Thermochronology Laboratory (BAHTL) in the University of Connecticut, USA.

The BATHL houses analytical instrumentation and sample preparation facilities to support research in (U-Th)/He thermochronology, including crystal preparation and imaging facilities using a Leica 165C high resolution stereomicroscope and a Leica MC170 HD Camera, a dedicated helium gas extraction and measurement line composed of a Santa Cruz Laser Microfurnace helium gas extraction and measurement system for Helium isotopes, a mineral dissolution lab, and a Thermo Scientific iCAP quadrupole ICPMS for U, Th and Sm parent isotope measurements.

3.4 Results

3.4.1 Newly identified crustal faults in the Aysén Region

New mapping has identified six previously undocumented faults along the Carretera Austral within the Aysén Region, located from north to south near Puyuhuapi, the Queulat Valley and the vicinities of Cerro Castillo and Cochrane (Figure 3.2). In addition, a

previously documented fault in the Exploradores Valley (i.e. Exploradores Fault; Georgieva et al., 2016) is better constrained using Structure from Motion 3D models. In this section I describe these previously unmapped faults, documenting their location, orientation, fault rock characteristics and their relation with local geomorphology and/or sediment stratigraphy. Orientation of structures are given as azimuth and dip with direction (e.g. 070/82ºW) with respect to the north. See Appendix II for more photographs of faults described below.

One of the main goals of this work was to find and evaluate the main LOFZ in the Aysén Region, but we did not find any evidence for it in the field, probably because it is buried by young volcanic and glacial deposits or because it is underwater in lakes and fiords.

3.4.1.1 Risopatrón Fault

3.4.1.1.1 Structural observations

The Risopatrón Fault (RF) is an east-west (E-W) striking fault located along the Western side of the Lake Risopatrón, 10 km north of the Puyuhuapi town along the Carretera Austral (Figure 3.2; Figure 3.3). It is a 100-m wide (north-south) south-verging fault zone where that cuts through intrusive rocks of the Patagonian Batholith. It is characterized by a fault core of 50-m wide characterized by fault breccias, cataclasites and several gouge layers, surrounded by highly sheared and fractured damaged bedrock (Figure 3.4). Fracture and joint intensity increase and grain size reduces notably towards the main fault plane. Slickensides indicate a dip-slip motion with a small left-lateral component.

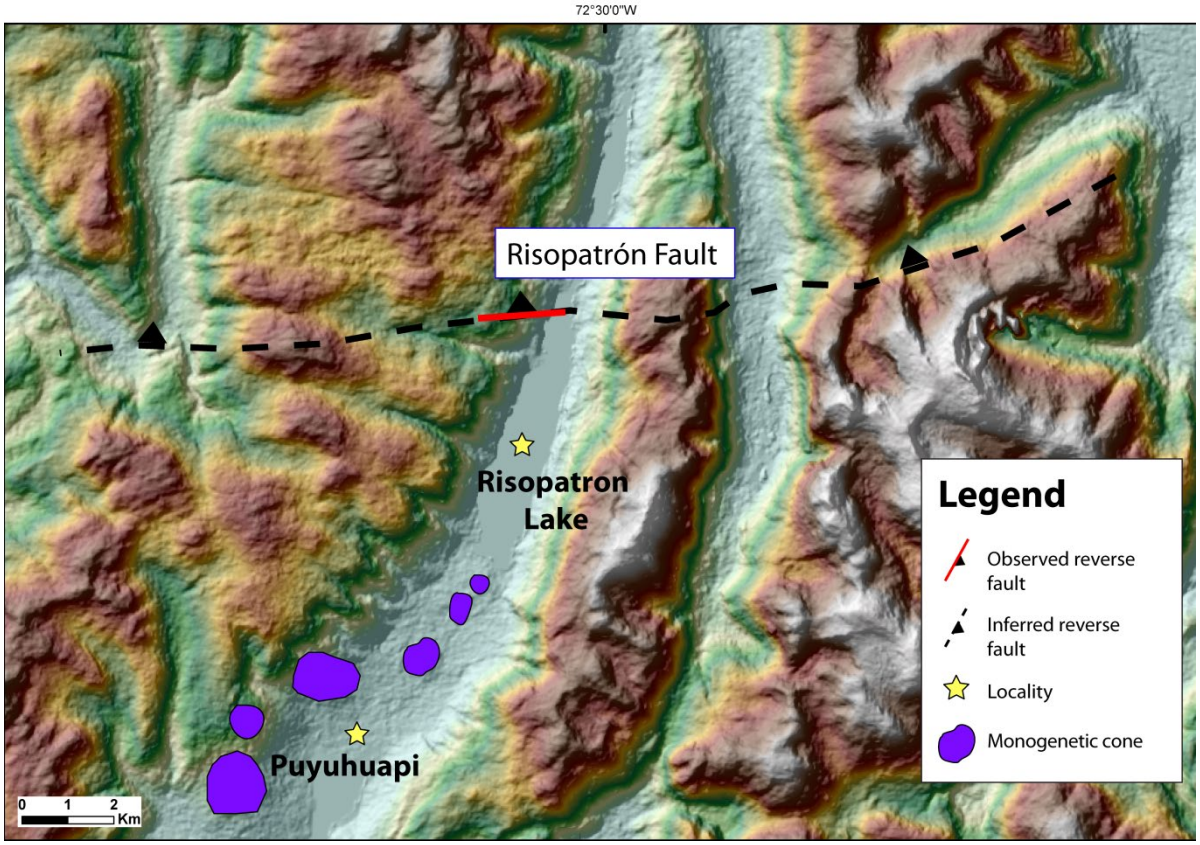

Figure 3.3. Simplified geological map showing the Risopatrón Fault trace north of Puyuhuapi.

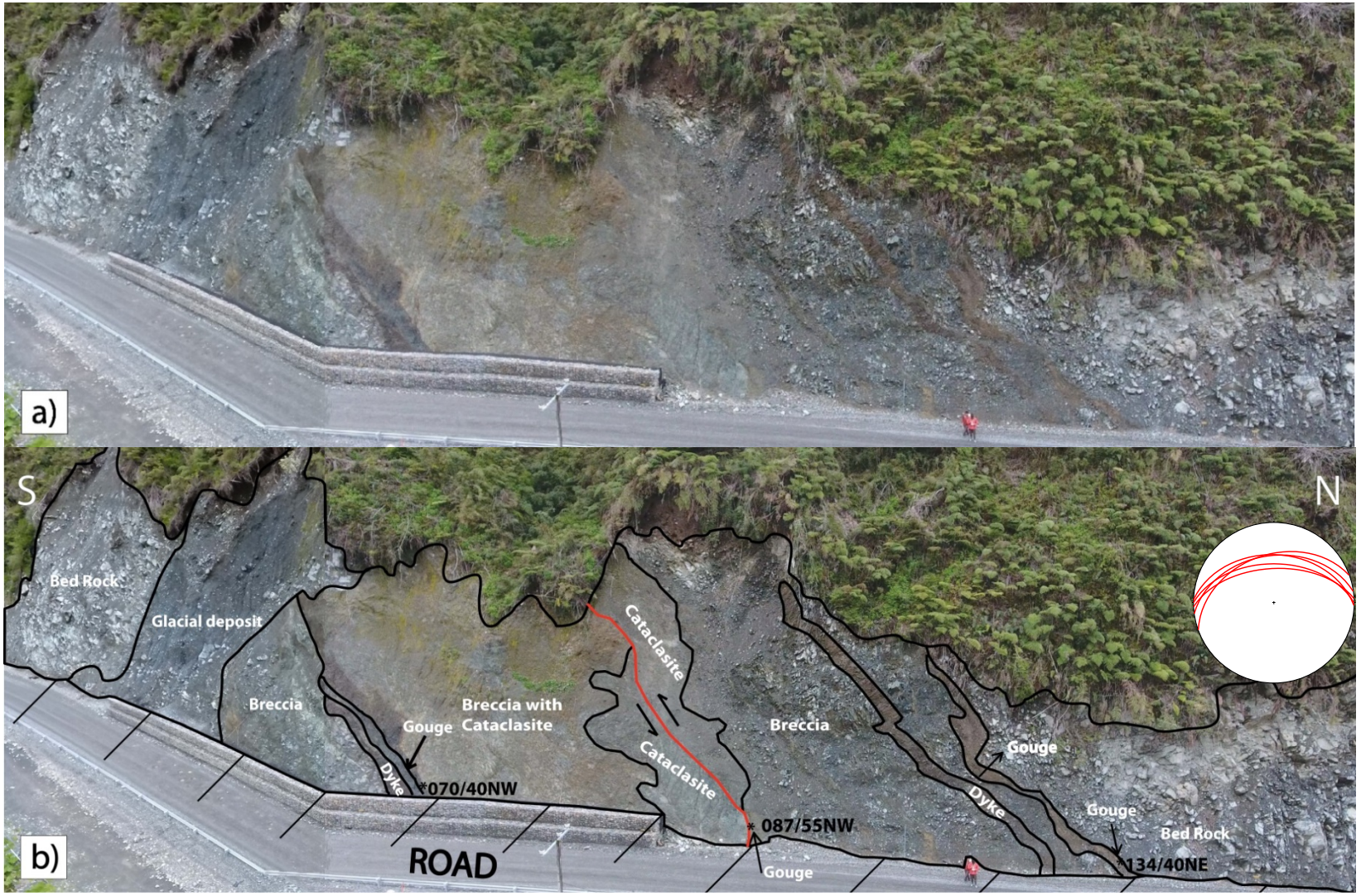

Figure 3.4. a) Stiched figure that combines oblique photographs taken by drone of the Risopatrón Fault and b) interpretation of the Risopatrón Fault. Main fault plane is shown in red. Note the person at the right bottom for scale. Stereonet shows the orientation of the main fault plane (n = 5).

The fault core is characterized by a main gouge zone composed of a 4-6 cm thick grey gouge layer of with an orientation of 090/40ºN, overlain by a 1-2 cm thick brown gouge layer with an orientation of 087/55ºN (Figure 3.5). Below the main gouge zone (within the footwall), the fault core is characterized by 50-m wide highly sheared fault rocks composed of foliated cataclasites, fault breccias and secondary gouge layers with a main azimuth of 070-080 dipping between 40 and 60º to the NW (Figure 3.4)

Fault breccia and cataclasites are yellow-green in color, with angular fragments with sizes ranging between 1 mm to 6 cm. Right below the main fault plane represented by the main gouge zone, the fault rocks consist of grey-greenish foliated cataclasites with angular fragments with sizes ranging from 5 to 15 mm with calcium carbonate cement. An angular block of 30 cm wide remaining as a lens within the fault core is overlain by a greenish gouge layer of 1 cm thick, in turn overlain by a matrix-supported fault breccia, with 15-20% of fragments of 5-10 cm in size that grades into a breccia with 60% of fragments with sizes between 0.5 and 1.5 cm. Towards the south, the fault core grades into green-yellowish, highly sheared fault breccias and cataclasites with several splayed patterns of yellow and brown clayish fault-gouge horizons of 1-10 mm wide, forming an anastomosing pattern with a main azimuth shear orientation of 044 dipping 35-60º to the NW. Fragments are totally angular and sizes range between 0.5 and 2 cm in diameter, conforming almost the total rock volume (< 90% of fragments) disposed in a fine-grained matrix. Occasional lens-shaped intact blocks up to 50-cm long are surrounded by thin (< 1-cm) gouge zones. To the south, the fault core is bounded by a wedge-shaped blueish gouge layer of 5-15 cm thick with a main orientation of 070/40ºNW. It is characterized by 15% of fragments with sizes ranging between 0.5 and 1.5 cm long within a clayish, highly plastic matrix. The contact between the damage zone and the footwall bedrock is unclear, where a fault breccia is cut by unconsolidated glacial deposits, with subangular and rounded plutonic and volcanic

fragments with sizes ranging from 2 cm to 1.5 m in diameter that compose almost a 30% of the volume of the deposit, within a fine-grained sandy matrix with high presence of clay.

To the north (hanging wall), the damage zone is less intense but also highly deformed, characterized by brown, matrix-supported fault breccia with black, angular fragments with sizes between 1 and 8 cm in a fine sand matrix. Fragments size get larger moving away from the main gouge zone, with sizes up to 60-cm wide. Two slightly sinuous brown gouge horizons of 1-cm wide are parallel to the main orientation of the fault, surrounded by cataclasites on both sides that grades into fault breccias. One brown dyke of 1-m wide is notably folded and deformed parallel to the main orientation of the fault zone (088/55ºN) (Figure 3.4). The contact between the fault breccia and the bedrock is diffuse with no clear planes.

The footwall bedrock corresponds to white, crystalline, foliated massive rocks, highly jointed and fractured. The most predominant joint set has an orientation of 035/75ºNW. In the hanging wall, the bedrock corresponds to intrusive rocks, conforming intact angular blocks of 1-2 m size with presence of epidote and calcite filled joints (115/83ºNE).

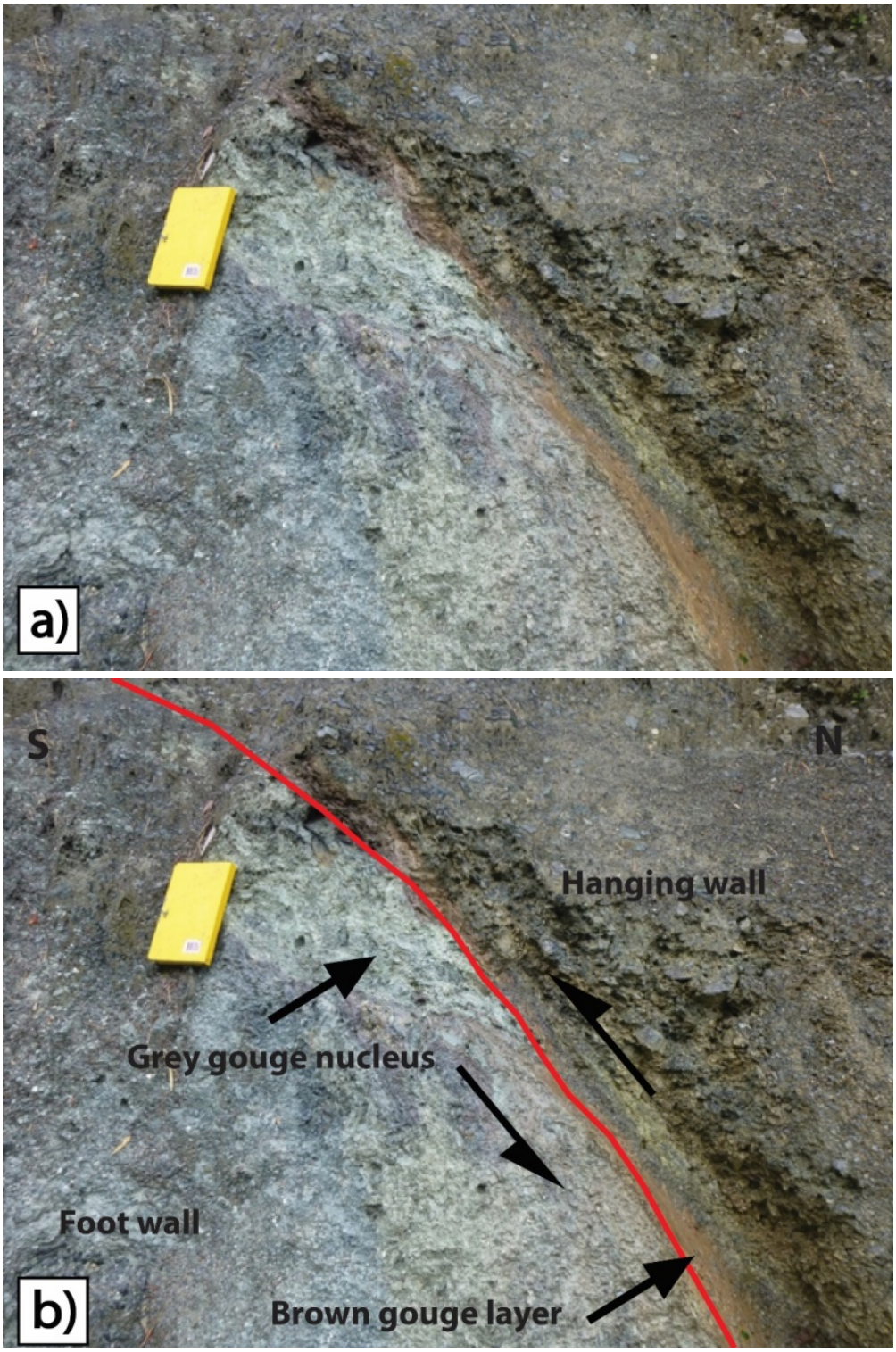

Figure 3.5. a) Field photograph of the Risopatrón fault plane. b) Interpretation of the photo in a, showing two different gouge layers (grey and brown) and the main fault plane in red. Note the fieldbook for scale.

3.4.1.1.2 Geomorphic and/or stratigraphic observations

The Risopatrón Fault trace coincides with a marked gully on the eastern side of the Risopatrón Lake aligned with the fault strike. From Google Earth, the fault trace is clearly seen as a lineament and can be mapped for at least 10 km. Likely, there may be Quaternary offsets here, but dense vegetation and steep slopes inhibited observations in addition to most of the fault being submarine under Risopatrón Lake.

3.4.1.2 Queulat Fault

3.4.1.2.1 Structural observations

The Queulat Fault (QF) is an ENE-WSW striking fault located at the southern flank of the Queulat Valley, 23 km to the southeast of the Puyuhuapi town along the Carretera Austral (Figure 3.2; Figure 3.6). It is a 3-m wide fault zone cutting intrusive rocks. It is characterized by a fault core composed on the eastern side by a 2-3 mm thick yellowish fault gouge layer (073/82ºSE), and fault breccia with 1 cm diameter angular fragments (Figure 3.7). Towards the west, the breccia turns into a cataclasite with fragments being less than 0.5 cm in diameter. At the western edge of the fault core, there is a 5-7 cm thick, yellowish fault gouge with an orientation of 073/82°SE composed of a clayish matrix with few mineral grains with sizes less than 0.5 mm in diameter (Figure 3.7). On both sides of the fault the bedrock is cut by joints with similar orientation than the main fault plane (074/81ºSE). Subhorizontal slickensides on the eastern fault plane indicate a strike-slip motion.

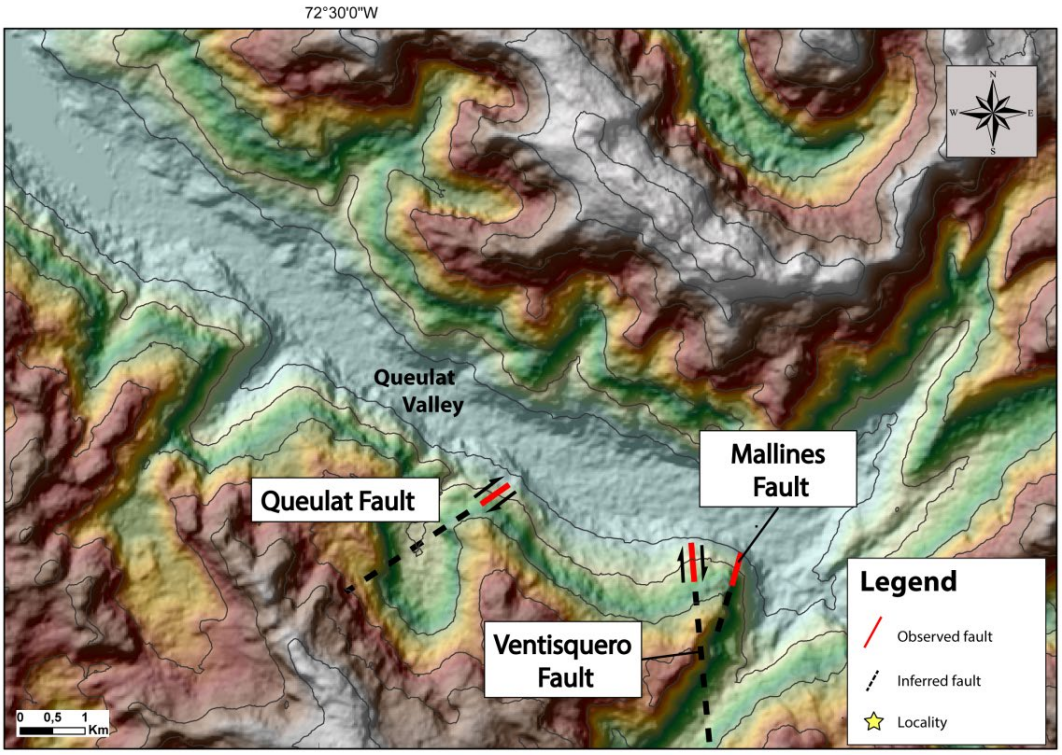

Figure 3.6. Simplified geological map of the Queulat Valley with the Queulat, Ventisquero and Mallines fault traces.

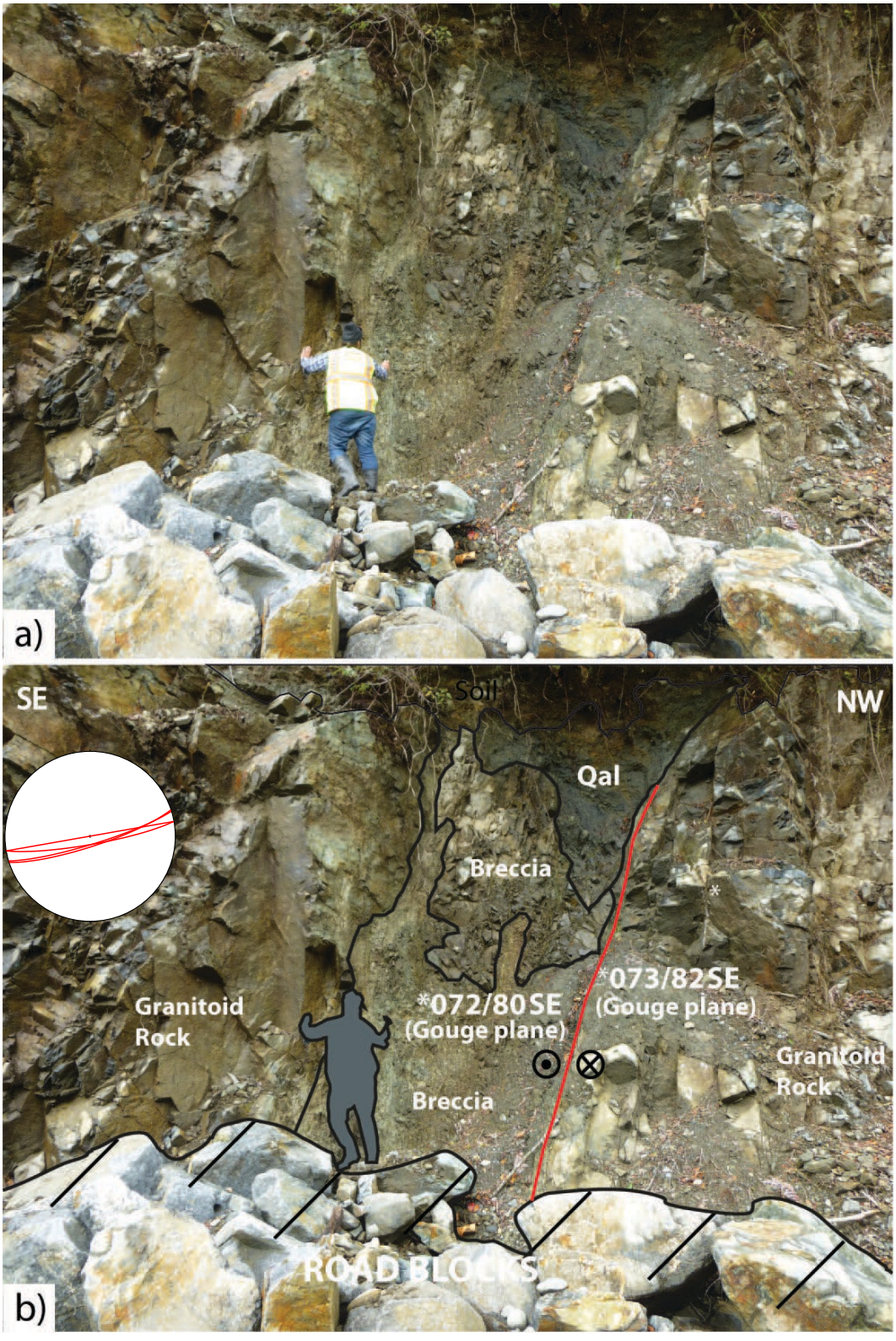

Figure 3.7. a) Oblique field photograph and b) interpretation of the Queulat Fault. B) The red line corresponds to the main fault plane. Note the person for scale. The stereonet shows the orientation of the main fault plane (n = 4).

3.4.1.2.2 Geomorphic and/or stratigraphic observations

To the NW of the fault core of the Queulat Fault, in the soil profile overlying the granitic bedrock, there is a blue-greyish, 20- thick silt layer (Figure 3.8). Towards the fault zone (to the SE) this layer falls into the fault core, conforming a fissure fill (Figure 3.8). The fault trace can be traced from Google Earth for at least 1 km.

Figure 3.8. Field photograph of the Queulat fault looking south. The photo shows a grey silt layer (black lines) falling into the fault zone. The red line corresponds to the Queulat Fault plane. Note person below the fault plane for scale.

3.4.1.3 Ventisquero Fault

3.4.1.3.1 Structural observations

The Ventisquero Fault (VF) is a N-S striking fault located at the southern flank of the upper Queulat Valley, 30 km to the southeast of the Puyuhuapi town along the Carretera Austral (Figure 3.2; Figure 3.9). It is a 1 m-wide fault zone that cuts through intrusive rocks. It has a fault core of 50-cm wide, characterized by a white gouge layer of 1-2 mm thick with a main fault plane of 168/70ºE and a fault breccia with angular fragments of intrusive rocks with sizes ranging from 0.5 to 3 cm. In the southern flank of the Queulat River some grooves (i.e. slickensides) were observed at outcrop scale with a rake of 10º, indicating a strike-slip movement with a minor dip-slip component (Figure 3.9). The main fault plane splays in to two planes with decreasing angles towards the surface, conforming a positive flower geometry (Figure 3.9). Between the two fault planes, there is a Quaternary till composed of rounded boulders with varying sizes (1-50 cm) conforming 15-20% of the total volume deposit within a clay-rich fine-grained matrix (Figure 3.9).

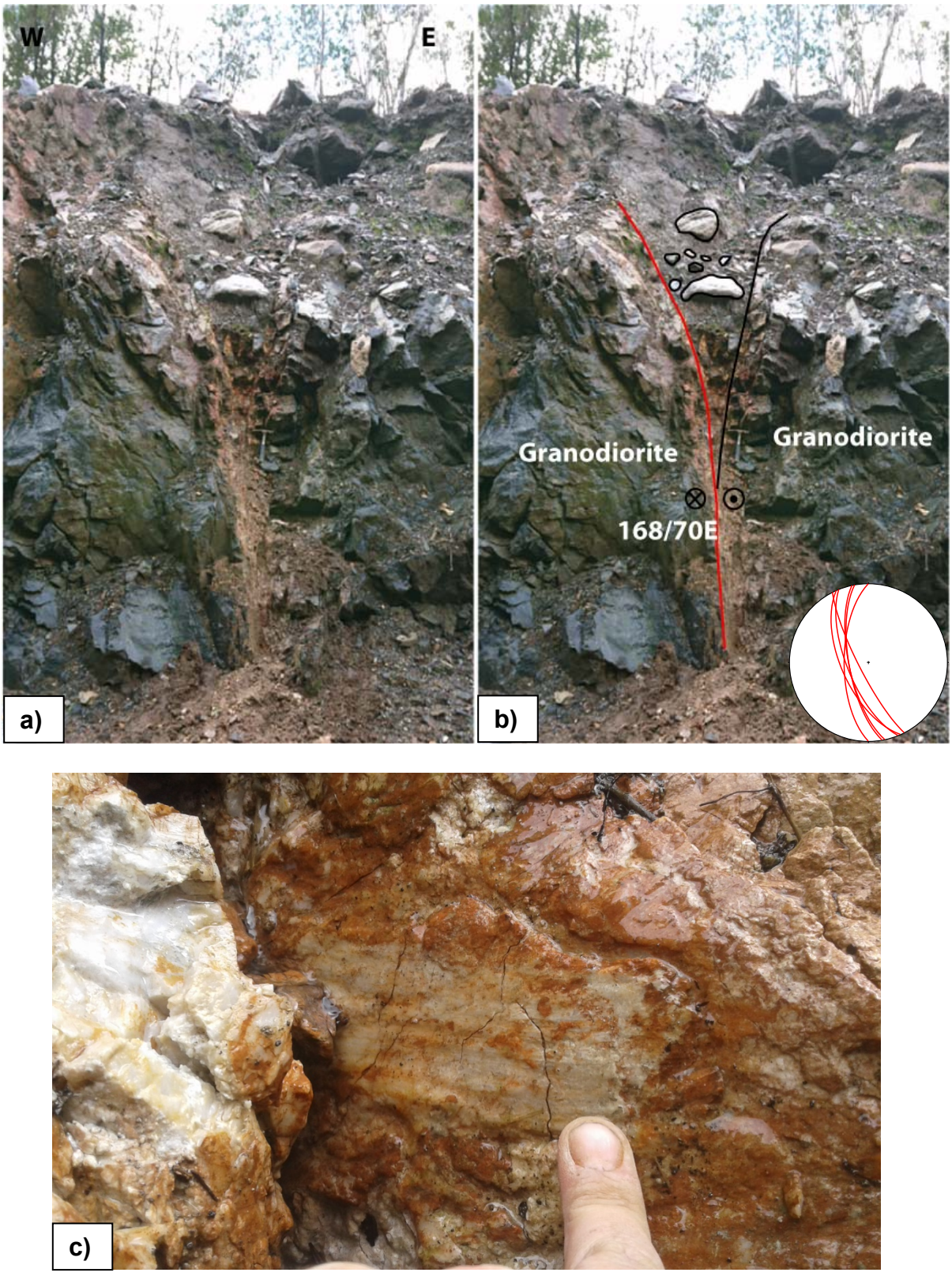

Figure 3.9. a) Field photograph looking north and b) interpretation of the Ventisquero Fault. Figure b) shows the main fault plane (red line) with a colluvial wedge bounded by a secondary fault (black line). Note hammer in the fault zone for scale. c) Horizontal striations in the fault plane, indicating strike-slip motion. Stereonet shows the fault plane orientation (n = 5).

3.4.1.3.2 Geomorphic and/or stratigraphic observations

A marked vertical offset is seen along the southern flank of the road, where the western side is approximately 1 m higher in topography than the eastern side of the fault zone, conforming an east-facing fault scarp (Figure 3.10). The fault trace can be seen in Google Earth for at least 2 km.

Figure 3.10. Field photograph looking south of the Ventisquero fault. A marked topographic change (i.e. fault scarp) can be seen at both sides of the fault plane, where the western block is 1-2 meters higher than the eastern block. Note person with orange jacket for scale.

3.4.1.4 Mallines Fault

3.4.1.4.1 Structural observations

The Mallines Fault (MF) is NE-SW striking fault located at the southern flank of the upper Queulat Valley, 1.5 km away towards the east of the Ventisquero Fault along the Carretera Austral in the upper Queulat Valley (Figure 3.2; Figure 3.11). It is a 1 m-wide fault zone that cuts through grey metamorphic rocks. It has a fault core of 50-cm wide, characterized by a white gouge layer of 1-2 mm thick (020/50ºSE) that cuts the schist folitation (140/40ºNW), and a fault breccia 1 m-wide with 1-cm diameter angular fragments of schist. No kinematic indicators were seen in the field.

3.4.1.4.2 Geomorphic and/or stratigraphic observations

No geomorphic or stratigraphic offsets were observed along this fault. However, the fault orientation is totally different and cuts the main foliation plane of the bedrock, so at least is younger than the age of metamorphism.

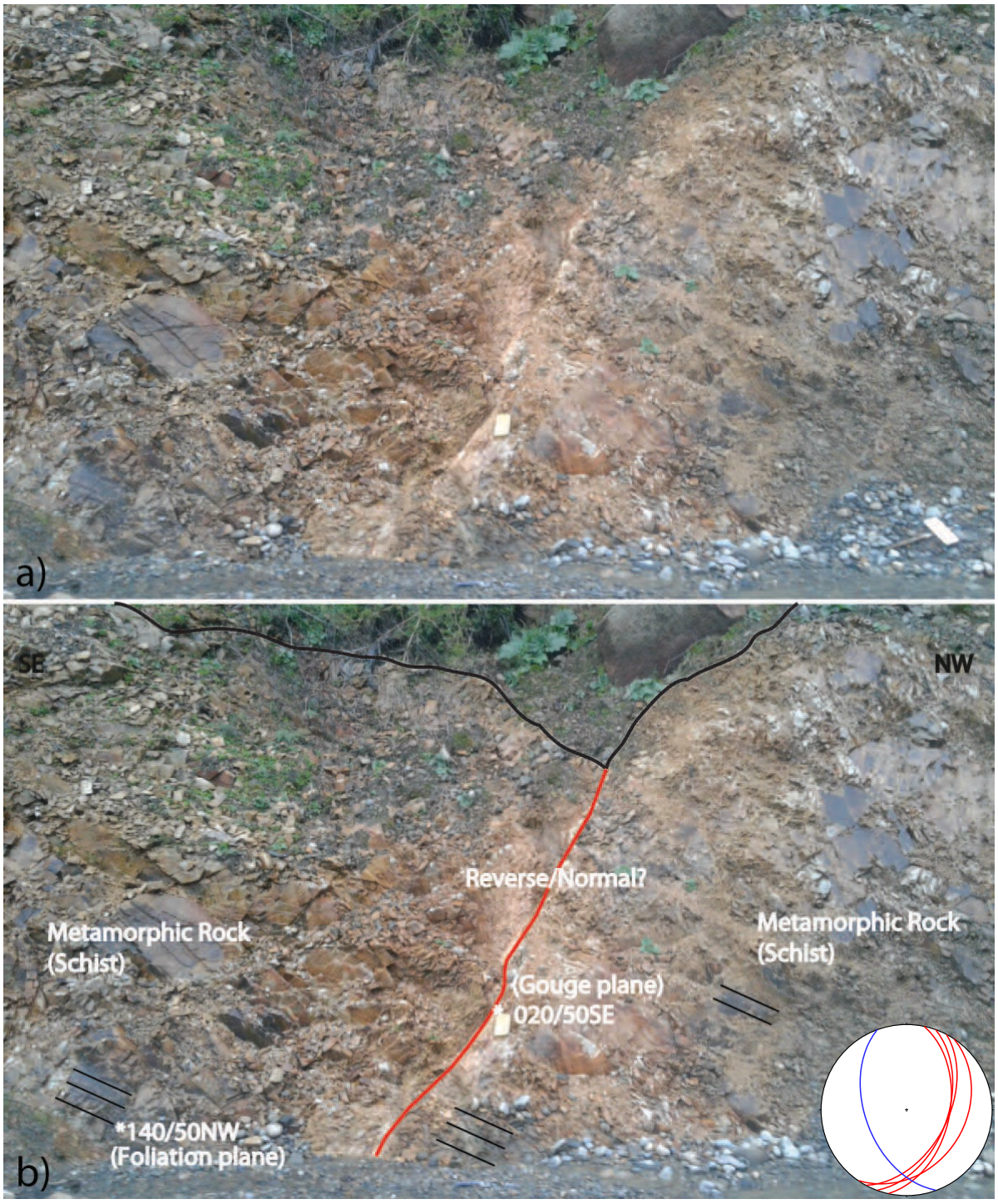

Figure 3.11. a) Field photograph and b) interpretation of the Mallines Fault. The red line corresponds to the main fault plane that cuts the older metamorphic foliation. Note the fieldbook for scale. Stereonet shows the foliation orientation (n = 1; blue line) and the fault plane orientation (n = 4).

3.4.1.5 Bosque Muerto Fault

3.4.1.5.1 Structural observations

The Bosque Muerto Fault (BMF) is an NW-SE striking fault, located 23 km to the west of Cerro Castillo Village along the Carretera Austral (Figure 3.2; Figure 3.12). It is characterized by a 1-m wide fault core that cuts through volcanic rocks (Figure 3.13). The fault core is composed of a yellow gouge layer of 2-cm thick with a main orientation fault plane of 115/64ºSW (Figure 3.13) surrounded by completely sheared, with fault breccias and with fragments size between 0.5 and 3 cm.

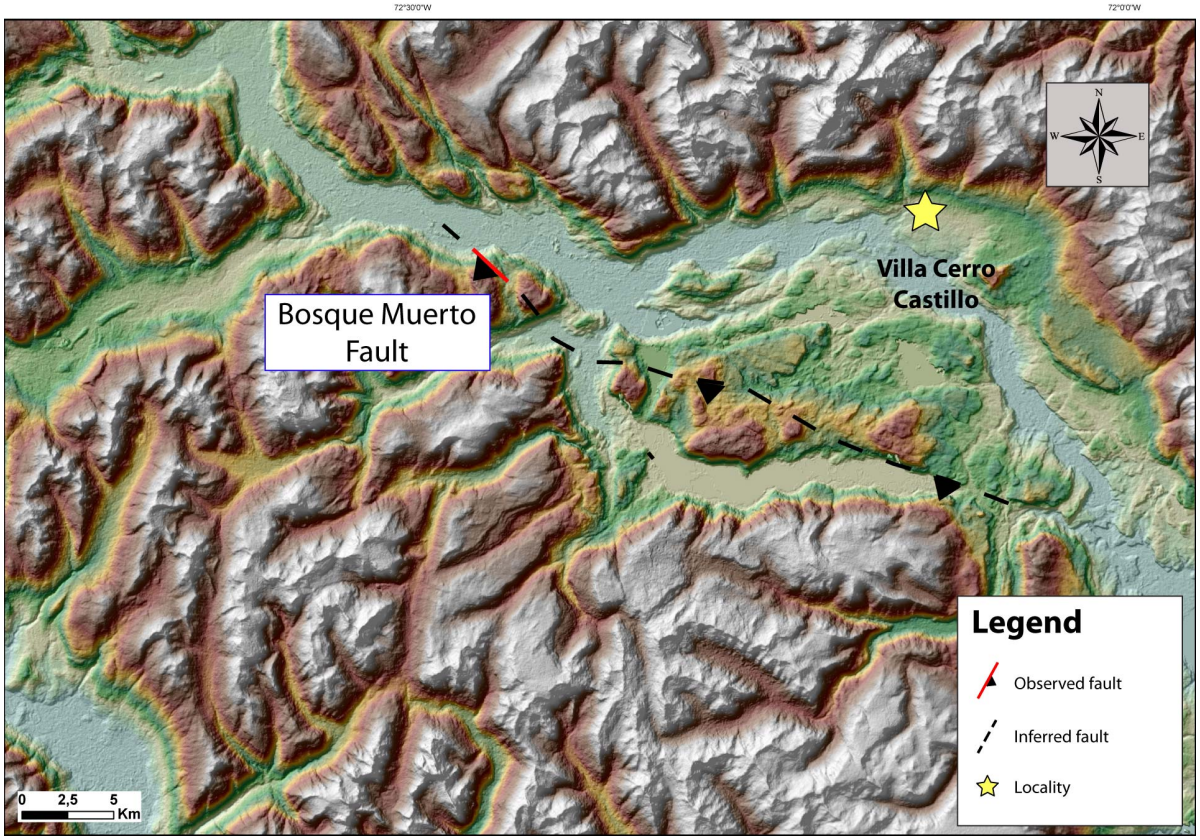

Figure 3.12. Simplified geological map showing Bosque Muerto Fault trace west of Villa Cerro Castillo.

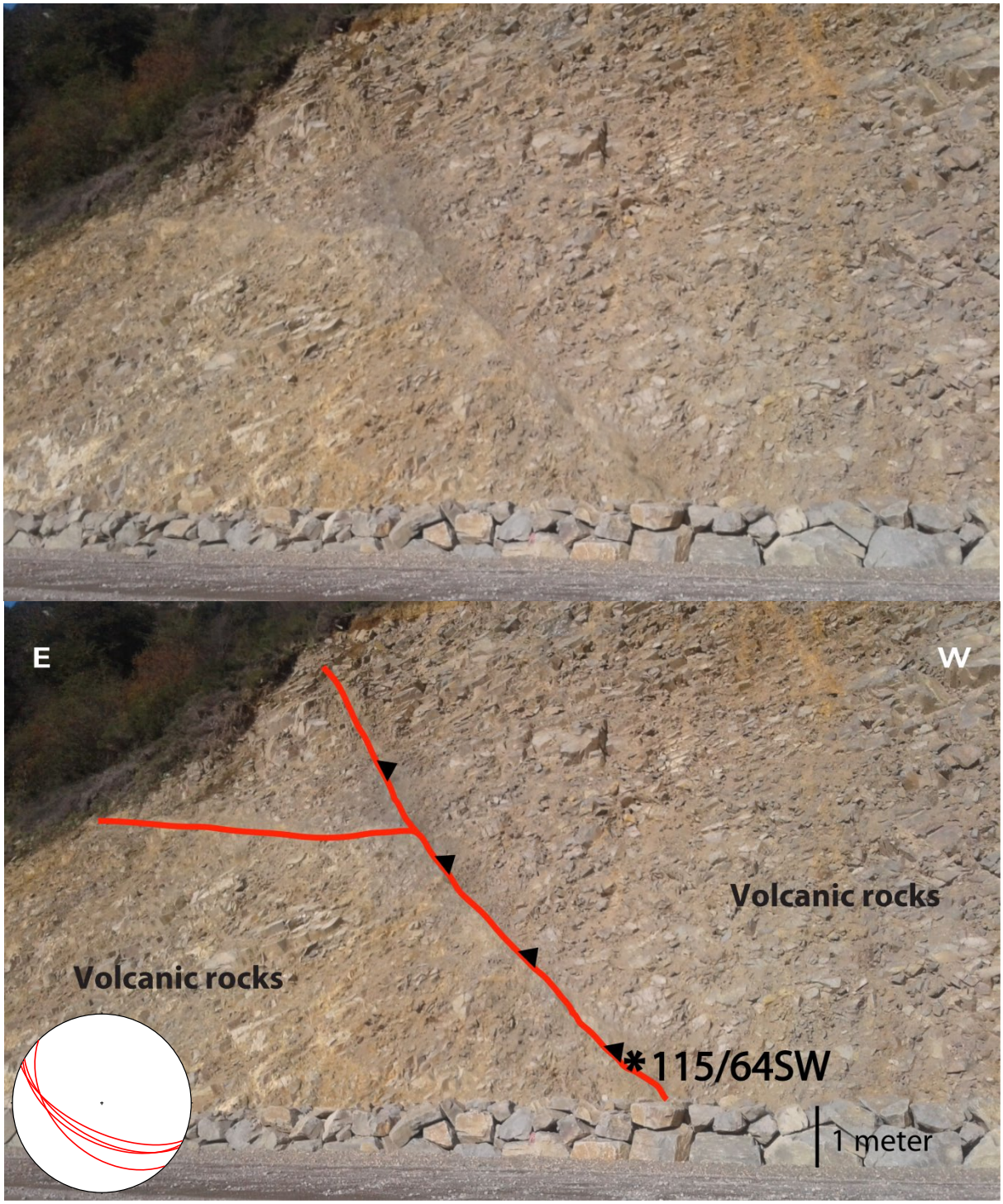

Figure 3.13. Field photograph looking south of the Bosque Muerto Fault. The red line corresponds to the Bosque Muerto fault plane. Stereonet shows the orientation of the main fault plane (n = 4).

West and east of the fault trace, the bedrock gets notably less fractured moving away from the main fault plane. Two main joint sets were identified. The main joint set has an orientation of 010/65ºW, while the second one has an orientation of 090/30ºN.

3.4.1.5.2 Geomorphic and/or stratigraphic observations

The Bosque Muerto Fault trace can be seen as a lineament in Google Earth for at least 12 km, where the footwall coincides with an extended depressed area basin to the southwest where Cerro Castillo village is located, in contrast with the hanging wall that conforms an elevated topography (Figure 3.13). No kinematic indicators were found along the fault zone, but the coincidence of the fault trace with the marked topographic change between the hanging wall and footwall suggests a reverse motion for the Bosque Muerto Fault.

3.4.1.6 Lago Esmeralda Fault

3.4.1.6.1 Structural observations

The Lago Esmeralda Fault (LEF) is an N-S striking fault located 6 km to the southwest of the town of Cochrane along the Carretera Austral (Figure 3.2; Figure 3.14). It is a 1-m wide fault zone that juxtaposes black volcanic rocks in the hanging wall with red sedimentary rocks in the footwall (Figure 3.15). It is characterized by a fault core composed of a 1-cm thick light grey gouge layer with an orientation of 000/45ºE (Figure 3.15).

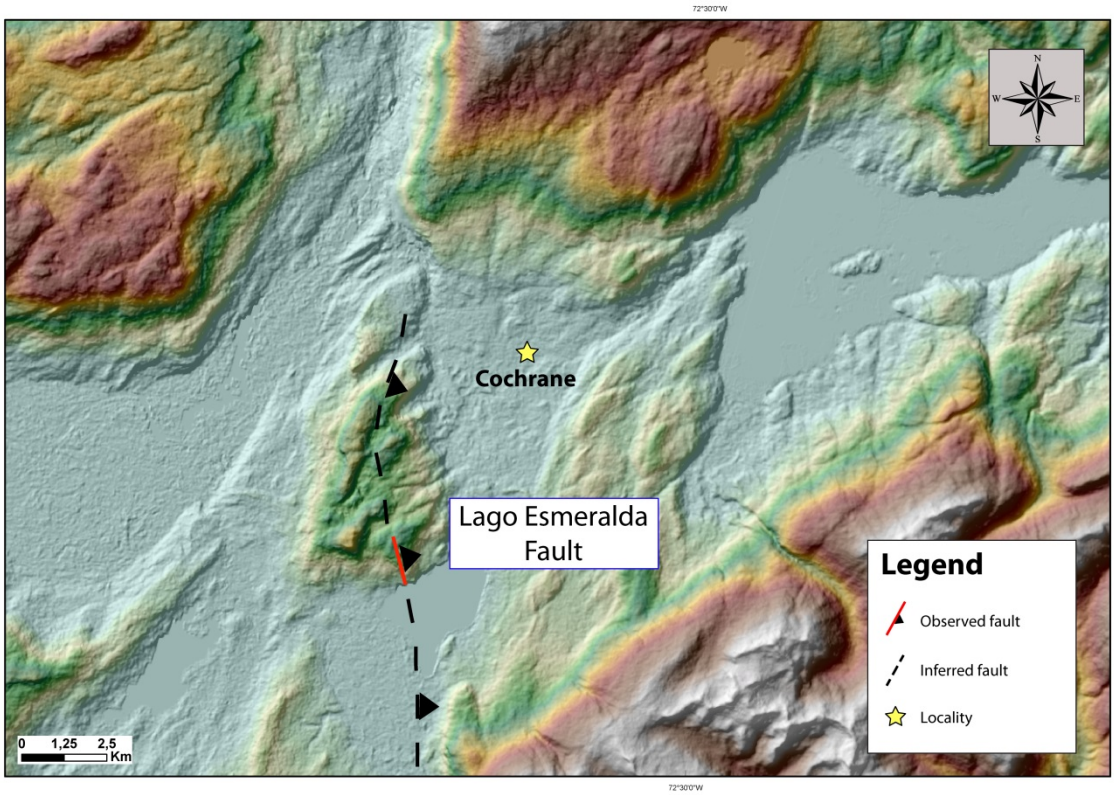

Figure 3.14. Simplified geological showing Lago Esmeralda Fault trace southwest of Cochrane.

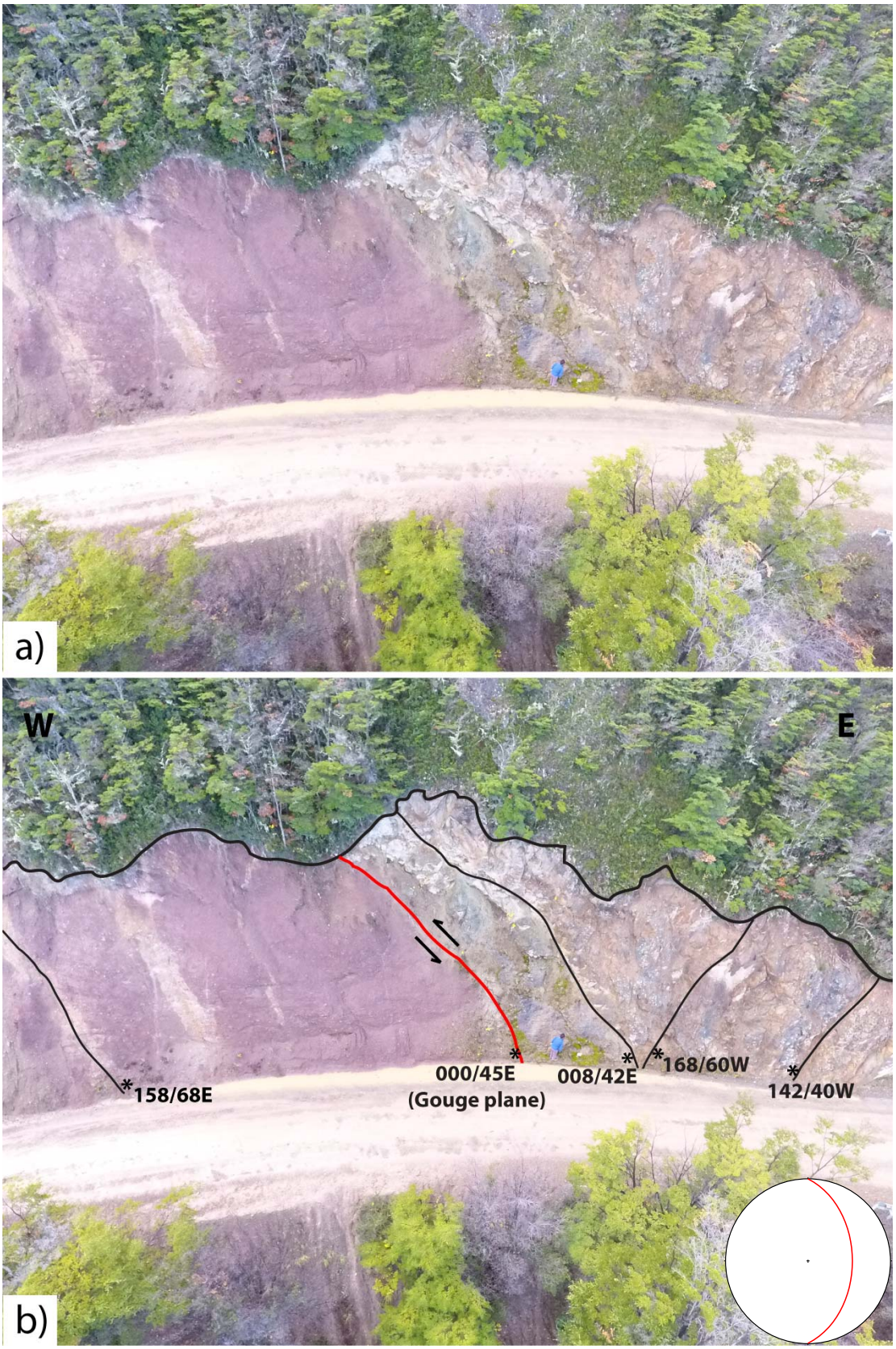

Figure 3.15. a) Oblique drone photograph looking north and b) interpretation of the Lago Esmeralda Fault. The red line corresponds to the main fault plane and black lines to secondary fault planes. Note person with blue jacket for scale. Stereonet shows the orientation of the main fault plane.

Within the footwall, 15 meters towards the west, the sedimentary red unit presents a 2-cm thick black gouge layer with an orientation of 158/68ºE, coincident with a yellow high altered strip probably associated with hydrothermal fluid alteration. In the hanging wall, the volcanic unit presents a secondary fault with a 2-mm thick grey gouge layer with a synthetic orientation of 008/42ºE and joints with the same orientation. Two antithetic secondary faults the east have an orientation of 168/60ºW and 142/40°W respectively.

3.4.1.6.2 Geomorphic and/or stratigraphic observations

No kinematic indicators were found along the fault zone, but there is a marked topographic change when crossing the fault, where the hanging wall is topographically higher than the footwall.

Another geomorphic feature of the Lago Esmeralda fault zone is observed in the drainage pattern. The river, that flows from east to west, changes from a straight river to a sinouse river towards the west, ending in a waterfall. This change in the drainage pattern is interpreted to be the effect of a popped up ridge that blocks the river flow towards the west (Figure 3.16).

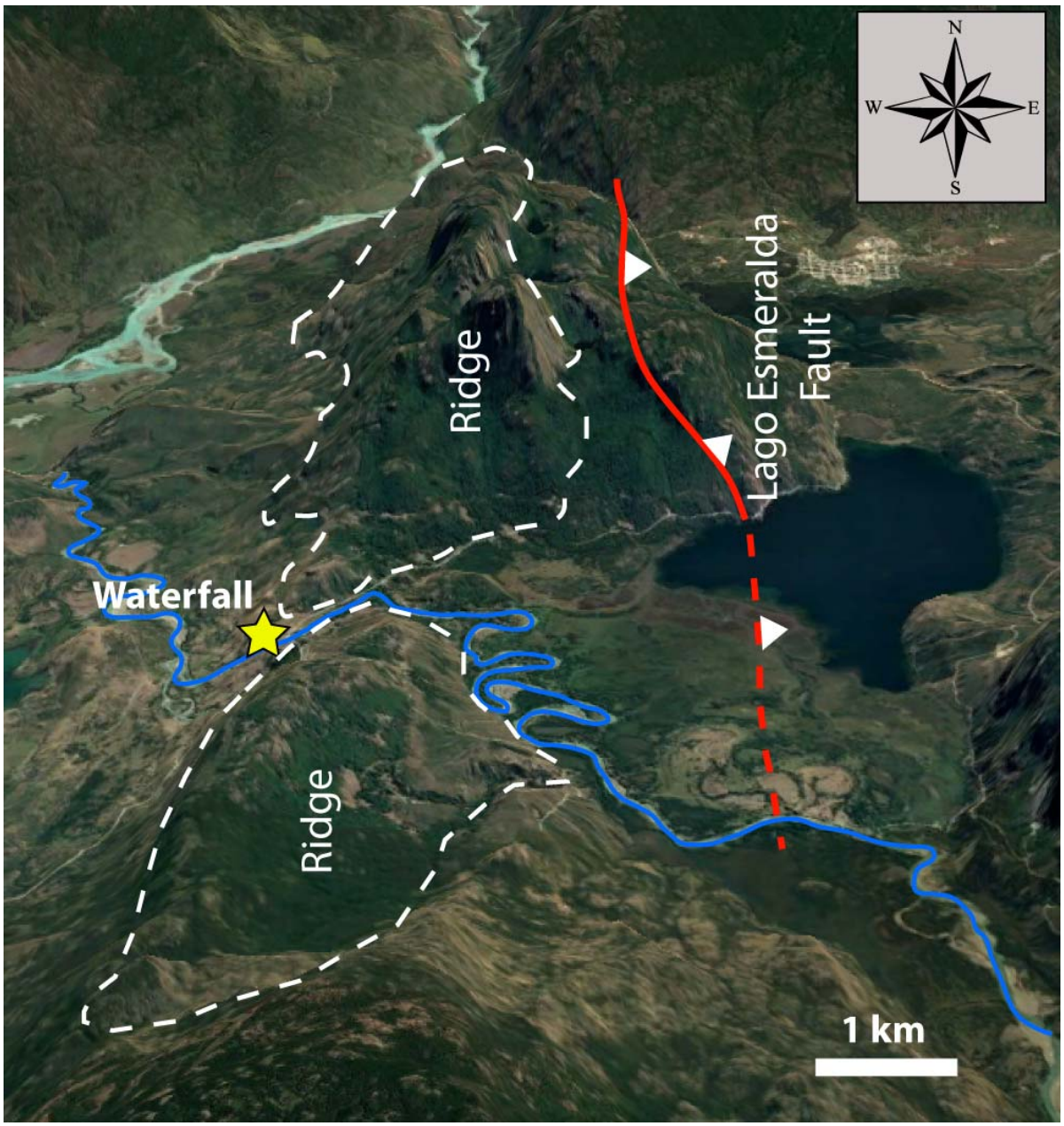

Figure 3.16. Oblique satellite image showing the Lago Esmeralda fault. Note how the drainage patterns changes from a straight river to a sinuous river towards the west as it hits an elevated ridge, for then conforming a waterfall.

3.4.1.7 Exploradores Fault

3.4.1.7.1 Structural observations

The Exploradores Fault Zone is a set of N120°E-striking reverse faults that dip southwest between 50-80° with a minor strike-slip component located at the northern foothills of the NPI (Figure 3.3; Figure 3.17; Georgieva et al., 2016). It coincides with the course of the Exploradores Valley, and with the almost 4 km pop up of the San Valentin Mount, the highest peak in Patagonia. The fault zone is 10-15 wide characterized by closely spaced brittle faults. The fault planes dip steeply toward the SW, and SE plunging lineations indicate oblique reverse faulting with a minor lateral component (Georgieva et al., 2016).

Based on differential tectonic uplift signatures revealed by low temperature thermochronological ages, this fault zone is interpreted to accommodate NS tectonic shortening as a consequence of northward translation of the North Patagonian Icecap, acting as a backstop and crustal ramp supporting high topography at the northern edge of the icefield (Georgieva et al., 2016). Additionally, this structure is proposed as an inherited structure that has been reactivated due to the favorable orientation with the current deformation regime (Georgieva et al., 2016).

Figure 3.17. Screen capture looking east of structure from Motion (SfM) 3-D model of the Exploradores Fault along. Two parallel fault planes with fault breccia between them compose the fault core.

3.4.1.7.2 Geomorphic and/or stratigraphic observations

Below the fault outcrop, there are wide rock fall deposits with several angular blocks with sizes up to 25-m wide. Over these blocks there are big trees (> 1-m trunk diameter) growing. In Figure 3.18, a 3-D Structure from Motion geomorphic model is presented. It can be seen a difference in the vegetation around the main fault zone, observed by a difference in height and color (Figure 3.18). Further work here will give insights into the recurrence and rupture parameters of this structure, but notably this suggest that this fault has had recent activity as vegetation is disturbed around this fault zone as a consequence of repeated landsliding below the fault.

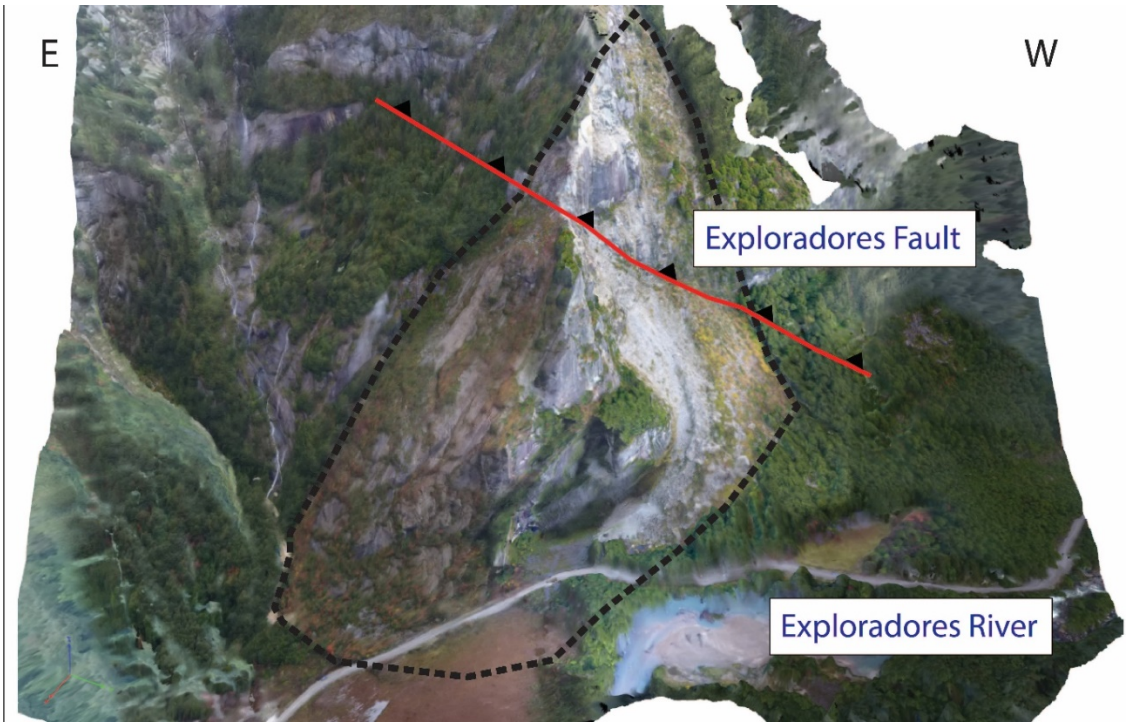

Figure 3.18. Screen capture of structure from Motion (SfM) 3-D model of the Exploradores Fault (red line) looking south. Note how vegetation is disturbed around the fault (black dashed line).

Figure 3.19. Field photograph showing huge (< 20 m) blocks with trees growing over them, evidencing rockfall around the Exploradores fault zone.

3.4.2 Kinematic analysis of newly identified crustal faults

Kinematic analysis were carried out on faults using the FaultKin7 software, following methodology outlined in Marrett and Allmendinger (1990) that define incremental strain tensors of compression (P) and extension (T). Stereonets are equal area, lower hemisphere projections. Where no kinematic indicators were observed, fault motion was inferred by either geomorphic or topographic expressions aligned with fault traces.

Fault orientation and slickenside data indicate that the most recent phase of motion on the faults described above was both reverse and strike-slip. The orientation of the principal directions of compression and extension were determined for individual faults with kinematic indicators described above. A regional moment tensor solution for faults studied in this work shows strike-slip and dip motion, with a horizontal shortening axis direction of 228°/013° (Figure 3.20).

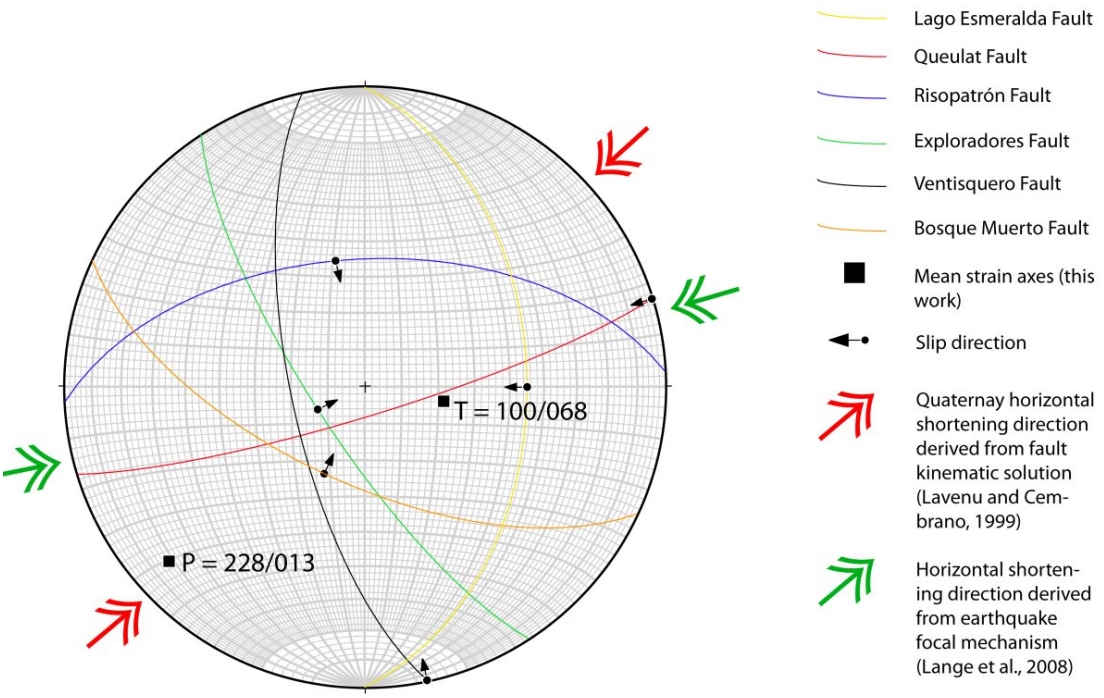

Figure 3.20. Stereonet showing kinematic solution for faults with kinematic indicators described above with mean strain compression (P = 228/13) and extension (T = 100/68) axes. Individual fault orientation with slip direction is shown in colours. Areas of extension (grey) and compression (white) are shown. Horizontal shortening directions obtained by Lavenu and Cembrano (1999) from fault slip data and by Lange et al. (2008) from earthquake focal mechanisms are shown for comparison. Faults with no kinematic indicators are not shown.

3.4.3 Preliminar potential earthquake magnitudes of crustal faults in the Aysén Region

As explained in the previous section, this work presents new documented faults that show some field evidence of potential paleoseismic indicators such as fissure fills and topographic offsets, and therefore potential earthquake magnitudes are calculated for each one in order to assess these structures as seismogenic sources for the Aysén Region.

Earthquake magnitudes can be estimated from the geometry of faults and their slip characteristics (e.g. Wells and Coppersmith, 1994). A downdip rupture width was determined by assuming complete fault rupture using a seismogenic depth of 10 km derived

from microseismicity studies (Lange et al., 2008; Legrand et al., 2011; Agurto-Detzel et al., 2014; Perez-Estay et al., 2020).

In Table 3.2 an updated list of crustal faults in the Aysén Region which their seismogenic parameters are presented, including the new documented faults characterized in this work. Fault coordinates which have no outcrop or specific location were taken from the maps which show those faults (see references in table).

Considering a range of potential fault lengths, minimum and maximum estimated magnitudes were calculated for the faults described above (Table 3.2). This was calculated based on the surface length trace of each fault. As these magnitudes are dependent only on the fault trace length, they should be considered only as first order magnitudes, being necessary paleoseismological studies to determine slip rates and recurrence times, to better constrain earthquake parameters.

Table 3.2. Summary of newly identified crustal faults for the Aysén Region. Main LOFZ is also included. Coordinates are in UTM (WGS84 Datum).

Fault Name	N (m)*	E (m)*	Style	Minimum Length (km)	Maximum Length (km)	Dip (°)	Seismogentic thickness (km)	Surface Width (m)	Estimated Mw (Min)	Estimated Mw (Max)	Relevant Study
Risopatrón	5098231	698474	Reverse	3	18	50	10	150 m	**5,6**	**6,5**	This study
Queulat	5062607	701530	Dextral	1	3	80	10	5 m	**5,1**	**5,6**	This study
Mallines	5061445	704654	Unknown	1	2	48	10	2 m	**5,1**	**5,4**	This study
Ventisquero	5061574	703756	Dextral	2	4	80	10	2 m	**5,3**	**5,8**	This study
Bosque Muerto	4888116	697624	Reverse	3	11	54	10	2 m	**5,6**	**6,3**	This study
Lago Esmeralda	4756878	680812	Reverse	2	8	45	10	30 m	**5,4**	**6,1**	This study
Exploradores	4845378	655615	Reverse	2	8	76	10	10 m	**5,4**	**6,1**	Georgieva et al 2016
Main LOFZ	41°S	47°S	Dextral / Reverse	200	1200	vertical?	10	?	**7,7**	**8,7**	Vargas et al., 2013

3.4.4 Geology of the Exploradores Valley

Field mapping was carried out along the Exploradores Valley (Figure 3.21). Rocks found in situ within the Exploradores Valley are plutonic, igneous intrusive rocks that correspond to the North Patagonian Batholith (Hervé et al., 2007). Two main rock units were recognized in this work. The first one corresponds to a mesocratic dioritic unit with phaneritic texture, characterized by a mineralogy composed by amphibole, K-feldpsar, minor biotite and quartz (Appendix III and IV). Crystal sizes range from 0.5 mm to 3 mm and show perthitic and reabsorption textures. The second corresponds to a leucocratic granodioritic unit with a mineralogy composed of biotite, K-feldspar and quartz, with minor amphibole crystals (Appendix IV). This second unit has sinuous and straight veins of 2-4 cm width composed mainly of quartz and calcite.

Structures in the Valley include joints, veins and faults. Two main joint set with NW and NE directions with low and high angles were mapped. Also, straight and sinous quartz veins cut both intrusive units with thicknesses up to 3 cm were documented. The most prominent structural feature is the Exploradores Fault that outcrops along the southern flank of Exploradores Valley. It consists in a NW-striking, north-east vergent reverse fault with a minor strike-slip component that cuts the Patagonian Batholith (Georgieva et al., 2016). It is characterized by two parallel fault planes surrounding a fault core of 1-2 meters composed of fault breccia and cataclasites.

Quaternary units along the Exploradores Valley correspond to alluvium, glacial deposits and landslides. Alluvium units correspond to modern river and stream deposits composed of non-consolidated matrix-supported gravels with rounded boulders. Also, there are two glaciers (Grosse and Exploradores glaciers) entering the Exploradores valley (Figure 3.21) to this day, with glacial till deposits that are exposed both as ground

basal and end moraines products on the southern flank of the Valley. They are characterized by a poor-grain selection, with angular and rounded blocks with sizes ranging from few millimeters to decameters.

Landslides are common features along the whole valley. They are characterized by talus and large angular blocks with sizes up to 20 m with trees growing over them. Close to the Exploradores Valley there is a rockfall deposit with large (up to 20m) angular blocks covered with soil and vegetation. Notably is the presence of big trees growing over rock blocks, whereas some of them are dead.

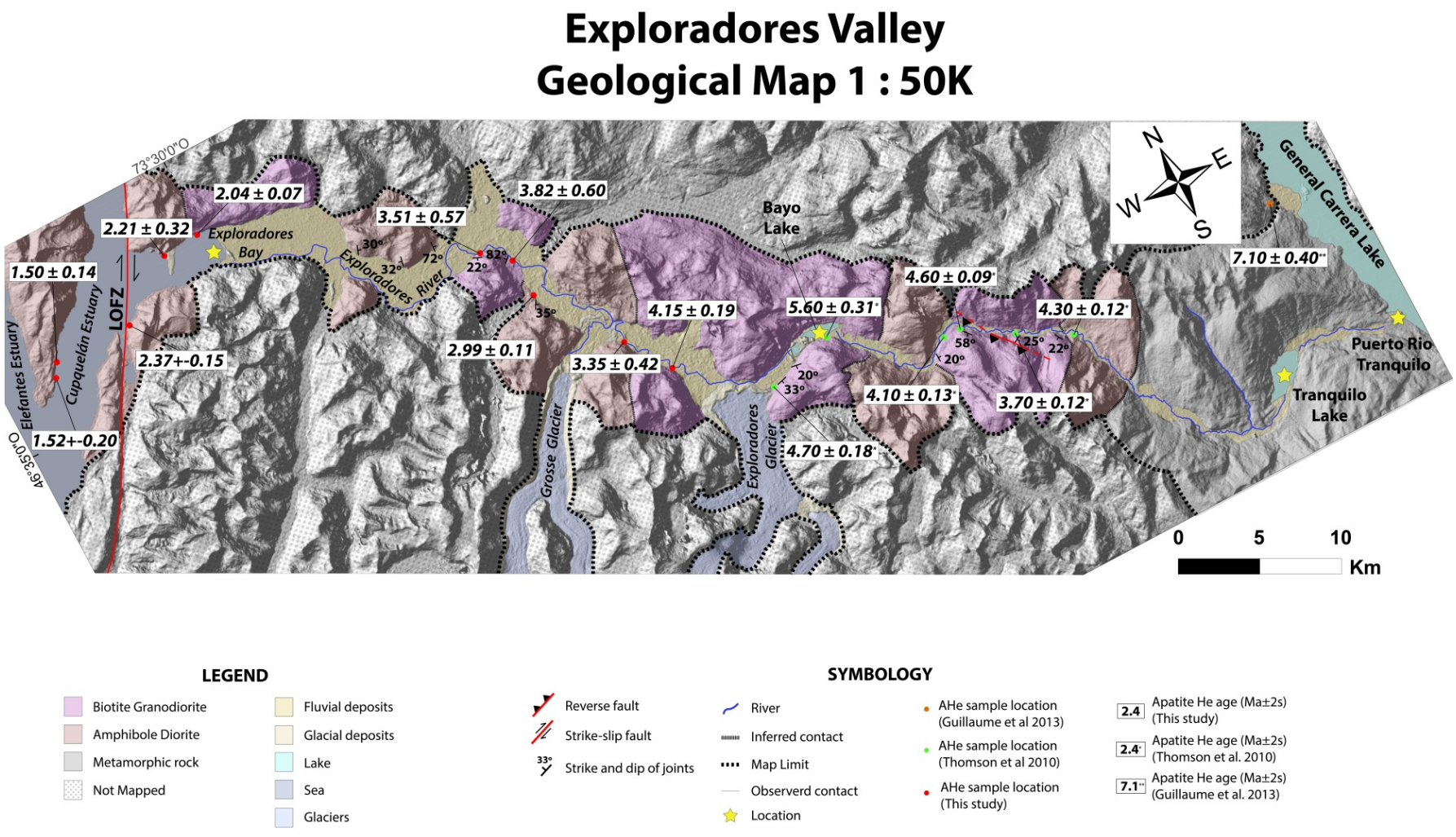

Figure 3.21. Geological map of the Exploradores valley with 8 new AHe ages (red dots) and previous AHe ages (orange and green dots).

3.4.5 Results from Apatite (U-Th)/He Thermochronometry from Exploradores Valley

We analyzed 8 intrusive bedrock samples collected as part of this study and compare this with 7 previously published (Thomson et al., 2010) apatite U-Th/He (AHe) ages along a 40 km east-west transect in the Exploradores Valley. This was done to better understand the neotectonics here including exploring the role of the LOFZ and the Exploradores Fault in the exhumation of the Patagonian Batholith. All samples correspond to the Patagonian Batholith diorites and granodiorites, with crystallization ages ranging from 100 to 15 Ma (e.g. Pankhurst et al., 1999; Hervé et al., 2007).

Table 3.3 and Appendix V shows the results of laboratory analysis while Figure 3.22 shows mean crystal ages with their associated standard error (2 sigma) versus distance (in km) from the LOFZ. AHe ages range from 1.5 to 7.1 Ma along the entire valley, with a first order general reduction of ages the closer they are to the LOFZ (Figure 3.22; Appendix IV). This relationship is regular, except for the 4 samples located in the vicinities of the Exploradores Fault Zone (Georgieva et al., 2016) that have younger ages than expected considering a linear correlation between age and distance east of the LOFZ (Figure 3.22). The closest samples are located in the proximities (< 5 km) of the LOFZ, which present the youngest ages (1.5 ± 0.07 Ma to 2.4 ± 0.15 Ma), while the further samples (> 40 km) from the LOFZ present the oldest ages, varying from 4.1 ± 0.19 to 7.1 ± 0.2 Ma. Additionally, samples from the same elevation present younger AHe ages at the eastern side of the LOFZ (1.5 ± 0.15 Ma) than samples located in the western side of the fault (2.0 ± 0.07 to 2.37 ± 0.32) (Table 3.3; Figure 3.21, 3.22 and 3.23).

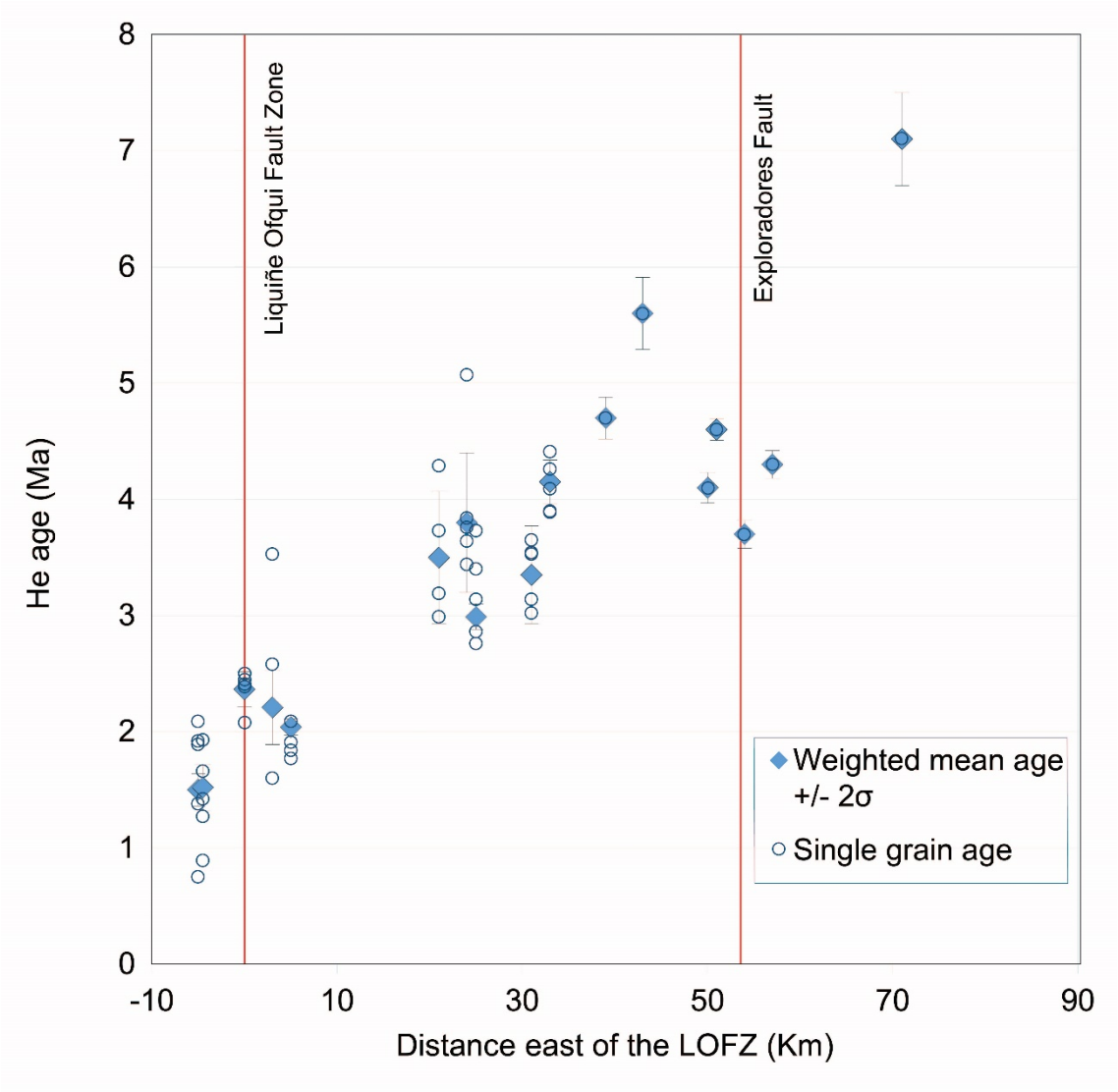

Figure 3.22. Age-distance relationships of apatite He ages along the Exploradores Valley. Empty circles show single grain ages for each sample and blue diamonds show weighted mean age for each sample.

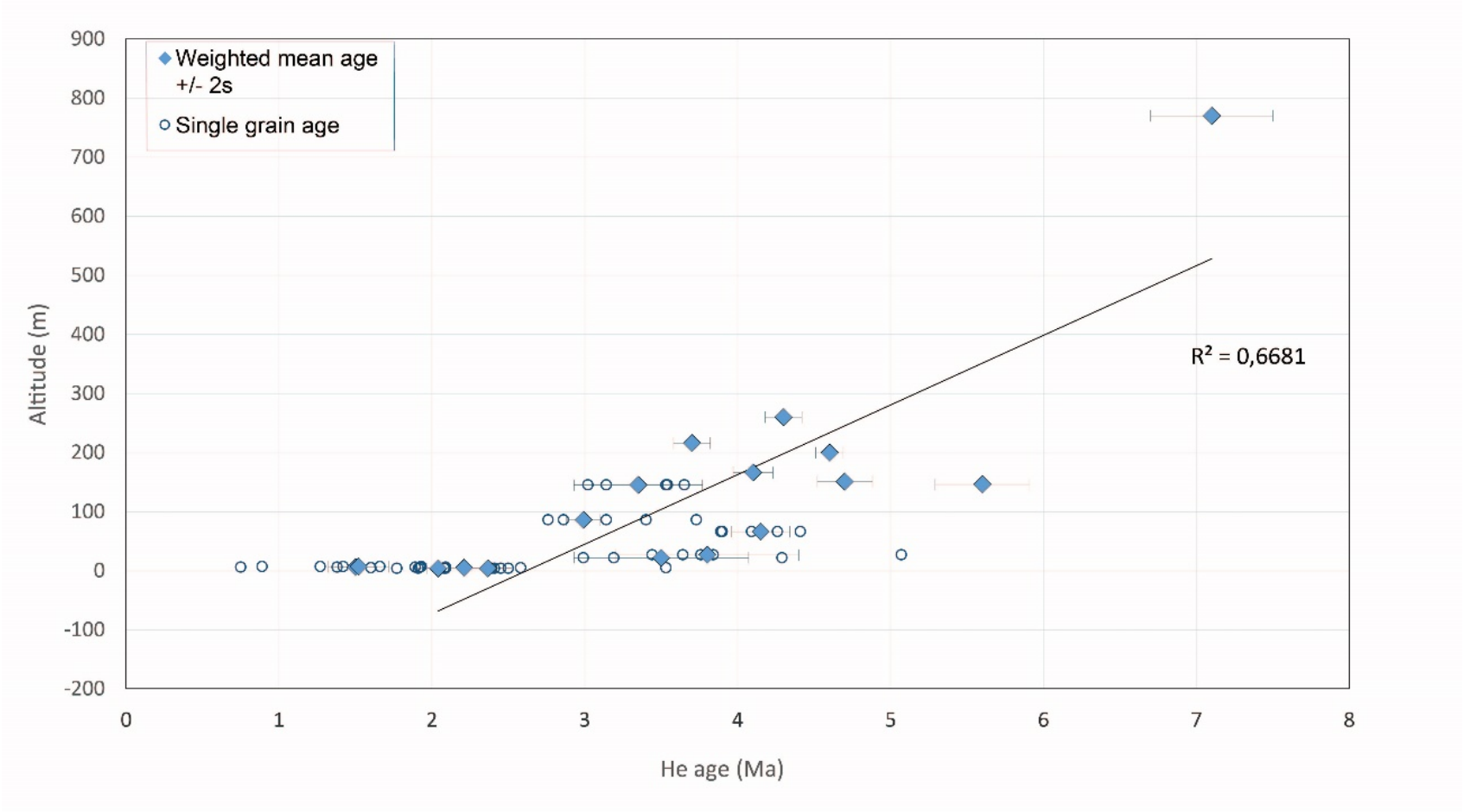

Figure 3.23. Age-elevation relationships of apatite He ages along the Exploradores Valley. Empty circles show single grain ages for each sample and blue diamonds show weighted mean age for each sample.

Table 3.3. Apatite (U-Th)/He mean ages and error (given in 2 σ). Positive values correspond to distance east of the LOFZ, while negative values correspond to distance west of the LOFZ.

Sample name	Latitude (ºS)	Longitude (ºW)	Distance east of LOFZ (km)	Altitude (m.a.s.l)	Mean He age (Ma)	Error (Ma)	Reference
GDP_MB6	46.3100	73.6479	-5	6	1.5	0.14	This study
GDP_MB7	46.3172	73.6518	-4.5	7	1.5	0.20	This study
GDP_MB4	46.3083	73.5794	0	4	2.4	0.15	This study
GDP_MB3	46.2849	73.5335	3	5	2.2	0.32	This study
GDP_MB2	46.2825	73.5043	5	4	2.0	0.07	This study
GDP MB11	46.3620	73.3092	21	22	3.5	0.57	This study
GDP MB12	46.3724	73.2883	24	27	3.8	0.60	This study
GDP_MB13	46.3949	73.2865	25	86	3.0	0.11	This study
GDP MB14	46.4412	73.2381	31	145	3.3	0.42	This study
GDP_MB15	46.4647	73.2149	33	66	4.1	0.19	This study
06PA05	46.5007	73.1497	39	151	4.7	0,18	Thomson et al. 2010
06PA06	46.4886	73.0934	43	146	5.6	0.31	Thomson et al. 2010
06PA08	46.5172	73.0101	50	166	4.1	0.13	Thomson et al. 2010
THC23	46.5187	72.9953	51	200	4.6	0.09	Thomson et al. 2010
06PA09	46.5330	72.9575	54	216	3.7	0.12	Thomson et al. 2010
06PA04	46.5476	72.9149	57	260	4.3	0.12	Thomson et al. 2010
PATC14-A	46.5310	72.7396	71	770	7.1	0.4	Guillaume et al. 2013

4 DISCUSSION

4.1.1 Style of deformation of newly identified crustal faults

New documented faults studied in this work have strikes preferentially NS with a few structures striking almost EW to NW, with kinematic indicators and geomorphic features indicating a reverse and/or strike-slip motion for these faults. As mentioned in section 3.4.1, one of the main purposes of this study was to look and assess the LOFZ around Puyuhuapi and Queulat Valley. Notably, we did not find any evidence in the field for fault rocks or geomorphic features that could be associated to the Liquiñe-Ofqui Fault, indicating that around the mentioned areas this fault is probably buried and underlying young deposits associated to Holocene volcanic deposits from monogenetic cones and big stratovolcanoes, glacial deposits and morraines associated with the LGM around 17 Ka ago, or because the main LOFZ is underwater in lakes and fiords around the region that make it impossible to observe this structure at the surface.

The Risopatrón Fault (RF), located north of Puyuhuapi, has an almost E-W orientation, oblique to the mainly north-south striking LOFZ and the northwest striking Andean Transverse Faults (ATF). Considering the hypothesis that oblique subduction is causing a crustal microplate (Chiloé Microplate) to be detached from the continent and translated northwards with its leading eastern edge being the LOFZ, (e.g. Forsythe and Nelson; 1985; Melnick et al., 2006; Wang et al., 2008; De Pascale et al., 2021), the RF could represent an internal structure within the Chiloé Microplate that responds to this northward migration, resulting in a south-vergent reverse fault. Beck et al. (1993) showed in their work that oblique subduction along convergent margins causes a "sliver" to detach, generating areas of tectonic extension, as it was proposed for the Golfo de Penas-Taitao Basin. In this context, as extension areas are generated and

basins are formed within the Chiloé Microplate, there are likely areas of shortening and compression as suggest by Wang et al. (2007), based on GPS data, possibly resulting in generation of thrusting and reverse faulting. Noting that northward motion of the Chiloe Microplate only started in the Late Miocene, RF fault likely started within LOFZ motion and thus validates north-south shortening as suggested by Wang et al (2007). Since the processes are still driving the LOFZ and thus the Chiloé microplate northwards, then the RF is likely still active and well-aligned for motion.

The Queulat, Ventisquero and Mallines faults, all located along the Queulat Valley, have been interpreted as strike-slip faults based on field observations. The Queulat Fault present subhorizontal kinematic indicators that indicate strike-slip motion. In the Ventisquero Fault, sub-horizontal slickensides observed in the fault gouge plane indicate a strike-slip movement. In the Mallines Fault, no kinematic indicators were observed, but based on the proximity of the other faults and considering the northeast regional stress state, it could be a dip-slip or strike-slip fault, being impossible to discriminate between both in this work. Interestingly, faults along the Queulat Valley have the same strike and coincide spatially with the Queulat shear zone, Río Mañihuales and Azul-Tigre faults mapped and described by Cembrano et al., 2002 and Thomson et al., 2002 (Figure 3.1) who interpreted these fault zones as east branches of the LOFZ; however, this works are based on petrographic and thermochronological studies, while no fault characterization nor structural information is presented. In this context, the data presented in this work along the Queulat Valley would represent the first geological field and structural evidence of the Queulat shear zone.

The Bosque Muerto Fault is interpreted as an NNW striking, reverse fault dipping 64° to the SW, conforming a hangingwall coincident with an elevated topographic area

and a footwall conforming a depressed basin, suggesting that relief and topography in this region are to some extent structurally controlled.

The Lago Esmeralda fault trace coincides with a NNE oriented, strike-slip fault mapped by Scalabrino et al. (2010). These authors map and describe a series of normal and strike-slip faults at 46ºS based on geomorphological analysis of lineaments, topographic analysis in satellite images and digital elevation models of the area, but with limited field evidence. They propose a negative tectonic inversion (e.g. reverse faults reactivated as normal faults) as a consequence of the Chile-Ridge spreading center subduction. In this context, they describe the Tamango Fault Zone, a NNE striking normal fault located 10 km north of the Cochrane town. This fault zone would partially coincide with the Lago Esmeralda Fault described in this work because of its proximity. Nevertheless, we have interpreted this structure as a reverse fault instead of a normal fault based on the dip angle and topographic changes across the fault plane. No kinematic indicators were observed in the field, but the marked topographic control of the landscape by this fault where the hanging wall composed of volcanic rocks is much higher and pops up strongly argues in favor of this hypothesis. Following this, we propose the Lago Esmeralda Fault as a new documented reverse fault. As drainage pattern perturbation suggests, this new documented fault is proposed as potentially active and may indicate that perhaps some of the previous mapped faults by Scalabrino et al. (2010) are also likely potentially active faults that are favourably oriented with the current main shortening direction derived from kinematic analysis obtained in this work.

The previously documented Exploradores fault, better characterized in this work, is proposed to be an inherited basement structure that accommodates a northward

translation of the Northern Patagonian Icecap that it is detached and decoupled from the continent along the LOFZ at the western side and by the Cachet Fault by the eastern side of this block, forming a crustal sliver (Georgieva et al., 2016). These authors suggest that this block translation results in localized N-S shortening accommodated by reverse faults of the Exploradores Fault Zone system described along the Exploradores Valley. In this context, the Bosque Muerto Fault has a similar orientation and kinematics than the Exploradores Fault, thus could be a prolongation to the north of this northward translation of this crustal sliver that accommodates N-S shortening as is also suggested by Wang et al. (2007) from GPS data.

So how do these observations fit with previous understanding of recent tectonic deformation in Aysén? There are two conflicting theories on deformation neotectonic in Aysén east of the LOFZ. In one (e.g. Scalabrino et al., 2010) suggest that the subduction of the Chile Ridge spreading centre below Aysén is causing former reverse faults to be reactivated as normal faults due to extension (which they term negative tectonic inversion). In contrast, recent thermochronological analysis by Stevens Goddard and Fosdick (2019) suggest that a rock cooling signature with uplift from 20 Ma to 5 Ma was driven by a thickened crust in front of the obliquely subducted ridge which would be associated with reverse faulting due to shortening. Many of the new faults first identified in this thesis or with better characterization due to work in the field including the Bosque Muerto and Exploradores faults help support existing theories that until this work had no field validation. Specifically, Bosque Muerto and Exploradores faults help support the Stevens Goddard and Fosdick (2019) theory that ridge subduction generates a thickened crustal along the leading edge of the obliquely subducted ridge. Husson et al. (2019) argued that because no reverse structures were observed in the field to confirm this theory of crustal thickening at the northern edge of the Chile ridge, it is

unlikely that shortening is occurring in the upper crust here due to oblique subduction "because this would be difficult to miss in the field" (Husson et al., 2019). Thus, the documentation of new, young, reverse faults there support the results of Stevens Goddard and Fosdick (2019) and thus lead support to the theory that shortening is occurring in the upper crust in front of the northward migration of the subducted Chile Ridge. Additionally, in this same area, Scalabrino et al., (2010) that negative tectonic inversion is taking place, i.e. that reverse faults are now operating as normal faults due to the subducted Chile Ridge. In the area near Cerro Castillo, where Scalabrino et al., 2010 propose normal faulting, there is found no evidence of this and instead found northeast-vergent reverse faults with hangingwall topography (up to the south) in direct contrast with their proposed deformation style (i.e. reverse faulting versus the normal faulting they proposed). Because I only saw evidence for strike slip and reverse faults in this field surveys, especially from Cochrane to Cerro Castillo, results from this work do not support evidence for ongoing normal faulting (again in support of the Stevens Goddard and Fosdick Model (2019)).

4.1.2 Potentially active faults as seismogenic sources in the Aysén Region

Exploring how these structures may operate regarding regional seismic hazard is insightful. The presence of uncemented fault rocks, soft and highly plastic clay-rich gouge layers, in addition with clear topographic expression, supports the idea that most of the structures described in Chapter 3 have had recent (Quaternary) movement and thus are potentially active (e.g. Cox et al., 2012). This is based on the argument that any ancient structure, for example Andean Mesozoic and Cenozoic faults (pre-Quaternary) would have cemented fault rocks as a consequence of fluid circulation and mineral precipitation if no fault movement recent has occurred. By the other side, young

structures should present uncemented faults rocks, with any previous cementation being probably erased because of repeated recent fault rupturing.

In the same context, kinematic analysis compression axes obtained in this work are consistent with Quaternary brittle deformation stress patterns for the southern Andes, where a NE-SW horizontal shortening direction was obtained by Lavenu and Cembrano (1999) (Figure 3.20). Also, it partially coincides with seismological estimates, where a principal shortening direction of 256° was obtained from focal mechanisms of shallow (< 10 km depth) crustal earthquakes in the Aysén Region (Agurto-Detzel et al., 2014; Perez-Estay et al., 2020). Kinematic solutions are also consistent with modern geodetic models for the region, which show a north-east principal shortening direction for the late Quaternary (Wang et al., 2007).

This is consistent with structural, stratigraphic and geomorphic features observed for almost all faults documented in this work. The Risopatrón Fault is proposed as potentially active due to the presence of uncemented fault rocks and recent microseismicity studies in the same location that show evidence for E-W reverse faulting with a left-lateral strike-slip component (Perez-Estay et al., 2020), in agreement with the main shortening direction obtained from kinematic analysis, where a left-lateral component should be expected if this fault is currently active.

The Queulat and Ventisquero faults are composed of uncemented fault rocks and present vertical topographic offsets and fissure fills, suggesting that these faults have interacted with soil profile and have modified landscape after the last glacial maximum, where any topographic expression as a consequence of ancient fault motions would have been erased by glacial erosion. These faults are oblique with respect to the main shortening direction obtained from regional kinematic analysis as shown in Figure 3.20,

consistent with the strike-slip movement that kinematic indicators show in the field. In this context, these structures should behave as right-lateral strike-slip faults inferred from kinematic analysis and field observations.

As is shown in Figure 3.20, Bosque Muerto, Lago Esmeralda and Exploradores are reverse faults that are oriented almost perpendicular to the main shortening direction obtained from kinematic analysis, indicating that they could be potentially reactivated. This would be consistent with evidence for recent tectonic deformation in the area of Lago Esmeralda fault suggested by drainage perturbation and in the Exploradores Fault as suggested by huge rock falls and vegetation modification around the fault zone. For Bosque Muerto Fault, the relation between the high topography in the hanging wall (located to the south), with respect to the low topography to the north (where the Rio Ibanez flows), supports the idea that this fault is controlling deformation here now and would correspond to a Quaternary active structure.

Furthermore, the reverse faults that are well-oriented with the modern stress field for activation (e.g. Boseque Muerto, Lago Esmeralda, and Exploradores), lend support to the proposed crustal welt theory (or upper crustal shortening) due to oblique subduction through the passage and northern migration of an active spreading center (i.e. the Chile Ridge) as suggested by Stevens Goddard and Fosdick (2019), and in direct contrast with theories proposed by Scalabrino et al. (2010) and by Husson et al. (2019).

Additionally, the relatively well-developed and well-defined fault planes and gouge layers in all the described faults are in agreement with faults being large structures that had accommodated kilometers of displacement and multiple rupturing events in the past (e.g. Engelder, 1974; Chester and Logan, 1986).

4.1.3 Uncertainties in the estimation of potential earthquake magnitudes

The estimated earthquake Mw for the described faults was calculated using the Wells and Coppersmith (1984) equation based on the trace length of the fault. Considering this, the estimations are very sensitive and depend exclusively on the length of the mapping of these faults, as they were observed in one outcrop and its continuity was made using digital elevation maps and Google Earth to see any geomorphic lineaments or morphologies that suggest the fault trace could pass through. Where faults become concealed or hidden by widespread glacial and volcanic deposits, or wide alluvium-filled valleys, we cannot know for certain whether faults are continuous along strike or become arrested at some point. For example, even after extensive field mapping, no fault outcrop of the north striking LOFZ was found near Puyuhuapi nor until Cochrane. Additionally, faults described here are characterized as individual structures, but they also could be part of previously unrecognized structures that have not been mapped yet. For this reason, the estimated magnitudes for all the faults are conservative and could be slightly underestimated, despite assuming that they ruptured along their full length and the full seismogenic thickness of the upper crust. Unfortunately, there is a lack of geomorphic indicators as guide levels for most faults described in this work to obtain a magnitude of rock displacement, which is another method to estimate earthquakes magnitudes. So, the potential underestimation of the calculated Mw is recognized and acknowledged, and earthquake magnitudes should be considered as first order values.

4.1.4 Geothermal implications of newly identified crustal faults for the Aysén Region

The newly identified faults presented in Chapter 3 are important structures regarding geothermal exploitation resources, as crustal structures and their associated damage zones enhances rock permeability and controls the pathways for heat and hydrothermal fluid flow of geothermal systems in the crust (e.g. Sibson, 1994, 1996; Cox, 1999; Zhang et al., 2008; Sanchez et al., 2013; Perez-Flores et al., 2016). In this context, the Risopatrón Fault appears to be a major controller in the volcanic and hydrothermal fluid flow of geothermal systems in the Puyuhuapi area. The location of monogenetic cones, in addition to the several thermal hotsprings that are present in the proximities of the Puyuhuapi fiord, are located within and to the south of the footwall of the RF, while in the hanging wall they are absent. This suggests that at least part of the RF is acting as a barrier for fluid flow, impeding the volcanic activity to develop to the north of this structure. At the same time, and because of the spatial coincidence with the thermal hotsprings, this structure may act as a channel for hydrothermal fluid flow, with a footwall highly fractured that allows water to flow and come up to the surface. The high presence of carbonate cement in the footwall of this fault, and the presence of several silica and carbonate veins suggest that different sources of fluids, probably with different temperatures and from different depths are being channelized by this structure. It is widely accepted that fault zones may affect and modify drastically the permeability of the upper crust (e.g. Sibson, 1979; Chester and Logan, 1896). It is common that in most fault zones, the progressive deformation and fracturing of the damage host rock towards the main gouge zone causes and increase in the permeability for fluids, but abruptly decreases within the main gouge zone because of alteration of gouge to clay, impermeable minerals and cementation of the main fault plane (e.g. Chester and Logan,

1986). Said this, the main gouge zone with high presence of clay would act as a barrier for fluid flow, while the fault core (excepting the main gouge zone) and the damaged host rock would act as a permeable channel for geothermal and volcanic activity.

Additionally, understanding the location of crustal faults is important for geothermal energy exploitation, as hydraulic fracturing (fracking) processes can be expected to aid geothermal energy extraction due to the several reservoirs in the whole region. In this context, the new faults presented in this work must be considered as a potential geological hazard in any future energy development, as the high-pressure liquid injected into the host rock may enhance potential seismic activity on these structures. On the same way, identification of crustal faults can provide useful information for geothermal sources and their pathways towards the surface, as the geometry and architecture of upper crustal faults and their damage zones enhances rock permeability and controls the pathways for heat and hydrothermal fluid flow of geothermal systems in the upper crust (e.g. Sibson, 1994, 1996; Cox, 1999; Zhang et al., 2008; Sanchez et al., 2013; Perez-Flores et al., 2016). The Northern Patagonian Andes has abundant thermal springs that show potential for geothermal energy, so understanding fault networks and where potential seismic sources are located in this region is critical prior to exploration or development of these geothermal fields, in addition to better characterization of the seismic hazard.

4.1.5 Interpretation of thermochronolical ages from the Aysén Region

New reported AHe ages along the Exploradores Valley are interpreted as cooling ages of the Patagonian Batholith, as crystallization ages range from 100 to 15 Ma (e.g. Pankhurst et al., 1992). In general, young AHe ages (< 4 Ma) reflect progressive younger cooling ages towards the main trace of the LOFZ along the Exploradores

Valley, which can be explained by accelerated exhumation rates because of the fault activity or possible resetting of the apatite AHe system caused by an elevated crustal heat flow product of the slab-window. These results are different when compared with the recent work of Christeleit et al. (2017), where they interpret fast cooling signals from 10 to 5 Ma due to an increase in valley relief as a consequence of early glaciations in Patagonia.

Data reported in this work show cooling ages much younger than ages reported by Christeleit et al. (2017) and younger AHe ages at the eastern side of the LOFZ (1.5 ± 0.15 Ma) than samples located in the western side of the fault (2.0 ± 0.07 to 2.37 ± 0.32) which are at least 0.5 Ma older, suggesting post-Miocene accelerated exhumation rates, compatible with recent published Quaternary activity along the LOFZ above the subducted Chile ridge (De Pascale et al., 2021). This is also consistent with Georgieva et al. (2016) results, where they propose neotectonic activity along the Exploradores Valley represented by the Exploradores Fault, complemented with apatite (U-Th)/He cooling ages that are interpreted to reflect faulting since 2-3 Ma.

Additionally, Thomson et al (2002) reported several thermochronological data for the whole Aysén Region, where he defined different crustal blocks based on different exhumation rates revealed by zircon and apatite fission track ages. Interestingly, around Puyuhuapi and the Queulat Valley, both apatite and zircon fission track ages are very young (< 10 Ma), while 10-15 km towards the east these ages start to increase considerably. He estimated exhumation rates of > 0.5 – 1.3 mm / yr for this area. This means that in 1 Ma there is a removal of 0.5 to 1.3 km of rock by exhumation, resulting in erosion of any geological feature that it is within the first kilometer of the surface. Following this, and assuming a brittle-ductile transition depth of 10 km obtained from

microseismicity studies (e.g. Agurto-Detzel et al., 2014, Perez-Estay et al., 2020), any fault with presence of brittle fault rocks (i.e. fault breccia, cataclasite, gouge) would be eroded and erased from the surface in 8-20 Ma at maximum, being preserved only deep fault rocks formed by ductile deformation (i.e. mylonites). As described above, all faults characterized along the Queulat Valley and Puyuhuapi present evidence of brittle deformation with presence of fault breccias, cataclasites and gouge, without presence of mylonites. This means that all observed faults must be younger than 8-20 Ma, otherwise they would be eroded with no evidence at surface (Figure 4.1), assuming that the Thompson rates of exhumation were consistent during these times. This idea is supported by Georgieva et al. (2016) and Christeleit et al. (2017), where they show high exhumation rates since 8 Ma before present. This strongly suggests that newly documented faults presented in this work are young structures, thus presenting potential for rupturing and triggering shallow crustal earthquakes.

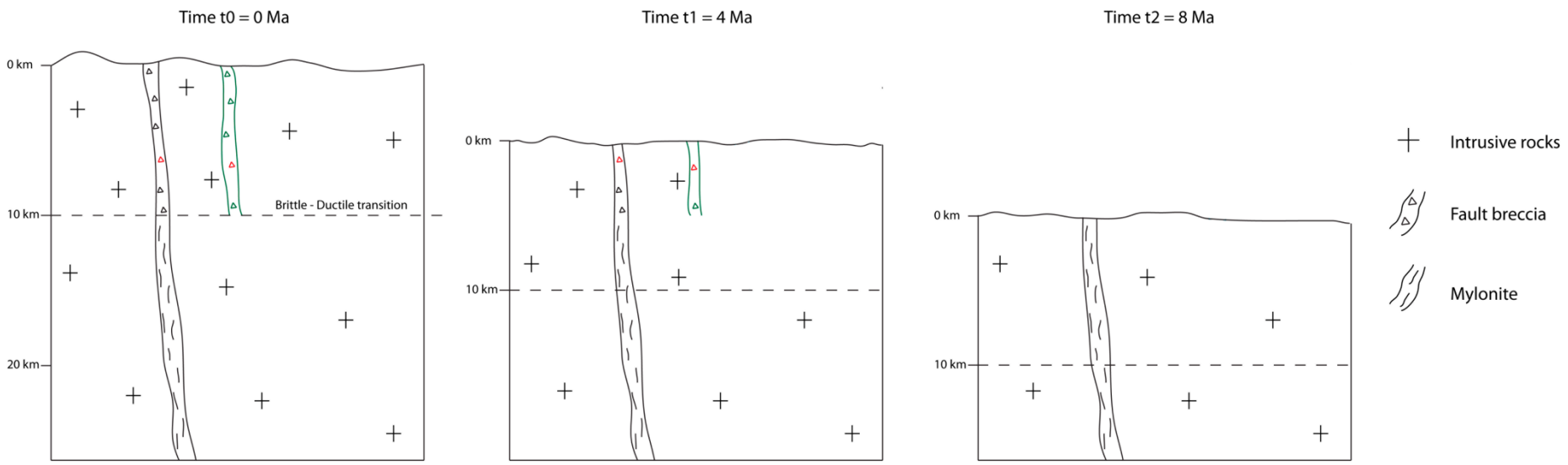

Figure 4.1. Schematic diagram showing exhumation and erosion effects on faults at the surface considering a maximum exhumation rate of > 1,3 mm/yr (or > 0,5 mm/yr; see text above) obtained from Thomson (2002). At time t0 = 0 Ma, a major regional crustal fault with brittle and ductile fault rocks is formed, together with a minor crustal with development of brittle fault rocks. As time passes (t1 = 4 (or 8) Ma), 5 km of rock is removed by exhumation, with the consequent erosion of the upper part of faults. At time t2 = 8 (or 20) Ma, 10 km of rock has been removed, eroding completely the brittle fault rocks with only the deep-formed mylonites preserved.

5 CONCLUSIONS

5.1 Main conclusions of this thesis

Using conventional fieldwork mapping methods, combined with remote sensing using satellite data, Structure from Motion (SfM) models and thermochronological data, I document and characterize previously unmapped crustal faults near the LOFZ and further inland in the Aysén Region. In addition, 8 new apatite (U-Th)/He (AHe) ages along the Exploradores Valley are reported in this work.

The Risopatrón Fault, located along the western side of the Lake Risopatrón, 10 km north of the Puyuhuapi town along the Carretera Austral, corresponds to a reverse, E-W striking fault with uncemented fault breccias, cataclasites and soft clay-rich gouges conforming a ~50 m wide fault core. This fault is proposed as potentially active due to the presence of uncemented fault rocks and recent microseismicity studies in the same location that show evidence for E-W reverse faulting.

The Queulat and Ventisquero faults, located at the southern flank of the Queulat Valley, ~25 km to the southeast of the Puyuhuapi town along the Carretera Austral, correspond to N-E to N-S, strike-slip faults with cores composed of soft clay-rich gouge and uncemented fault breccias. These faults are proposed as potentially active structures based on uncemented fault rocks, geomorphic and stratigraphic observations such as fissure fills and topographic offsets that suggest recent deformation.

The Bosque Muerto Fault, located 23 km to the west of Cerro Castillo Village along the Carretera Austral, corresponds to a reverse, NW striking fault characterized by

a soft clay-rich gouge fault core that cuts through volcanic. No kinematic indicators were found along the fault zone, but the coincidence of the fault trace with the marked topographic change between the hangingwall and footwall suggests a reverse motion for the Bosque Muerto Fault.

The Lago Esmeralda Fault, located 6 km to the southwest of the town of Cochrane along the Carretera Austral, corresponds to a N-S reverse fault characterized by soft clay-rich gouges. This fault is proposed as potentially active based on drainage pattern perturbation and elevated ridges to the west of the fault.

Based on the presence of uncemented (unhealed) fault rocks, geomorphological and stratigraphic observations, in addition to recent microseismicity studies in the Puyuhuapi area, I propose that these faults are potentially active, and thus correspond to sources of potential coseismic hazard for the Aysén Region. Regional kinematic solutions for these faults show a NNE principal shortening direction, consistent with previous proposed Quaternary principal shortening direction and recent crustal deformation models. Based on scaling relationships, these faults are capable of generating earthquakes of magnitudes up to at least Mw 6.5.

New thermochronological cooling ages along the Exploradores Valley reflect progressive younger cooling ages towards the main trace of the LOFZ. Notably, samples from the same elevation present younger AHe ages at the eastern side of the LOFZ (1.5 ± 0.15 Ma) than samples located at the western side of the fault (2.0 ± 0.07 to 2.37 ± 0.32), which are at least 0.5 Ma older. These results are consistent with recent published Quaternary activity along the LOFZ above the subducted Chile ridge (e.g. De Pascale et al., 2021). Additionally, anomalous AHe ages and vegetation perturbation near the Exploradores Fault suggest recent tectonic deformation along the Exploradores

Valley, similar to that proposed by Georgieva et al. (2016). This is consistent with wide rock fall deposits around the fault zone, with several angular blocks with sizes up to 25-m wide.

Many of the new faults first identified in this thesis or with better characterization due to work in the field including the Bosque Muerto and Exploradores faults help support existing theories that until this work had no field validation. Specifically, the Bosque Muerto and Exploradores faults helps support the Stevens Goddard and Fosdick (2019) theory that ridge subduction generates a thickened crustal along the leading edge of the obliquely subducted Chile ridge. Husson et al. (2019) argued that because no reverse structures were observed in the field to confirm this theory of thickened crust, it is unlikely that shortening is occurring in the upper crust here due to oblique subduction "because this would be difficult to miss in the field" (Husson et al., 2019). Thus, the documentation of new, young, reverse faults there support the results of Stevens Goddard and Fosdick (2019) and thus lead support to the theory that shortening is occurring in the upper crust in front of the northward migration of the subducted Chile Ridge. Additionally, in this same area, Scalabrino et al., (2010) suggest that negative tectonic inversion is taking place, i.e. that reverse faults are now operating as normal faults due to the subducted Chile Ridge. Because I only saw evidence for strike slip and reverse faults in this field surveys, especially from Cochrane to Cerro Castillo, results from this work do not support the idea for ongoing normal faulting (again in support of the Stevens Goddard and Fosdick Model (2019)).

In conclusion, new field mapping, geomorphic and stratigraphic observation, in addition with low temperature thermochronological ages, present evidence of previously unmapped structures that are compatible with the current stress regime in the Aysén

Region, and thus probably correspond to new sources of coseismic hazard for the region that should be considered and included in local and regional seismic hazard models. This study also demonstrates again the fundamental importance of first order primary fieldwork to constrain areas that are not well-characterized due to limited natural exposures due to vegetation and lack of roads. Certainly, future fieldwork in this region will reveal more structures here that will aid in the understanding of the Late-Cenozoic and Quaternary neotectonic framework and relationship with seismic and co-seismic geohazards.

Table 5.1. Summary of faults for the Aysén Region.

Fault Name	N (m)*	E (m)*	Style	Minimum Length (km)	Maximum Length (km)	Dip (degrees)	Seismogentic thickness (km)	Surface Width (Fault Zone – m)	Estimated Mw (Min)	Estimated Mw (Max)	Relevant Study
Rio Cuervo	4975422	653180	Dextral	30-40		60-90		313 - 852 m	**7.1**	**7.1**	Vargas et al. 2013; Villalobos 2017
Punta Cola	4972832	656374	Dextral-Reverse	15-20		80		242 - 1000 m	**6.2**	**6.2**	Vargas et al. 2013; Villalobos 2017
Los Palos	4979036	679416	Dextral	10-15		50-80		250 - 300 m	**6.2**	**6.5**	Vargas et al. 2013
Quitralco	4975422	653180	Dextral	15		75-85		?	**6.2**	**6.5**	Vargas et al. 2013; Villalobos 2017
Exploradores	4845378	655615	Reverse	~ 15		60-80		10 - 15 m			Georgieva et al. 2016
Cachet	4762482	632522	Dextral	~ 60		60-90		?			Georgieva et al. 2016
El Saltón	4734576	648547	Normal	~ 20		50-80		?			Georgieva et al. 2016
Rio Mañihuales (Riesco)	4943112	665636	Dextral-Reverse	~ 30		50-80		?	**7.1**	**7.1**	Thomson 2002; Vargas et al. 2013

Azul-Tigre (Queulat shear zone)	4999360	691310	Dextral-Reverse	15-200?		?		?			Thomson 2002; Cembrano et al. 2002
Risopatrón	5098231	698474	Reverse	3	18	50	10	150 m	**5.6**	**6.5**	This study
Queulat	5062607	701530	Dextral	1	3	80	10	5 m	**5.1**	**5.6**	This study
Mallines	5061445	704654	Reverse/ Strike-slip?	1	2	48	10	2 m	**5.1**	**5.4**	This study
Ventisquero	5061574	703756	Dextral-Reverse?	2	4	80	10	5 m	**5.3**	**5.8**	This study
Bosque Muerto	4888116	697624	Reverse	3	6	54	10	100 m	**5.6**	**6.0**	This study
Lago Esmeralda	4756878	680812	Reverse	2	6	45	10	50 m	**5.4**	**6.0**	This study
Exploradores	4845378	655615	Reverse	1	3	76	10	10 m	**5.1**	**5.6**	Georgieva et al 2016
Main LOFZ	41°S	47 °S	Dextral reverse	400	1200	vertical?	10	?	**7.1**	**8.7**	Vargas et al., 2013

Previous work

This work

5.2 Suggestions for future work regarding neotectonics in the Aysén Region

As presented in the sections above, recognition, mapping and characterization of crustal faults it is a first order input for seismic hazard models. Several suggestions or future work regarding active tectonics in the Patagonian Andes are outlined in Table 5.2.

Table 5.2. Suggestion for future work regarding neotectonics in the Aysén Region.

Suggestion for future work	What for?
Lidar Mapping	Lidar images are a very useful tool for mapping in areas with highly dense vegetation. Lidar mapping around new documented fault zones can provide better constrains on fault trace lengths and offset data to constrain geological fault slip rates for seismic hazard assessment.
Dating glacial deposits	Glacial deposits within fault zones or overthrusted by faults have been recognized in this work. Dating these deposits with OSL or cosmonuclides (e.g. Be10) can provide the age of these deposits and thus constrain post-glacial fault rupture events. In particular, fissure fills present in Queulat and Ventisquero faults should be dated to get information about timing of possible recent ruptures of these faults.
Trenching at faults	Risopatrón Fault should be revisited and excavated to obtain paleoseismological records and provide long-term slip rates and recurrence times. Trenching is suggested across the principal slip zone that corresponds to the main fault plane shown in chapter 3.

Marine geophysics	Given the high number of fiords and lakes in the Patagonian Andes, marine geophysics must be a first order tool for studying quaternary deformation around the LOFZ, as much of its surface trace is not exposed onshore. In this sense, high resolution bathymetry and reflection seismic profiles can provide evidence of recent sediment seafloor deformation and location of active fault traces.
Seismic network	Seismic network consisting of land stations and offshore station should be implemented for recording microseismicity in the region around fault zones to better constrain seismogenic depths and focal mechanisms of earthquakes.
Thermochronological dating and modelling	Low temperature thermochoronlogical data is a good geological tool to understand recent tectonic motions occurring shallow in the crust. Dating on opposite blocks (hanging and footwall) of each fault is suggested to detect relative uplift across faults. Modeling of cooling ages can give insight on the time-cooling path of rocks and thus reconstruct tectonic evolution of Patagonian landscape.

BIBLIOGRAPHY

Agurto-Detzel, H., Rietbrock, A., Bataille, K., Miller, M., Iwamori, H., Priestley, K. 2014. Seismicity distribution in the vicinity of the Chile Triple Junction, Aysén Region, southern Chile, J. South Am. Earth Sci., 51,1 –11, doi:10.1016/j.jsames.2013.12.011.

Allen, C. 1974. Geological criteria for evaluating seismicity, Bull. Geol. Soc. Am. 86, 1041-1057.

Anderson, J. 1979. Estimating the Seismicity from Geological Structure for seismic-risk studies, Bull Seism. Soc. Am. 69, 135-158.

Angermann, D., Klotz, J., Reigber, C. 1999. Space-geodetic estimation of the Nazca-South America Euler vector, Earth Planet. Sci. Lett., 171(3), 329–334, doi:10.1016/S0012-821X(99)00173-9.

Arancibia, G., Cembrano, J., Lavenu, A. 1999. Transpresión dextral y partición de la deformación en la Zona de Falla Liquiñe-Ofqui, Aisén, Chile (44-45ºS), Revista Geologica de Chile. http://dx.doi.org/10.4067/S0716-02081999000100001

Barrientos, S., Bataille, K., Aranda, C., Legrand, D., Baez, J.C., Agurto, H., Pavez, A., Gen-Rich, J., Vigny, C., Bondoux., F. 2007. Complex sequence of earthquakes in Fiorland, Southern Chile, in: Geosur 2007, International Geological Congress on the Southern Hemisphere. Santiago de Chile, pp. 19–20.

Beck, Jr., M. E., Rojas, C., Cembrano, J. 1993. On the nature of buttressing in margin-parallel strike-slip fault systems, Geology, 21(8), 755. doi:10.1130/0091-7613(1993)021<0755:otnobi>2.3.co;2

Caine, J., Evans, J., Forster, C. 1996. Fault zone architecture and permeability structure. Geology, 24(11), 1025-1028. doi: 10.1130/0091-7613(1996)024<1025:fzaaps>2.3.co;2

Caine, J., Minor, S., Grauch, V., Budahn, J., Keren, T. 2017. A comprehensive survey of faults, breccias, and fractures in and flanking the eastern Española Basin, Rio Grande rift, New Mexico. Geosphere, 13(5), 1566-1609. https://doi.org/10.1130/GES01348.1

Catalán, N., Bataille, K., Tassara, A., Araya, R. 2017. Depth-dependent geometry of margin-parallel strike-slip faults within oblique subduction zones. Andean Geology 44(1)79. doi: 10.5027/andgeoV44n1-a05.

Cembrano, J., Moreno, H. 1994. Geometría y Naturaleza contrastante del volcanismo cuaternario entre los 38°S y 46°S. ¿Dominios compresionales y tensionales en un régimen transcurrente?. Congreso Geológico Chileno No. 7, Actas, vol. 1, p.240-244, Concepción.

Cembrano, J., Hervé, F., Lavenu, A. 1996. The Liquiñe-Ofqui fault zone: a long-lived intra-arc fault system in southern Chile. Tectonophysics, 259, 55 –66, doi:10.1016/0040-1951(95)00066-6.

Cembrano, J., Lavenu, A., Reynolds, P., Arancibia, G., López, G., Sanhueza, A. 2002. Late Cenozoic transpressional ductile deformation north of the Nazca–South America–Antarctica triple junction, Tectonophysics, 354, 289–314, doi:10.1016/S0040-1951(02)00388-8.

Cembrano, J., Lara, L. 2009. The link between volcanism and tectonics in the southern volcanic zone of the Chilean Andes: A review. Tectonophysics, 471, 96-113, doi:10.1016/j.tecto.2009.02.038.

Chester, F., Logan, J. 1986. Implications for mechanical properties of brittle faults from observations of the Punchbowl fault zone, California. Pure and Applied Geophysics, 124(1-2), 79-106, doi: 10.1007/BF00875720.

Christeleit, E., Brandon, M., Shuster, D. 2017. Miocene development of alpine glacial relief in the Patagonian Andes, as revealed by low-temperature thermochronometry. Earth and Planetary Science Letters. 460: 152-153, doi: 10.1016/j.epsl.2016.12.019.

Cifuentes, I. 1989. The 1960 Chilean earthquakes. Journal of Geophysical Research Atmospheres 94(B1):665-680, doi: 10.1029/JB094iB01p00665.

Cisternas, M., Carvajal, M., Wesson, R., Ely, L. 2017. Exploring the Historical Earthquakes Preceding the Giant 1960 Chile Earthquake in a Time-Dependent Seismogenic Zone. BSSA, doi: 10.1785/0120170103.

De la Cruz, R., Suárez, M., Demant, A. 1994. Facies volcánicas del Mesozoico de Aisén (sector noreste), 44–47 Latitud Sur, Chile (Formaciones Ibáñez y Divisadero). Actas Congreso Geológico Chileno No. 7, Concepción 1, 27–31.

De Mets, C., Gordon, R., Argus, D. 2010. Geologically current plate motions, Geophys. J. Int., 181(1), 1–80, doi:10.1111/j.1365246X.2009.04491.x.

De Pascale, G.P., Froude, M., Penna, I., Hermanns, R, Sepúlveda, S., Moncada, D., Persico, M., Easton, G., Villalobos, A., Gutiérrez, F. 2021. Liquiñe-Ofqui's fast slipping intra-volcanic arc crustal faulting above the subducted Chile Ridge. Sci Rep 11, 7069 (2021). https://doi.org/10.1038/s41598-021-86413-w.

Dewey, J., Bird, J. 1970. Mountain belts and the new global tectonics. Journal Geophysical Research 75 (14): 2625-2647, doi: 10.1029/JB075i014p02625.

Dimaté, C., Drake, L., Yepez, H., Ocola, L., Rendon, H., Grünthal, G., Giardini, D. 1999. Seismic Hazard Assesment in the Northern Andes (PILOTO PROJECT). Annali Di Geofisica, Vol. 42, N.6, doi: 10.4401/ag-3787.

Dzierma, Y., Thorwart, M., Rabbel, W., Siegmund, C., Comte, D., Bataille, K., Iglesia, P., Prezzi, C. 2012. Seismicity near the slip maximum of the 1960 Mw 9.5 Valdivia

earthquake (Chile): Plate interface lock and reactivation of the subducted Valdivia Fracture Zone, Journal of Geophysical Research Atmospheres 117(B6):6312, doi: 10.1029/2011JB008914.

Forsythe, R., Nelson, E. 1985. Geological manifestations of ridge collision: evidence from the Golfo de Penas–Taitao basin, southern Chile. Tectonics 4 (5), 477–495, doi:10.1029/TC004i005p00477.

Georgieva, V., Melnick, D., Schildgen, T., Ehlers, T., Lagabrielle, Y., Enkelmann, E., Strecker, M. 2016. Tectonic control on rock uplift, exhumation, and topography above an oceanic ridge collision: Southern Patagonian Andes (47°S), Chile. Tectonics, 35, doi:10.1002/ 2016TC004120.

Gorring, M., Kay, S., Zeitler, P., Ramos, V., Rubiolo, D., Fernandez, M., Panza, J. 1997. Neogene Patagonian plateau lavas: Continental magmas associated with ridge collision at the Chile Triple Junction, Tectonics, 16, 1–17, doi:10.1029/96TC03368.

Guivel, C., Lagabrielle, Y., Bourgois J., Maury R.C., Fourcade S., Martin H., Arnaud N. 1999. New geochemical constraints for the origin of ridge-subduction-related plutonic and volcanic suites from the Chile Triple Junction (Taitao Peninsula and Site 862, LEG ODP141 on the Taitao Ridge). Tectonophysics, 311, 83–111, doi: 10.1016/S0040-1951(99)00160-2.

Guivel, C., Morata, D., Pelleter, E., Espinoza, F., Maury, R.C., Lagabrielle, Y., Polvé, M., Bellon, H., Cotten, J., Benoit, M., Suárez, M., De la Cruz, R. 2006. Miocene to Recent Patagonian basalts (46-47°S): geochronometric and geochemical evidence for slab tearing during ridge collision. Journal of Volcanology and Geothermal Research 149 (3-4): 346-370.

Guillaume, B., Gautheron, C., Simon-Labric, T., Martinod, J., Roddaz., M., Douville, E, 2013. Dynamic topography control on Patagonian relief evolution as inferred from low

temperature thermochronology, Earth Planet. Sci. Lett., 364, 157–167, doi:10.1016/j.epsl.2012.12.036.

Hervé, F., Pankhurst, R.J., Drake, R, Beck, M. Jr., Mpodozis, C. 1993. Granite generation and rapid unroofing related to strike-slip faulting, Aysén, Chile. Earth and Planetary Science Letters 1203-4:375-386.

Herve, F., Ota, Y. 1993. Fast Holocene uplift rates at the Andes of Chiloe, southern Chile. Andean Geology, Vol. 20 N°1, doi: 10.5027/andgeoV20n1-a02.

Herve, F. 1994. The southern Andes between 39 ° and 44°S latitude: the geological signature of a transpressive tectonic regime related to a magmatic arc. In: K.-J. Reutter, E. Scheuber and P.J. Wigger (Editors), Tectonics of the Southern Central Andes. Springer, Berlin, pp. 243-248.

Hervé, F., Aguirre, L., Godoy, E., Massone, H., Morata, D., Pankhurst, R., Ramírez, E., Sepúlveda, V., Willner, A. 1998. Nuevos antecedentes acerca de la edad y las condiciones P-T de los complejos metamórficos en Aysén. In Congreso Latinoamericano de Geología, No. 10 y Congreso Nacional de Geología Económica, No. 6, Actas 2: 134-137. Buenos Aires.

Hervé, F., Faúndez, V., Calderón, M., Massonne, H., Willner, A. 2007. Metamorphic and plutonic basement complexes. In: The Geology of Chile (Moreno, T. and Gibbons, W. Eds.). The Geology of Chile. The Geological Society, of London, p. 5-19.

Hervé, F., Pankhurst, R., Fanning, M., Calderon, M., Yaxley, G. 2007. The South Patagonian batholith: 150 my of granite magmatism on a plate margin. Lithos, 97(3-4), 373–394, doi:10.1016/j.lithos.2007.01.007.

Hervé, F., Calderón, M, Faúndez, V. 2008. The metamorphic complexes of the Patagonian and Fuegian Andes. Geologica Acta, Vol. 6 N°1, p.43-53.

Hildreth, W., Moorbath, S. 1998. Crustal contributions to arc magmatism in the Andes of Central Chile. Contributions to Mineralogy and Petrology, Vol. 98 N°4, p.455-489, doi: 10.1007/BF00372365.

Hulton, N., Purves, R., McCulloch, R., Sugden, D., Bentley, M. 2002. The Last Glacial Maximum and deglaciation in southern South America, Quat. Sci. Rev., 21(1), 233–241, doi:10.1016/S0277-3791(01)00103-2.

Husson, L., Guillaume, B., Martinod, J. 2019. Multichronometer thermochronologic modeling of migrating spreading ridge subduction in southern Patagonia. Geology. https://doi.org/10.1130/G46629C.1

Jalowitzki, T., Gervasoni, F., Conceicao, R., Orihashi, Y., Bertotto, G., Sumino, H., Schilling, M., Nagao, K., Morata, D., Sylvester, P. 2017. Slab-derived components in the subcontinental lithospheric mantle beneath Chilean Patagonia: Geochemistry and Sr-Nd-Pb isotopes of mantle xenoliths and host basalt, Lithos; 292-293; 11-2017; 179-197, doi: 10.1016/j.lithos.2017.09.008.

Johnson, K., Nissen, E., Saripalli, S., Arrowsmith, J., McGarey, P., Scharer, K., Williams, P, Blisnuik, K. 2014. Rapid mapping of ultrafine fault zone topography with structure from motion. Geosphere (2014) 10 (5): 969-986, doi: 10.1130/GES01017.1.

Lagabrielle, Y., Scalabrino, B., Suárez, M., J, Ritz. 2010. Mio-Pliocene glaciations of Central Patagonia: New evidence and tectonic implications, Andean Geol., 37(2), 276–299.

Lange, D., Cembrano, J., Rietbrock, A., Haberland, C., Dahm, T., Bataille, K. 2008. First seismic record for intra-arc strike-slip tectonics along the Liquine-Ofqui fault zone at the obliquely convergent plate margin of the Southern Andes. Tectonophysics, 455(1-4), 14–24, doi:10.1016/j.tecto.2008.04.014.

Lara, L., Cembrano, J., Lavenu, A. 2008. Quaternary Vertical Displacement along the Liquiñe-Ofqui Fault Zone: Differential Uplift and Coeval Volcanism in the Southern Andes?. International Geology Review, Number 11, 975-993, doi: 10.2747/0020-6814.50.11.975.

Lavenu, A., Cembrano, J. 1999. Compressional and traspressional-stress pattern for Pliocene and Quaternary brittle deformation in fore arc and intra-arc zones (Andes of Central and Southern Chile). Journal of Structural Geology 21, 1669–1691, doi: 10.1016/S0191-8141(99)00111-X.

Legrand, D., Barrientos, S., Bataille, K., Cembrano, J, Pavez, A. 2011. The fluid-driven tectonic swarm of Aysén Fjord, Chile (2007) associated with two earthquakes (Mw 6.1 and Mw 6.2) within the Liquiñe-Ofqui Fault Zone. Continental Shelf Research, 31(3-4), 154-161, doi: 10.1016/j.csr.2010.05.008.

López-Escobar, L., Cembrano, J., Moreno, H. 1995. Geochemistry and tectonics of the Chilean Southern Andes basaltic Quaternary volcanism (37-46°S). Revista Geológica de Chile. Vol. 22 (2): 219-234, doi:10.5027/andgeoV22n2-a06.

Marrett, R., Allmendinger, R. 1990. Kinematic analysis of fault-slip data. Journal of structural geology, 12(8), 973-986, doi: 10.1016/0191-8141(90)90093-E.

Matsuda, T. 1977. Estimation of future destructive earthquakes from active faults on land in Japan, J.Phys. Earth, Suppl. *25* 795-855.

Mercer, J.H. 1983. Cenozoic glaciation in the southern hemisphere. Annual Reviews of Earth and Planetary Science 11: 99-132, doi: 10.1146/annurev.ea.11.050183.000531.

Melnick, D., Bookhagen, B., Strecker, M., Echtler, H. 2009. Segmentation of megathrust rupture zones from fore-arc deformation patterns over hundreds to millions of years, Arauco peninsula, Chile. Journal of Geophysical Research, 114, B01407, doi:10.1029/2008JB005788.

Miller, M., Bataille, K., Priestley, K., Iwamori, H., Calisto, I. 2005. Seismic imaging of a subducted ridge, southern Chile, paper presented at AGU Fall Meeting San Francisco, U.S., Dec 01.

Pankhurst, R., Hervé, F., Rojas, L., Cembrano, J. 1992. Magmatism and Tectonics in continental Chiloé, Chile (42°-42° 30'). Tectonophysics, Vol. 205, Issues 1–3, p. 283-294, doi: 10.1016/0040-1951(92)90431-5.

Pankhurst, R., Leat, P., Sruoga, P., Rapela, C., Márquez, M., Storey, B., Riley, T. 1998. The Chon Aike province of Patagonia and related rocks in West Antarctica: A silicic large igneous province. Journal of Volcanology and Geothermal Research, Vol. 81, N°1, p: 113-136, doi: 10.1016/S0377-0273(97)00070-X.

Pankhurst R., Weaver, S., Hervé, F., Larrondo, P. 1999. Mesozoic-Cenozoic evolution of the North Patagonian Batholith in Aysén, Southern Chile. Journal of the Geological Society, Vol. 156(4):673-694, doi: 10.1144/gsjgs.156.4.0673.

Parada, M., Lahsen, A., Palacios, C., 2001. Ages and geochemistry of Mesozoic-Eocene back–Arc volcanic rocks in the Aysén Region of the Patagonian Andes, Chile. Revista Geológica de Chile 28 (1), 25–46, doi: 10.4067/S0716-02082001000100002.

Pardo-Casas, F., Molnar, P. 1987. Relative Motion of the Nazca (farallon) and South American Plates Since Late Cretaceous Time. Tectonics 6, 233–248, doi: 10.1029/TC006i003p00233.

Perez, A., Ruiz, J., Vargas, V., Rauld, R., Rebolledo, S., Campos, J. 2013. Improving seismotectonics and seismic hazard assessment along the San Ramón Fault at the eastern border of Santiago city, Chile, Natural Hazards, Volume 69(ISSN 0921-030X), doi: 10.1007/s11069-013-0908-3.

Perez-Estay, N., Yáñez, G., Roquer, T., Cembrano, J., Valdenegro, P., Aravena, D., Arancibia, G., Morata, D. 2020. Seismicity in a transpressional volcanic arc: the Liquiñe-Ofqui Fault

System in the Puyuhuapi area, Southern Andes, Chile (44°S). Tectonics, doi:10.1029/2020TC006391.

Pérez-Flores, P., Cembrano, J., Sánchez-Alfaro, P., Veloso, E., Arancibia, G., Roquer, T. 2016. Tectonics, magmatism and paleo-fluid distribution in a strike-slip setting: Insights from the northern termination of the Liquiñe–Ofqui fault System, Chile. Tectonophysics, doi:10.1016/j.tecto.2016.05.016.

Ramos, V., Ghiglione, M., 2008. Tectonic Evolution of the Patagonian Andes. Developments in Quaternary Sciences, 11: 57-71, doi: 10.1016/S1571-0866(07)10004-X.

Ramos, V., Kay, S., 1992. Southern Patagonian plateau basalts and deformation - backarc testimony of ridge collisions, Tectonophysics, 205(1-3), 261–282, doi: 10.1016/0040-1951(92)90430-e.

Rosenau, M., Melnick, D., Ecthler, H. 2006. Kinematic constraints on intra-arc shear and strain partitioning in the southern Andes between 38 degrees S and 42 degrees S latitude, Tectonics, 25, TC4013, doi: 10.1029/2005TC001943.

Ruiz, S., Moreno, M, Melnick, D., Del Campo, F., Poli, P., Báez, J., Leyton F., Madariaga, R. 2017. Reawakening of large earthquakes in south central Chile: The 2016 *Mw* 7.6 Chiloé event, Geophysical Research Letters, doi: 10.1002/2017GL074133.

Sánchez, P., Pérez-Flores, P., Arancibia, G., Cembrano, J. 2013. Crustal deformation effects on the chemical evolution of geothermal systems: the intra-arc Liquiñe–Ofqui fault system, Southern Andes, International Geology Review, doi: 10.1080/00206814.2013.775731.

Scalabrino, B., Lagabrielle, Y., Malavieille, J., Domínguez, S., Melnick, D., Espinoza, F., Suárez, M., Rossello, E. 2010. A morphotectonic analysis of central Patagonian Cordillera: Negative inversion of the Andean belt over a buried spreading center?. Tectonics 29, TC2010, doi: 10.1029/2009TC002453.

Sepulveda et al. 2010. Landslides induced by the April 2007 Aysén Fjord earthquake, Chilean Patagonia, Landslides 7(4):483-492, doi: 10.1007/s10346-010-0203-2.

Sibson, R., 1977. Fault rocks and fault mechanisms. Journal of the Geological Society, 133(3), 191-213, doi: 10.1144/gsjgs.133.3.0191.

Sibson, R., 2003. Thickness of the seismic slip zone. Bulletin of the Seismological Society of America, Vol. 93, No. 3, pp. 1169–117.

Siegfield, G., Cembrano, J., Lara, L. 2016. Transtension driving volcano-edifice anatomy: Insights from Andean transverse-to-the-orogen tectonic domains. Quaternary International, doi: 10.1016/j.quaint.2016.01.002.

Stevens Goddard, A., Fosdick, J., 2019. Multichronometer thermochronologic modeling of migrating spreading ridge subduction in southern Patagonia. Geology, https://doi.org/10.1130/G46091.1

Thomson, 2002. Late Cenozoic geomorphic and tectonic evolution of the Patagonian Andes between latitudes 428S and 468S: An appraisal based on fission-track results from the transpressional intra-arc Liquiñe-Ofqui fault zone, Geol. Soc. Am. Bull., 114(9), 1159–1173, doi:10.1130/0016-7606(2002)114<1159:LCGATE>2.0.CO;2.

Thomson, S., Brandon, M., Tomkin, J., Reiners, P., Vásquez, C., Wilson, N. 2010. Glaciation as a destructive and constructive control on mountain building, Nature, 467, 313-317, doi: 10.1038/nature09365.

Ton-That, T., Singer, B., Mörner, N., 1999. Datación de lavas basálticas por 40 Ar/39 Ar y geología glacial de la región del lago Buenos Aires, Provincia de Santa Cruz, Argentina, Rev. Asoc. Geol. Argent., 54(4), 333–352.

Vargas, G., Rebolledo, S., Sepúlveda, S., Lahsen, A., Thiele, R., Townley B., Padilla, C., Rauld, R., Herrera, M.J., Lara, M. 2013. Submarine earthquake rupture, active faulting and

volcanism along the major Liquiñe-Ofqui Fault Zone and implications for seismic hazard assessment in the Patagonian Andes. Andean Geology, Vol. 40 (1), 141-171, doi: 10.5027/andgeoV40n1-a07.

Wang, K., Hu, Y., Bevis, M., Kendrick, E., Smalley Jr, R., Barriga, R., Lauría, E. 2007. Crustal motion in the zone of the 1960 Chile earthquake: Detangling earthquake-cycle deformation and forearc-sliver translation. Geochemistry, Geophysics, Geosystems, doi: 10.1029/2007GC001721.

Wesnousky, 1984. Integration of geological and seismological data for the analysis of seismic hazarsd. A case study of Japan. BSSA, Vol. 74 (2): 687-708.

Wesnousky, 1986. Earthquakes, Quaternary Faults and Seismic Hazard in California. Journal of Geophysical research, doi: 10.1029/JB091iB12p12587.

APPENDIX I

Author's congress participations

Appendix I.I. *Abstract presented in the Chilean Geological Congress, held during 18-23 of November 2018 in Concepción, Chile.*

XV CONGRESO GEOLÓGICO CHILENO
"GEOCIENCIAS HACIA LA COMUNIDAD"
18 AL 23 DE NOVIEMBRE DE 2018, UNIVERSIDAD DE CONCEPCIÓN, CONCEPCIÓN, CHILE

Crustal fault characterization and seismic hazard and geothermal assessment In Aysén, Patagonian Andes, Chile

Mario Persico[1], Gregory De Pascale[1], Daniel Moncada[1]

(1) Geología, Facultad de Ciencias Físicas y Matemáticas, Universidad de Chile

The Northern Patagonian Andes constitutes part of one of the most geologically active orogens in the world, with the longest active volcanic chain and the greatest recorded earthquake in history (Mw 9.5 Valdivia 1960 Earthquake). In 2007, a seismic swarm with magnitudes up to Mw 6.2 occurred in the Aysén fiord associated to submarine crustal faults related to the Liquiñe-Ofqui Fault Zone (LOFZ), triggering earthquakes and landslides that induced a tsunami, causing 12 deaths. However, very little is known about the active tectonic framework, and relation with these fault and regional geothermal systems and the potential seismogenic crustal structures in the Aysén region, mainly due to dense vegetation and widespread Quaternary volcanic and glacial cover. Using conventional fieldwork mapping methods, combined with remote sensing using satellite data and Structure from Motion (SfM) models, we document and characterize six previously un-identified crustal faults near the LOFZ in Aysén. Based on geomorphological observations and fault rock characteristics, such as deflected rivers and cataclasite, fault breccia and gouge, we propose that these faults, which are reverse or strike slip are potentially active, and thus crustal sources of coseismic hazard for the region. Based on scaling relations, these faults are capable of generating earthquakes of magnitudes up to Mw 6.0-7.0, in addition to accommodating crustal deformation during late Cenozoic evolution of the Patagonian Andes. Further work here will allow a better understanding and characterization of these faults, however these should be included in local and regional seismic hazard and fault rupture models. Because of the coincidence of these faults (e.g. Queulat and Ristopatrón Faults) with evidence of geothermal systems (thermal springs, etc), work on these faults may also allow better insight to the geothermal systems here.

This work was funded by CEGA and Fondecyt Iniciacion Project number 11160038: Quantifying Seismic Hazard Along Chile´s fastest slipping crustal Fault, the Liquiñe-Ofqui Fault Zone (LOFZ), Patagonia.

Appendix I.II. *Abstract presented in Cities on Volcanoes congress, held during 20-25 of November 2016 in Puerto Varas, Chile.*

Abstract for S3.1 - Volcano-tectonic processes from basement to surface: control on activity and hazard, in Cities On Volcanoes, Puerto Varas 2016

Title: Active tectonics along the Liquiñe--Ofqui Fault Zone and influence on Volcano distribution in Chile's Southern Volcanic Zone (SVZ)

Authors: **Mario Persico**, Gregory De Pascale, Daniel Moncada

Abstract

The ~1200-km-long Liquiñe-Ofqui Fault Zone (LOFZ) is a crustal system of dextral faults that appear to accommodate northward migration of the Chiloe Microplate (CM), and is associated with the Chilean Southern Volcanic Zone (SVZ), however little is known about the LOFZ's Holocene activity. Although major volcanoes are well-documented along the LOFZ, a number of smaller eruptive centres are not well documented due to the scale of regional geological and geomorphic mapping (oftentimes at 1:1,000,000). Here we map distribution of major (e.g. stratovolcanoes) and minor (e.g. monogenetic cones) along what appear to be active traces of the LOFZ. Our new mapping shows a coincidence of volcanic centres along the LOFZ and helps provide insight into active structural control on distribution of volcanic centres in the SVZ. Based on our new mapping a number of clearly post-glacial volcanic centres exhibit permanent deformation due to the active tectonics, which demonstrates that: a) LOFZ is active, b) the LOFZ is important source of seismic hazard, c) most monogenetic cones are located proximal to the LOFZ and decrease in frequency away from active traces of the fault zone, and d) the LOFZ is perhaps a local trigger (i.e. seismic triggering during large earthquakes) for SVZ eruptions and a major structural control on distribution of volcanic centres (e.g. with local pull-apart basins between strands of the fault facilitating monogenetic cone development). Further mapping and field investigations here will further unravel the interplay between active crustal tectonics in Southern Chile, earthquakes, and the SVZ.

Appendix I.III. *Poster presented in Cities on Volcanoes congress, held during 20-25 of November 2016 in Puerto Varas, Chile.*

Active tectonics along the Liquiñe-Ofqui Fault Zone (LOFZ) and influence on volcano distibution in Chile's Southern Volcanic Zone (SVZ)

Mario Persico [1,2], Gregory De Pascale [1,2], Daniel Moncada [1,2]

(1) Facultad de Ciencias Físicas y Matemáticas, Depto. de Geología, Universidad de Chile, Plaza Ercilla 803, Santiago, Chile
(2) Centro de Excelencia en Geotermia de Los Andes (CEGA), Universidad de Chile, Plaza Ercilla 803, Santiago, Chile
email: mcaa.mario07@gmail.com, snowyknight@gmail.com, dmoncada@ing.uchile.cl

INTRODUCTION AND METHODOLOGY

The ~1200-km-long Liquiñe-Ofqui Fault Zone (LOFZ) is a system of crustal dextral faults that appear to accommodate northward migration of the Chiloe Microplate (CM), associated with the Chilean Southern Volcanic Zone (SVZ) (Stern, 2004; Cembrano and Lara, 2009) and is also associated with high enthalpy potential and related geothermal prospects, **however little is known about the LOFZ's Holocene and postglacial (~17 ka BP) activity.** A number of smaller eruptive centres are not well documented due to the scale of regional mapping (oftentimes at 1:1,000,000). Here we map distribution of major (e.g. stratovolcanoes) and minor (e.g. monogenetic cones - oftentimes primative in composition) along what appear to be active traces of the LOFZ. Also, fluid inclusion samples were collected near Puyuhuapi to explore PTX.

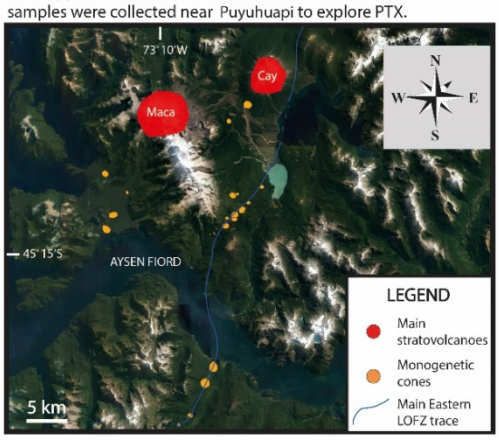

Maca and Cay stratovolcanoes and minor monogenetic cones (>20 here) in relation with LOFZ faults near Aysen Fiord. Note lack of cones east of LOFZ.

RESULTS AND DISCUSSION

Our new mapping shows a coincidence of minor volcanic centres along the LOFZ, supports previous observations (e.g. Cembrano and Lara 2009), and helps provide insight into active structural control on distribution of volcanic centres in the SVZ. This demonstrates that: a) LOFZ is a major structural boundary with no monogenetic cones or stratovolcanoes to the east of the fault zone (except Hudson in slab window), b) most monogenetic cones are proximal to the LOFZ and decrease in frequency away from LOFZ, c) the LOFZ perhaps an important source of seismic hazard d) the LOFZ is perhaps a local trigger (i.e. seismic triggering during large earthquakes) for SVZ eruptions and a first-order structural control on distribution of volcanic eruptive centres. Further mapping (including submarine volcanoes in fiords), dating and analysis of the cones, and field investigations here will further unravel the interplay between active crustal tectonics and fluid flow (e.g. PTX - which at Puyuhuapi, fluid inclusions register at least 200°C at the surface) along LOFZ faults in Southern Chile, megathrust earthquakes, and the SVZ.

Distribution of volcanic centres of the Southern Volcanic zone (SVZ) in relation with the main trace of the Liquiñe-Ofqui Fault Zone (LOFZ).

ACKNOWLEDGEMENTS

This work was funded by CEGA, FCFM (UCHILE) AND CONICYT (Chile) through the research grant to De Pascale: Fondecyt 11160038.

REFERENCES

Cembrano, J., Lara, L., 2009. The link between volcanism and tectonics in the southern volcanic zone of the Chilean Andes: a review. Tectonophysics, v. 471 n. 1&2, p. 96-113.
Stern, C.R., 2004. Active Andean volcanism: its geologic and tectonic setting. Revista Geologica de Chile, v. 31, n. 2, p. 161-206.

Appendix I.IV. *Abstract presented in the PATA meeting, held during 13-16 of November 2017 in Blenheim, New Zealand.*

8th International INQUA Meeting on Paleoseismology, Active Tectonics and Archeoseismology (PATA), 13 – 16 November, 2017, New Zealand

INQUA Focus Group Earthquake Geology and Seismic Hazards

New school faults and seismic hazard, guilty (i.e. active) until proven innocent (i.e. inactive)?

De Pascale, Gregory (1), Araya, Jose (1), ***Persico, Mario*** *(1), Sandoval, Francisca (1), Medina, Javiera (1), Sepulveda, Sergio (1), Moncada, Daniel (1)*

(1) Department of Geology, University of Chile, Plaza Ercilla 803, Santiago, Chile. snowyknight@gmail.com.

Abstract: Of primary importance in Seismic Hazard Assessments (SHA) is finding, mapping, and then investigating faults in order to determine if they are "active", and potential seismic sources. Thus, faults are considered innocent (i.e. inactive) until proven guilty (i.e. active). Recent evidence demonstrates that lack of evidence of activity (or mapping) due to lack of investigation along these faults does not mean the faults are inactive. By comparing all identified faults in three regions, we find that 71% of faults in California, 24% of faults in New Zealand, and 5% of faults in Chile are considered "active". Thus, in the best studied area (California), most of the faults are active. Thus to answer the question in the title, perhaps yes it is better to consider all faults in tectonically active zones guilty (active) until proven inactive (not guilty) and we should invest in mapping to best understand seismic sources.

Key words: Active Faults, Inactive Faults, New Zealand, California, Chile

APPENDIX II

Field photographs of fault outcrops

Figure II.1. Field photograph looking south of the Risopatrón Fault showing secondary minor faults with brown-yellowish thin gouge layers in the footwall damage zone. Note grey pencil for scale.

Figure II.2. Field photograph looking south of the damage zone in the footwall of the Risopatrón Fault showing a highly foliated fault breccia. Note fieldbook for scale.

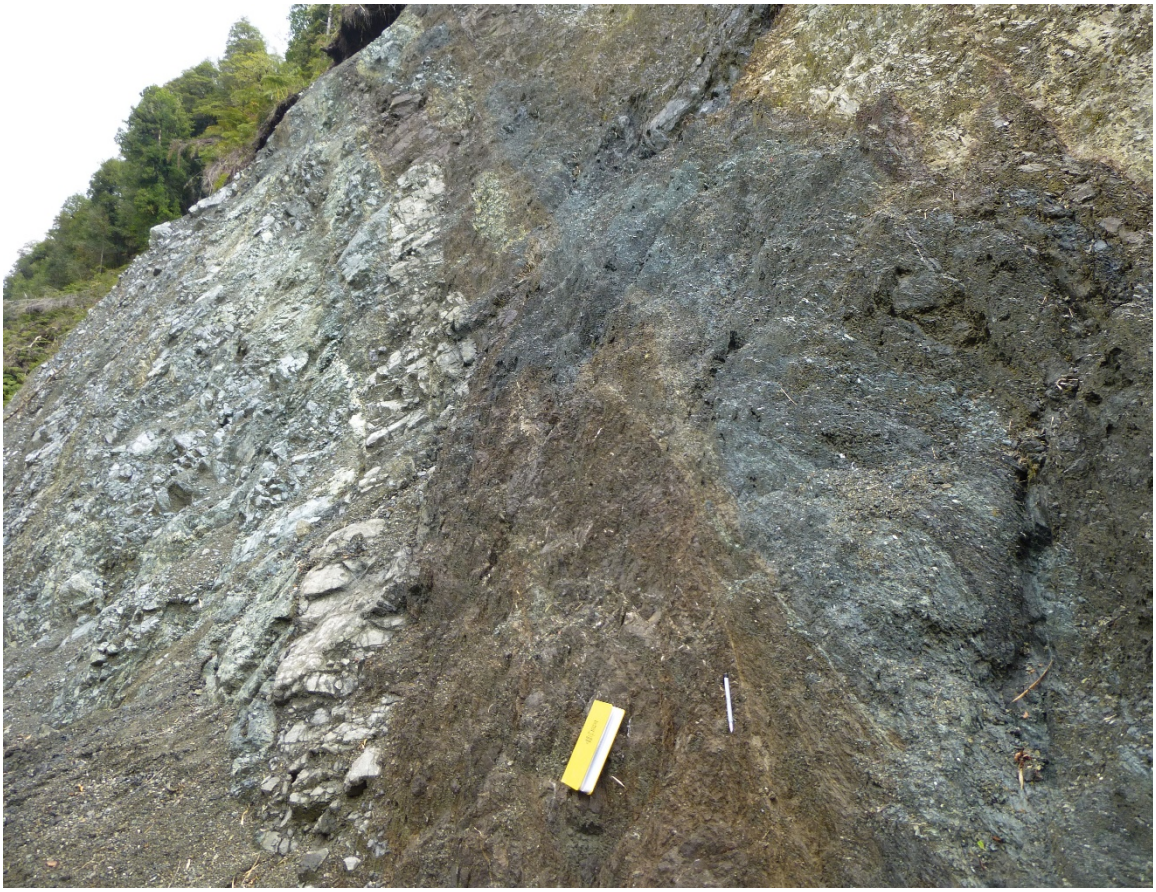

Figure II.3. Field photograph looking south of the damage zone in the footwall of the Risopatrón Fault showing a blue gouge layer in contact with a brown sheared dyke. Note fieldbook and pencil for scale.

Figure II.4. Field photograph looking south of the damage zone in the footwall of the Risopatrón Fault showing the contact between fault breccia and and gouge blue layer to the right with uncemented deposits to the left. Roadwall is 2 meters high for scale.

Figure II.5. Field photograph looking south of the damage zone in the hanging wall of the Risopatrón Fault, showing a fault breccia with angular fragments with sizes ranging 1 and 8 cm. Note fieldbook for scale.

Figure II.6. Field photograph looking south of the damage zone in the footwall of the Risopatrón Fault, showing the contact between the main fault plane and the damage zone (black unit) in the hanging wall. Note red backpack at the left for scale.

Figure II.7. Field photograph looking south of the Queulat fault plane showing the main fault plane with a 2 cm-thick yellowish gouge layer. Note pencil for scale.

Figure II.8. Field photograph looking south of the Bosque Muerto fault plane. The shear zone is 50-cm thick.

Figure II.9. Field photograph of the Bosque Muerto fault plane, showing grey and black gouge layers of the main fault plane. Note pencil for scale.

Figure II.10. Field photograph looking south showing the west side of the Bosque Muerto Fault. Note how towards the west (right of the photo) the rock gets much less fractured. Also note the reddish vein that is offset to the east (left of the photo).

Figure II.11. Field photograph of the Lago Esmeralda Fault plane. The white-greyish layer corresponds to a fault gouge layer of 2-3 cm thick.

APPENDIX III

Field photographs from Exploradores Valley

Figure III.1. Field photograph of intrusive dioritic outcrops of the Patagonian Batholith along the Exploradores Valley. Note person for scale.

Figure III.2. Field photograph of grandioritic intrusive along the Exploradores Valley, affected by subhorizontal joints. Note person for scale.

Figure III.3. Field photograph of intrusive contact between dioritic and granodioritic intrusive units along the Exploradores Valley.

Figure III.4. Drone photograph looking east of the Exploradores Fault along the southern side of the Exploradores Valley.

APPENDIX IV

Hand sample description from Exploradores Valley units used for apatite (U-Th)/He thermochronological analysis

SAMPLE NAME
MB-2

Description
Holocrystalline, medium-grained, leucocratic colored rock with homogeneous structure and planar fabric, with oriented quartz and biotite crystals. The mineralogy is composed of Quartz, Biotite and K-Feldspar in order of abundance. There is uncertainty if the fabric is magmatic or metamorphic (foliation) in origin.

SAMPLE NAME
MB-3

Description
Holocrystalline, medium-grained, mesocratic colored rock with homogeneous structure and isotropic fabric. The mineralogy is composed of Pyroxene, Plagioclase and Amphibole in order of abundance.

SAMPLE NAME
MB-4

Description
Holocrystalline, fine-grained, mesocratic colored rock with homogeneous structure and isotropic fabric. The mineralogy is composed Plagioclase, Pyroxene, Biotite and Quartz in order of abundance.

SAMPLE NAME
MB-6

Description
Matrix-supported breccia, with angular clasts with sizes between 5-10 mm and 5 cm in diameter of dioritic composition. It seems to be a fault-breccia.

SAMPLE NAME
MB-7

Description
Holocrystalline, medium-grained, mesocratic colored rock with homogeneous structure and isotropic fabric. The mineralogy is composed of Plagioclase, Amphibole, Biotite, Quartz and K-Feldspar in order of abundance.

SAMPLE NAME
MB-8

Description
Holocrystalline, medium-grained, leucocratic colored rock with homogeneous structure and isotropic fabric. The mineralogy is composed of Quartz, Plagioclase, K-Feldspar, Amphibole and Biotite in order of abundance.

SAMPLE NAME
MB-11

Description
Holocrystalline, medium-grained, leucocratic colored rock with homogenous structure and isotropic fabric. The mineralogy is composed of Quartz, Biotite, Amphibole and K-Feldspar in order of abundance.

SAMPLE NAME
MB-12

Description
Holocrystalline, medium-grained, leucocratic colored rock with mafic cumulates of ~3 cm diameter and isotropic fabric. The mineralogy is composed of Quartz, Plagioclase and Biotite in order of abundance. When crushed, mafic cumulates where removed.

SAMPLE NAME
MB-13

Description
Holocrystalline, inequigranular, leucocratic colored rock with coarse grains of plagioclase and fine grains of quartz, biotite and amphibole. In order of abundance, the mineralogy is composed of Biotite, Plagioclase, Quartz and Amphibole.

SAMPLE NAME
MB-14

Description
Holocrystalline, medium-grained, mesocratic colored rock with nodules of quartz surrounded by biotite crowns and an isotropic fabric. The mineralogy is composed of Plagioclase, Biotite, Amphibole and Quartz in order of abundance.

SAMPLE NAME
MB-15

Description
Holocrystalline, medium-grained, leucocratic colored rock with mafic cumulates, and isotropic fabric. The mineralogy is composed of Quartz, Amphibole, Plagioclase and K-feldspar in order of abundance.

APPENDIX V

Apatite U-Th-He ages from Exploradores Valley

Table V.1. Simplified U-Th-He data in apatites from samples of the Exploradores Valley. Data from Julie Fosdick.

Crystal No	Sample	Sample #	He date	2 sig unc.	He date (filtered)	2 sig unc.	Error weighted mean	2sigma unc.	Ft	Th/U	eU	Rs
			Ma	Ma	Ma	Ma	Ma	Ma			ppm	microns
GDP_MB-4_ap1	MB-4	6	2.50	0.16	2.50	0.16	**2.37**	**0.15**	0.66	2.63	125.3	42.09
GDP_MB-4_ap2	MB-4	6	2.41	0.12	2.41	0.12	**0.00**	**0.00**	0.64	1.19	98.7	32.53
GDP_MB-4_ap3	MB-4	6	2.39	0.27	2.39	0.27	**0.00**	**0.00**	0.60	1.72	72.7	35.41
GDP_MB-4_ap4	MB-4	6	2.45	0.21	2.45	0.21	**0.00**	**0.00**	0.62	1.55	60.3	37.91
GDP_MB-4_ap5	MB-4	6	2.08	0.17	2.08	0.17	**0.00**	**0.00**	0.70	1.91	55.3	47.88
GDP_MB-2_ap1	MB-2	4	2.30	0.06	2.30	0.06	**2.04**	**0.07**	0.78	0.08	44.9	62.02
GDP_MB-2_ap2	MB-2	4	1.77	0.08	1.77	0.08	**0.00**	**0.00**	0.72	0.04	39.4	50.03
GDP_MB-2_ap3	MB-2	4	2.09	0.08	2.09	0.08	**0.00**	**0.00**	0.77	0.08	34.5	59.30
GDP_MB-2_ap4	MB-2	4	1.91	0.11	1.91	0.11	**0.00**	**0.00**	0.71	0.09	21.3	48.06
GDP_MB-2_ap5	MB-2	4	1.84	0.09	1.84	0.09	**0.00**	**0.00**	0.74	0.06	32.5	52.39
GDP_MB3_ap1	MB3	5	2.49	0.34	0.00	0.00	**2.21**	**0.32**	0.76	4.06	56.3	62.20
GDP_MB3_ap2	MB3	5	1.60	0.23	1.60	0.23	**0.00**	**0.00**	0.83	1.53	37.9	86.90
GDP_MB3_ap3	MB3	5	2.58	0.27	0.00	0.00	**0.00**	**0.00**	0.76	3.66	55.1	62.95
GDP_MB3_ap4	MB3	5	3.53	0.44	3.53	0.44	**0.00**	**0.00**	0.69	3.68	64.0	48.20
GDP_MB3_ap5	MB3	5	2.58	0.26	2.58	0.26	**0.00**	**0.00**	0.80	3.10	113.5	75.67
GDP_MB11_ap1	MB11	10	4.29	0.58	4.29	0.58	**3.51**	**0.57**	0.75	1.80	17.5	57.73
GDP_MB11_ap2	MB11	10	3.19	0.59	3.19	0.59	**0.00**	**0.00**	0.70	3.65	28.3	48.97
GDP_MB11_ap3	MB11	10	2.99	0.51	2.99	0.51	**0.00**	**0.00**	0.65	3.57	37.3	42.71
GDP_MB11_ap4	MB11	10	3.73	0.63	3.73	0.63	**0.00**	**0.00**	0.67	3.08	49.1	44.96
GDP_MB11_ap5	MB11	10	11.69	1.26	0.00	0.00	**0.00**	**0.00**	0.68	2.41	23.8	45.60
GDP_MB12_ap1	MB12	11	3.44	0.82	3.44	0.82	**3.82**	**0.60**	0.55	4.23	43.4	32.92

GDP_MB12_ap2	MB12	11	3.64	0.42	3.64	0.42	**0.00**	**0.00**	0.72	4.19	30.0	53.24
GDP_MB12_ap3	MB12	11	3.84	0.98	3.84	0.98	**0.00**	**0.00**	0.61	3.71	17.6	37.92
GDP_MB12_ap4	MB12	11	5.07	0.86	5.07	0.86	**0.00**	**0.00**	0.64	4.44	30.0	42.13
GDP_MB12_ap5	MB12	11	3.76	0.80	3.76	0.80	**0.00**	**0.00**	0.65	3.33	29.8	42.61
GDP_MB14_ap1	MB14	12	3.14	0.33	3.14	0.33	**3.35**	**0.42**	0.65	3.42	36.6	42.54
GDP_MB14_ap2	MB14	12	3.02	0.77	3.02	0.77	**0.00**	**0.00**	0.87	2.19	15.9	108.69
GDP_MB14_ap3	MB14	12	3.54	0.57	3.54	0.57	**0.00**	**0.00**	0.73	3.56	20.7	54.62
GDP_MB14_ap4	MB14	12	3.53	0.38	3.53	0.38	**0.00**	**0.00**	0.71	3.31	37.7	51.80
GDP_MB14_ap5	MB14	12	3.65	0.71	3.65	0.71	**0.00**	**0.00**	0.60	2.23	55.0	36.21
GDP_MB-13_ap1	MB-13	13	3.40	0.34	3.40	0.34	**2.99**	**0.11**	0.67	2.92	21.4	44.25
GDP_MB-13_ap2	MB-13	13	3.14	0.12	3.14	0.12	**0.00**	**0.00**	0.67	2.98	372.2	45.16
GDP_MB-13_ap3	MB-13	13	2.86	0.11	2.86	0.11	**0.00**	**0.00**	0.69	2.56	377.0	46.69
GDP_MB-13_ap4	MB-13	13	2.76	0.10	2.76	0.10	**0.00**	**0.00**	0.68	2.86	260.6	45.34
GDP_MB-13_ap5	MB-13	13	3.73	0.18	3.73	0.18	**0.00**	**0.00**	0.66	2.65	567.8	42.26
GDP_MB-15_ap1	MB-15	14	3.89	0.18	3.89	0.18	**4.15**	**0.19**	0.64	3.30	82.9	41.06
GDP_MB-15_ap2	MB-15	14	4.41	0.22	4.41	0.22	**0.00**	**0.00**	0.79	3.79	41.0	69.95
GDP_MB-15_ap3	MB-15	14	4.26	0.15	4.26	0.15	**0.00**	**0.00**	0.71	4.35	52.4	51.93
GDP_MB-15_ap4	MB-15	14	4.09	0.30	4.09	0.30	**0.00**	**0.00**	0.64	3.03	34.9	40.79
GDP_MB-15_ap5	MB-15	14	3.90	0.42	3.90	0.42	**0.00**	**0.00**	0.71	3.64	12.5	51.82

Table V.2. Full U-Th-He data reduction in apatites from samples of the Exploradores Valley. Data from Julie Fosdick.

Full Sample Name	Sample	Sample Name	Sample #	Corrected date (Ma)	1s ± date (Ma)	2s ± date (Ma)	Mean	std dev	Norm Dist	$\tau_{max}N\tau_{max}N\tau_{max}N\tau_{max}N\tau_{max}N\tau_{max}N$	Single Age (treated) ± 1σ (Ma)		Mean Date (treated) ± 1σ (Ma)		√σ√σ√σ√σ√σ√σ	χ√σ	Weighted Mean Date ± 2σ (Ma)	
GDP_MB-4_ap1	GDP_MB-4_ap1	MB-4	6	2.50	0.08	0.16	2.37	0.17	1.72	8.61	2.50	0.16	**2.37**	**0.19**	40.92	102.34	**2.37**	**0.15**
GDP_MB-4_ap2	GDP_MB-4_ap2	MB-4	6	2.41	0.06	0.12			2.30	11.48	2.41	0.12			68.49	165.17		
GDP_MB-4_ap3	GDP_MB-4_ap3	MB-4	6	2.39	0.13	0.27			2.36	11.81	2.39	0.27			14.06	33.56		
GDP_MB-4_ap4	GDP_MB-4_ap4	MB-4	6	2.45	0.11	0.21			2.08	10.38	2.45	0.21			21.71	53.27		
GDP_MB-4_ap5	GDP_MB-4_ap5	MB-4	6	2.08	0.09	0.17			0.53	2.67	2.08	0.17			33.58	69.72		
GDP_MB-2_ap1	GDP_MB-2_ap1	MB-2	4	2.30	0.03	0.06	1.98	0.21	0.62	3.12	2.30	0.06	**1.98**	**0.09**	264.59	608.33	**2.04**	**0.07**
GDP_MB-2_ap2	GDP_MB-2_ap2	MB-2	4	1.77	0.04	0.08			1.16	5.80	1.77	0.08			148.58	263.70		
GDP_MB-2_ap3	GDP_MB-2_ap3	MB-2	4	2.09	0.04	0.08			1.64	8.20	2.09	0.08			152.27	318.70		
GDP_MB-2_ap4	GDP_MB-2_ap4	MB-2	4	1.91	0.06	0.11			1.77	8.85	1.91	0.11			76.32	145.91		
GDP_MB-2_ap5	GDP_MB-2_ap5	MB-2	4	1.84	0.04	0.09			1.48	7.41	1.84	0.09			127.22	233.75		
GDP_MB3_ap1	GDP_MB3_ap1	MB3	5				2.57	0.97	0.01	0.04	outlier		**2.57**	**0.31**			**2.21**	**0.32**

GDP_MB3_ap2	GDP_MB3_ap2	MB3	5	1.60	0.11	0.23			0.25	0.75	1.60	0.23			19.74	31.49			
GDP_MB3_ap3	GDP_MB3_ap3	MB3	5						0.01	0.04	outlier								
GDP_MB3_ap4	GDP_MB3_ap4	MB3	5	3.53	0.22	0.44			0.25	0.76	3.53	0.44			5.23	18.46			
GDP_MB3_ap5	GDP_MB3_ap5	MB3	5	2.58	0.13	0.26			0.41	1.24	2.58	0.26			14.51	37.45			
GDP_MB11_ap1	GDP_MB11_ap1	MB11	10	4.29	0.29	0.58	3.55	0.58	0.31	1.23	4.29	0.58	**3.55**	**0.58**	2.99	12.84	**3.51**	**0.57**	
GDP_MB11_ap2	GDP_MB11_ap2	MB11	10	3.19	0.30	0.59			0.57	2.26	3.19	0.59			2.85	9.08			
GDP_MB11_ap3	GDP_MB11_ap3	MB11	10	2.99	0.26	0.51			0.43	1.73	2.99	0.51			3.78	11.31			
GDP_MB11_ap4	GDP_MB11_ap4	MB11	10	3.73	0.31	0.63			0.65	2.61	3.73	0.63			2.55	9.52			
GDP_MB11_ap5	GDP_MB11_ap5	MB11	10								outlier								

Table V.3. Full U-Th-He data reduction in apatites from samples of the Exploradores Valley (continuation).

Full Sample Name	Sample	Sample Name	Sample #	Corrected date (Ma)	1s ± date (Ma)	2s ± date (Ma)	Mean	std dev	Norm Dist	$\tau_{max}N\tau_{max}N\tau_{max}N\tau_{max}N\tau_{max}N\tau_{max}N$	Single Age (treated) ± 1σ (Ma)		Mean Date (treated) ± 1σ (Ma)		$\sqrt{\sigma\sqrt{\sigma\sqrt{\sigma\sqrt{\sigma\sqrt{\sigma}}}}}$	$\chi\sqrt{\sigma}$	Weighted Mean Date ± 2σ (Ma)	
GDP_MB12_ap1	GDP_MB12_ap1	MB12	11	3.44	0.41	0.82	3.95	0.64	0.45	2.27	3.44	0.82	**3.95**	**0.78**	1.49	5.11	**3.82**	**0.60**
GDP_MB12_ap2	GDP_MB12_ap2	MB12	11	3.64	0.21	0.42			0.55	2.77	3.64	0.42			5.65	20.57		
GDP_MB12_ap3	GDP_MB12_ap3	MB12	11	3.84	0.49	0.98			0.61	3.06	3.84	0.98			1.03	3.96		
GDP_MB12_ap4	GDP_MB12_ap4	MB12	11	5.07	0.43	0.86			0.14	0.68	5.07	0.86			1.34	6.79		
GDP_MB12_ap5	GDP_MB12_ap5	MB12	11	3.76	0.40	0.80			0.59	2.97	3.76	0.80			1.56	5.86		
GDP_MB14_ap1	GDP_MB14_ap1	MB14	12	3.14	0.17	0.33	3.37	0.28	1.02	5.11	3.14	0.33	**3.37**	**0.55**	9.12	28.68	**3.35**	**0.42**
GDP_MB14_ap2	GDP_MB14_ap2	MB14	12	3.02	0.38	0.77			0.62	3.11	3.02	0.77			1.70	5.14		
GDP_MB14_ap3	GDP_MB14_ap3	MB14	12	3.54	0.29	0.57			1.22	6.09	3.54	0.57			3.03	10.71		
GDP_MB14_ap4	GDP_MB14_ap4	MB14	12	3.53	0.19	0.38			1.24	6.18	3.53	0.38			6.88	24.27		
GDP_MB14_ap5	GDP_MB14_ap5	MB14	12	3.65	0.35	0.71			0.89	4.45	3.65	0.71			2.01	7.33		
GDP_MB-13_ap1	GDP_MB-13_ap1	MB-13	13	3.40	0.17	0.34	3.18	0.40	0.86	4.30	3.40	0.34	**3.18**	**0.17**	8.73	29.63	**2.99**	**0.11**

GDP_MB-13_ap2	GDP_MB-13_ap2	MB-13	13	3.14	0.06	0.12			1.00	4.98	3.14	0.12			73.32	230.31		
GDP_MB-13_ap3	GDP_MB-13_ap3	MB-13	13	2.86	0.05	0.11			0.73	3.63	2.86	0.11			87.64	250.48		
GDP_MB-13_ap4	GDP_MB-13_ap4	MB-13	13	2.76	0.05	0.10			0.57	2.86	2.76	0.10			109.90	302.83		
GDP_MB-13_ap5	GDP_MB-13_ap5	MB-13	13	3.73	0.09	0.18			0.38	1.90	3.73	0.18			31.43	117.29		
GDP_MB-15_ap1	GDP_MB-15_ap1	MB-15	14	3.89	0.09	0.18	4.11	0.23	1.09	5.44	3.89	0.18	**4.11**	**0.25**	30.65	119.11	**4.15**	**0.19**
GDP_MB-15_ap2	GDP_MB-15_ap2	MB-15	14	4.41	0.11	0.22			0.74	3.72	4.41	0.22			20.87	91.93		
GDP_MB-15_ap3	GDP_MB-15_ap3	MB-15	14	4.26	0.08	0.15			1.42	7.10	4.26	0.15			44.32	188.77		
GDP_MB-15_ap4	GDP_MB-15_ap4	MB-15	14	4.09	0.15	0.30			1.77	8.84	4.09	0.30			10.94	44.77		
GDP_MB-15_ap5	GDP_MB-15_ap5	MB-15	14	3.90	0.21	0.42			1.17	5.83	3.90	0.42			5.72	22.31		